MORPHOLOGIC AND CLIMATIC CONTROLS ON SOIL EVOLUTION

IN THE BITTERROOT AND SAPPHIRE MOUNTAINS, MONTANA

by

Sarah Sarojini Benjaram

A thesis submitted in partial fulfillment
of the requirements for the degree
of

Master of Science

in

Earth Sciences

MONTANA STATE UNIVERSITY
Bozeman, Montana

April 2017

DEDICATION

I would like to thank my advisor, Dr. Jean Dixon, for her guidance in carrying out this project and writing this thesis. Thank you for your good example and your patience.

Thanks to my committee members, Dr. Tony Hartshorn and Dr. Dave Mogk, for their input on my project. Tony, thanks especially for visiting me in the field during the summer.

I am grateful to George Furniss for his hospitality in letting me stay at his beautiful place in the Bitterroots. I couldn't have managed such a long field trip without taking breaks at the little house.

Thanks to Dr. Andrew Wilcox for his insight, advice and support.

Thanks to Sam Shelafo, Darrell Schwartz, and Aaron Feldhaus for helping me out in the field and Karsten Lorentz for help in the lab.

TABLE OF CONTENTS

TABLE OF CONTENTS – CONTINUED

LIST OF TABLES

Table Page

LIST OF FIGURES

Figure Page

ABSTRACT

To what extent is chemical weathering governed by a landscape's topography? Two neighboring mountain ranges in the northern Rockies of western Montana, USA, provide an ideal natural laboratory in which to investigate the relationship between soil chemical weathering, persistence of soil cover, and topography. We also examine the connection between the topography and climate history. The mountain ranges we explore are the previously glaciated Bitterroot Mountains, which consist of steep, rock-dominated hillslopes, and the neighboring unglaciated Sapphire Mountains which display convex, soil-mantled hillslopes. Soil thickness measurements, soil and rock geochemistry, and digital terrain analysis reveal that soils in the rock-dominated Bitterroot Mountains are less thoroughly weathered than those in the Sapphire Mountains. These differences are even greater when we adjust weathering for rock fragments and consider surface weathering intensity at a landscape scale using our newly developed metric, the rock-adjusted chemical depletion fraction (RACDF) and rock-adjusted mass transfer coefficient (RAτ). The Bitterroots overall are 30% less weathered than the Sapphires despite higher mean annual precipitation in the former, with an average RACDF of 0.38 in the postglacial Bitterroots catchment and 0.61 in the nonglacial Sapphire catchment, suggesting that 38% of rock mass is lost in the conversion to soil in the Bitterroots, whereas 61% of rock mass is lost in the nonglaciated Sapphires. Though we find little evidence for modern climate influence on weathering, data suggest that precipitation may influence slope thresholds for soil cover. Forested soils persist on slopes that are 5° higher in the Bitterroots than the Sapphires (25° and 20° respectively), based on land cover data. Because the previously glaciated Bitterroots are less weathered despite being wetter, we conclude that the glacial history of this landscape exerts more influence on soil chemical weathering than does modern climate. However, while previous studies have correlated weathering intensity with topographic parameters such as slope gradient, we find little topographic indication of specific controls on weathering in these complex systems.

CHAPTER 1

INTRODUCTION

Intent of this MS Thesis

Significant advancement has been made in our understanding of the controls on soil development and chemical weathering over the past several decades. However, some grand challenges remain untangling the relationships between past and present climate, topography, and soil formation and weathering. I bring together these important themes by addressing the critical question: To what extent do climate and morphology control soil evolution? I address this question through the examination of two landscapes in the northern Rockies of Montana: one of which, the Bitterroot Mountains, was glaciated in the LGM, while the other, the neighboring Sapphire Mountains, was not. My research, presented in this thesis, links the topographic legacy of glaciation to thresholds for soil cover and chemical weathering.

Background

The patterns of soil formation, weathering, and erosion shape terrestrial landscapes where the biosphere, atmosphere, hydrosphere, and lithosphere all meet, forming the foundation on which ecosystems and human civilizations are built. Landscapes record interactions between climatic and tectonic forcings; by linking observed landforms to surface processes and their rates we may better untangle how these forcings impact Earth's surface (Dietrich et al., 2003). In the last 50 years, quantitative

understanding of Earth surface processes has accelerated exponentially, and continues to grow in complexity and scope. Increasingly, the geomorphic community has recognized that feedbacks between climate (e.g. von Blanckenburg et al., 2004; Dixon et al., 2009), vegetation (Dietrich and Perron, 2006; Amundson et al., 2007), hydrology (Anderson and Dietrich, 2001), and regolith development (Anderson et al., 2007) play important roles in the evolution of landscapes. Each of these inputs influences the rate of mineral weathering in soils, which in turn controls the release of solutes that provide the nutritional basis of terrestrial ecosystems, neutralizes acidic precipitation, accelerates landscape evolution, and possibly stabilizes Earth's climate over millennial timescales (Garrels and Mackenzie, 1971; Likens et al., 1967; Drever, 1994; Kump et al., 2000; Berner 2003). Significant advances in our understanding of these complex feedbacks between air, water, rock and life have been made since Jenny (1941) first qualitatively described the five factors of soil formation, partially due to increased attention over the past decade and a half to this interface as a "Critical Zone" (National Research Council, 2001; Banwart et al., 2013).

A landscape bears the mark of its cumulative tectonic and climatic history, as tectonic motion leads to surface deformation (e.g. Kirby and Whipple, 2012), mantle convection and plumes cause vertical displacement (e.g. Rohrman and van der Beek, 1996; Saunders et al., 2007; Braun, 2010), ice sheets grow and recede (e.g. Dansgaard et al., 1993), and sea level changes by tens of meters (e.g. Lambeck and Chappell, 2001). In mountain belts, glaciers play an important role as they steepen and deepen valleys and create forms such as cirques, arêtes, horns, hanging valleys, truncated spurs, and U-

shaped troughs (e.g. Sugden and John, 1976; Brocklehurst and Whipple, 2002). The abrasion and plucking caused by ice scraping over bedrock can accelerate mountain erosion (Herman et al., 2013) and produce fine-grained sediments that weather quickly (Anderson et al., 2000), resulting in large changes in surface weathering post-glaciation (Taylor and Blum, 1995). After glacial retreat, mountain belts may rebound isostatically (Molnar and England, 1990; Champagnac et al., 2007) and glacial sediments serve as erosive tools for rivers through abrasion of bedload grains against the river bed (Jansen et al., 2011).

Because glaciers are so influential, numerous metrics have been developed to measure their topographic legacy. For example, by eroding topography above the snowline, glaciers change the elevation distribution, or hypsometry, of a landscape (Brozović et al., 1997; Montgomery et al., 2001; Brocklehurst and Whipple, 2004; Mitchell and Montgomery, 2006). Around the globe, the hypsometric maximum, or the greatest proportion of a landscape at a given elevation, occurs between the modern snowline and the Last Glacial Maximum (LGM) snowline, regardless of tectonic setting, lithology, or uplift rate (Egholm et al., 2009). Thus, the hypsometry of a landscape contains hints of its glacial history over millennial timescales. Slope-elevation distribution can also be used to detect a glacial signature, as the decrease in slope at the ELA shows up as a decrease in the slope-elevation curve at the ELA (Robl et al., 2015). Thirdly, by bulldozing short-wavelength topography, glaciers may decrease the drainage density of a landscape, and thus drainage density can be used to detect a glacial signature (Salcher et al., 2014).

The glacial imprint on landscape morphology has important implications for the evolution of critical zone processes, since topography influences soil production and weathering. Hillslope curvature, for example, is a predictor of soil thickness (Heimsath et al., 1997), which in turn controls the hydrologic regime of a landscape via infiltration rates (Woolhiser et al., 2006) and water storage potential (McGuire et al., 2005; Pelletier and Rasmussen, 2009). Topography may also control whether there is any soil cover at all, since slope thresholds may exist above which regolith cover cannot persist (e.g., Dietrich et al., 1992; Heimsath et al., 2012).

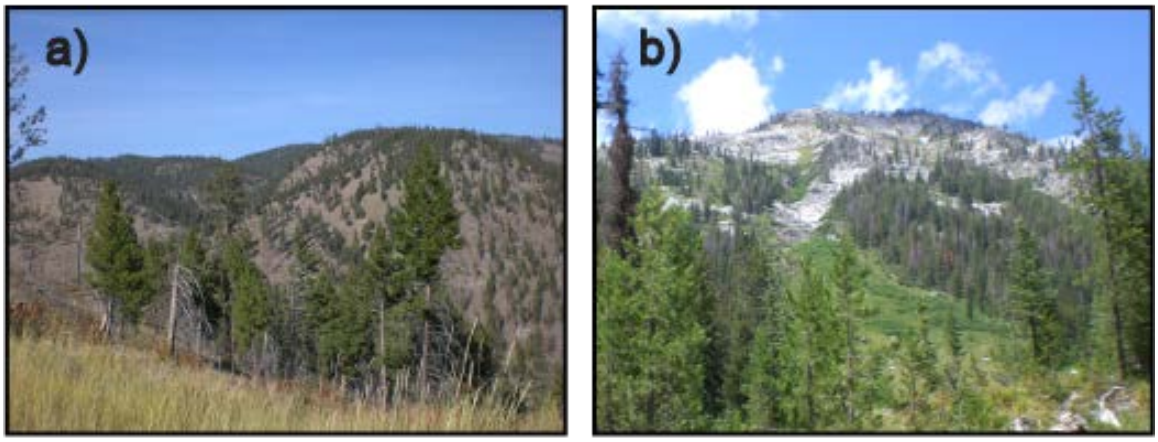

Figure 1.1. Illustration of contrasting landscapes. In panel (a), a soil mantle covers the entire hillslope and supports tree cover that spans the entire elevation. In panel (b), the ridge displays bare bedrock with no soil cover. Vegetation cover is dense near the bottom of the hillslope but becomes patchy partway up the slope and almost disappears at the highest elevations. This contrast is indicative of a change in soil production or transport processes.

Several fundamental questions remain regarding how soils evolve, especially in mountainous landscapes where tectonics and climate exert complex forcings on erosion and weathering. In these systems, soil cover is discontinuous and the regolith cover heterogeneous. Consider two landscapes distinct in their abundance of soil and rock

outcrops (figure 1.1). One is covered by vegetation that overlies a continuous soil mantle. In the other, soils and vegetation primarily cover the valley floor, extending upslope to some elevation where vegetation cover becomes patchy and bare rock is exposed. Why might one landscape be soil-mantled while another is rock-dominated? To answer this question, we must understand the processes that produce and transport soil at multiple spatial and temporal scales. The presence of a soil mantle indicates that soil production rate meets or exceeds the erosion rate at a given location, and a stabilizing feedback mechanism stabilizes soil thickness so a soil cover is maintained over much of Earth's surface (Carson and Kirkby, 1972; Ahnert, 1976; Anderson and Humphrey, 1989). In landscapes void of this continuous mantle, the exposure of bare rock at the surface suggests a breakdown of this stabilizing mechanism.

The original, but still widely used, models for soil and hillslope evolution are primarily derived for continuously soil mantled convex hillslopes, where soil erosion is understood to occur by diffusive, gradient-dependent processes and soil is formed by biomechanical disruption of rock at the bottom of the soil column (e.g., Gilbert, 1898; Dietrich et al., 1995). When soil particles become exposed at the surface, creep processes move them downslope in proportion to slope gradient in a continuous process. Soil production and transport influence each other in a negative feedback so that they tend to find a balance at a constant, usually thin, soil thickness (Heimsath et al., 1997). In these systems, uniformly eroding hillslopes have a parabolic shape, and therefore spatially varying steepnesses. Importantly, in such systems it has also been noted that at a landscape scale, the mean erosion rate generally increases with the mean landscape slope

and local relief (Gilbert, 1877; Ahnert, 1970; Milliman and Syvitski, 1992; Summerfield and Hulton, 1994; Harrison, 2000; Montgomery and Brandon, 2002). However, in some landscapes, erosion and slope become decoupled as slopes approach threshold steepnesses (Strahler, 1950; Penck, 1953; Anderson and Humphrey, 1989; Anderson, 1994; Howard, 1994, 1997; Schmidt and Montgomery, 1995; Burbank et al., 1996; Roering et al., 1999; Montgomery and Brandon, 2002). Once they reach their threshold steepness, catchments with similar mean slope gradients can have widely different denudation rates, especially in active orogens (Burbank et al., 1996). This theoretical relationship is supported by multiple empirical data sets across diverse mountain ranges that show catchment-average hillslope angle remains constant in regions with rapid erosion rates (often >250 m/My; e.g., Binnie et al., 2007; Ouimet et al., 2009). In such systems, hillslope processes are likely dominated by landsliding (e.g., Binnie et al., 2007; Schmidt and Montgomery, 1995; Burbank et al., 1996; Montgomery, 2001). Importantly, this transition between slope-dependent transport processes and landslide dominance is likely gradual, and carries important implications for rates of soil formation, which may keep up locally with high rates of erosion even in otherwise bedrock dominated systems (Heimsath et al., 2012).

The presence and thickness of soil cover at both local and landscape scales also have important implications for chemical weathering. Chemical weathering regimes have been described as two end-member conditions. In one, chemical erosion rates increase proportionally with soil production rate, which provides the weathering engine with fresh supply to act on. This is termed a supply-limited regime because chemical weathering

rates are coupled to the rate of mineral supply (Riebe et al., 2004a, 2004b; West et al., 2005; Gabet and Mudd, 2009; Hilley et al., 2010; Dixon et al., 2012). In the other endmember condition, the degree of chemical depletion decreases with increasing mineral supply rates, as erosion removes weatherable material before it has a long enough residence time on the hillslope to be completely weathered. This is termed kinetic limitation (West et al., 2005; Brantley and White, 2009; Brantley and Lebedeva, 2011; Brantley et al., 2013). Much of the world can largely be described as supply limited (Dixon and von Blanckenburg, 2012). Kinetically limited landscapes are less well documented (e.g., Dixon et al., 2012; Jin et al., 2010; Rasmussen et al., 2011), partially due to sampling biases to measure weathering in soil-mantled systems (Dixon and von Blanckenburg, 2012). Large uncertainties therefore exist in how weathering regimes may reflect erosion-weathering feedbacks or controls such as climate and landscape morphology.

Thesis Format and Outline

This thesis addresses the complex questions of how morphology and climate may influence soil evolution. In chapter 2, I present my examination, prepared for publication. The fundamental concepts behind my approach are described in figure 1.2. I explore the relationships between soil thickness, degree of chemical weathering, and topographic and climatic variables in order to better understand how soils evolve in mountainous landscapes. Addressing these relationships requires quantifying weathering and soil cover

across multiple spatial scales. Chapter 3 provides a summary and directions for future work.

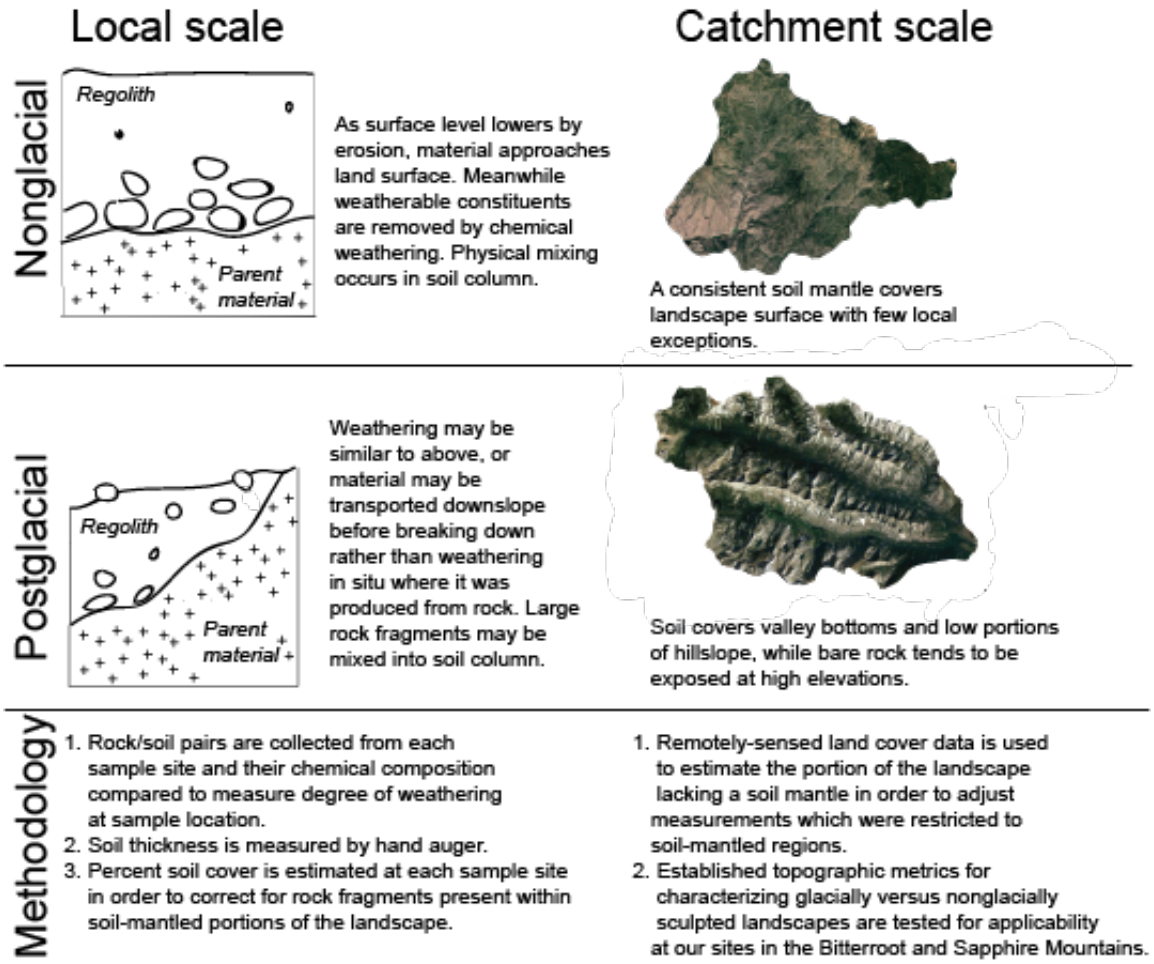

Figure 1.2. Glaciers carved steep-walled valleys in parts of the Northern Rockies during the Pleistocene. Thousands of years later, landscapes still bear this topographic signature. The aim of our study is to better understand the differences in chemical weathering regime in steep landscapes such as those formed by glaciers (middle panel) from the chemical weathering regime of gentle, convex hillslope systems where much of our understanding of geomorphology was developed (top panel). It is necessary to measure weathering patterns at both the local scale (left column) and catchment scale (right column), by which we mean the basin upslope from where the creek feeds into the river valley. The bottom panel describes our methodology for doing so.

References Cited

Ahnert, F., 1976. Quantitative slope models.

Ahnert, F., 1970. Functional relationships between denudation, relief, and uplift in large, mid-latitude drainage basins. *American Journal of Science*, *268*(3), pp.243-263.

Alden, W.C., 1953, Physiography and glacial geology of western Montana and adjacent areas: U.S. Geological Survey Professional Paper 231, pp. 200.

Amundson, R., Richter, D.D., Humphreys, G.S., Jobbágy, E.G. and Gaillardet, J. 2007. Coupling between biota and earth materials in the critical zone. *Elements*, *3*(5), pp.327-332.

Anderson, R.S., 1994. Evolution of the Santa Cruz Mountains, California, through tectonic growth and geomorphic decay. *Journal of Geophysical Research: Solid Earth*, *99*(B10), pp.20161-20179.

Anderson, S.P., Drever, J.I., Frost, C.D. and Holden, P., 2000. Chemical weathering in the foreland of a retreating glacier. *Geochimica et Cosmochimica Acta*, *64*(7), pp.1173-1189.

Anderson, S.P. and Dietrich, W.E. 2001. Chemical weathering and runoff chemistry in a steep headwater catchment. *Hydrological Processes*, *15*(10), pp.1791-1815.

Anderson, R.S. and Humphrey, N.F., 1989. Interaction of weathering and transport processes in the evolution of arid landscapes. *Quantitative Dynamic Stratigraphy*, pp.349-361.

Anderson, S.P., von Blanckenburg, F. and White, A.F. 2007. Physical and chemical controls on the critical zone. *Elements*, *3*(5), pp.315-319.

Banwart, S.A., Chorover, J., Gaillardet, J., Sparks, D., White, T., Anderson, S., Aufdenkampe, A., Bernasconi, S., Brantley, S.L., Chadwick, O. and Dietrich, W.L.E. Sustaining Earth's Critical Zone Basic Science and Interdisciplinary Solutions for Global Challenges (The University of Sheffield, 2013).

Beaty, C.B., 1962. Asymmetry of stream patterns and topography in the Bitterroot Range, Montana. *The Journal of Geology*, pp.347-354.

Berner, R.A. 2003. The long-term carbon cycle, fossil fuels and atmospheric composition. *Nature*, *426*(6964), pp.323-326.

Binnie, S.A., Phillips, W.M., Summerfield, M.A. and Fifield, L.K., 2007. Tectonic uplift, threshold hillslopes, and denudation rates in a developing mountain range. *Geology*, *35*(8), pp.743-746.

Brantley, S. L., and M. Lebedeva. 2011. Learning to read the chemistry of regolith to understand the Critical Zone. *Annu. Rev. Earth Planet. Sci.*, 39, 387–416, doi:10.1146/annurev-earth-040809-152321.

Brantley, S. L., and A. F. White. 2009. Approaches to modeling weathering regolith. *Rev. Mineral. Geochem.*, 70, 435–484.

Brantley, S.L., Holleran, M.E., Jin, L. and Bazilevskaya, E., 2013. Probing deep weathering in the Shale Hills Critical Zone Observatory, Pennsylvania (USA): the hypothesis of nested chemical reaction fronts in the subsurface. *Earth Surface Processes and Landforms*, *38*(11), pp.1280-1298.

Braun, J., 2010. The many surface expressions of mantle dynamics. *Nature Geoscience*, *3*(12), pp.825-833.

Brocklehurst, S.H. and Whipple, K.X., 2002. Glacial erosion and relief production in the Eastern Sierra Nevada, California. *Geomorphology*, *42*(1), pp.1-24.

Brozović, N., Burbank, D.W. and Meigs, A.J., 1997. Climatic limits on landscape development in the northwestern Himalaya. *Science*, *276*(5312), pp.571-574.

Burbank, D.W., Leland, J., Fielding, E., Anderson, R.S., Brozovic, N., Reid, M.R. and Duncan, C. 1996. Bedrock incision, rock uplift and threshold hillslopes in the northwestern Himalayas. *Nature*, *379*(6565), pp.505-510.

Burke, B.C., Heimsath, A.M. and White, A.F. 2007. Coupling chemical weathering with soil production across soil-mantled landscapes. *Earth Surface Processes and Landforms*, *32*(6), pp.853-873.

Carson, M.A. and Kirkby, M.J., 1972. Hillslope form and process.

Champagnac, J.D., Molnar, P., Anderson, R.S., Sue, C. and Delacou, B., 2007. Quaternary erosion-induced isostatic rebound in the western Alps. *Geology*, *35*(3), pp.195-198.

Dansgaard, W., Johnsen, S.J., Clausen, H.B., Dahl-Jensen, D., Gundestrup, N.S., Hammer, C.U., Hvidberg, C.S., Steffensen, J.P., Sveinbjörnsdottir, A.E., Jouzel, J. and Bond, G., 1993. Evidence for general instability of past climate from a 250-kyr ice-core record. *Nature*, *364*(6434), pp.218-220.

Dietrich, W.E., Bellugi, D.G., Sklar, L.S., Stock, J.D., Heimsath, A.M. and Roering, J.J. 2003. Geomorphic transport laws for predicting landscape form and dynamics. *Prediction in geomorphology*, pp.103-132.

Dietrich, W.E. and Perron, J.T., 2006. The search for a topographic signature of life. *Nature*, *439*(7075), pp.411-418.

Dietrich, W.E., Reiss, R., Hsu, M.L. and Montgomery, D.R., 1995. A process-based model for colluvial soil depth and shallow landsliding using digital elevation data. *Hydrological processes*, *9*(3-4), pp.383-400.

Dixon, J. L., A. S. Hartshorn, A. M. Heimsath, R. A. DiBiase, and K. X. Whipple. 2012. Chemical weathering response to tectonic forcing. A soils perspective from the San Gabriel Mountains, California. *Earth Planet. Sci. Lett.*, 323, 40–49.

Dixon, J.L., Heimsath, A.M., Kaste, J. and Amundson, R. 2009a. Climate-driven processes of hillslope weathering. *Geology*, *37*(11), pp.975-978.

Drever, J.I. 1994. The effect of land plants on weathering rates of silicate minerals. *Geochimica et Cosmochimica Acta*, *58*(10), pp.2325-2332.

Egholm, D.L., Nielsen, S.B., Pedersen, V.K. and Lesemann, J.E., 2009. Glacial effects limiting mountain height. *Nature*, *460*(7257), pp.884-887.

Evans, I.S., and Cox, N.J., 2005, Global variations in local asymmetry in glacier altitude: Separation of north-south and east-west components: *Journal of Glaciology*, v. **51** pp. 469-482.

Gabet, E.J. and Mudd, S.M., 2009. A theoretical model coupling chemical weathering rates with denudation rates. *Geology*, *37*(2), pp.151-154.

Gilbert GK. 1877. Report on the Geology of the Henry Mountains. Department of the Interior: Washington, DC.

Gilbert GK. 1909. The convexity of hilltops. *Journal of Geology* **17** : 344–350.

Green, E.G., Dietrich, W.E. and Banfield, J.F. 2006. Quantification of chemical weathering rates across an actively eroding hillslope. *Earth and Planetary Science Letters*, *242*(1), pp.155-169.

Harrison, C.G.A., 2000. What factors control mechanical erosion rates?. *International Journal of Earth Sciences*, *88*(4), pp.752-763.

Heimsath, A.M., Dietrich, W.E., Nishiizumi, K. and Finkel, R.C., 1997. The soil production function and landscape equilibrium. *Nature*, *388*(6640), pp.358-361.

Heimsath, A.M., DiBiase, R.A. and Whipple, K.X., 2012. Soil production limits and the transition to bedrock-dominated landscapes. *Nature Geoscience*, *5*(3), pp.210-214.

Herman, F., Seward, D., Valla, P.G., Carter, A., Kohn, B., Willett, S.D. and Ehlers, T.A., 2013. Worldwide acceleration of mountain erosion under a cooling climate. *Nature*, *504*(7480), pp.423-426.

Hilley, G.E., Chamberlain, C.P., Moon, S., Porder, S. and Willett, S.D., 2010. Competition between erosion and reaction kinetics in controlling silicate-weathering rates. *Earth and Planetary Science Letters*, *293*(1), pp.191-199.

Howard, A.D., 1994. A detachment-limited model of drainage basin evolution. *Water resources research*, *30*(7), pp.2261-2285.

Howard, A.D., 1997. Badland morphology and evolution: Interpretation using a simulation model. *Earth Surface Processes and Landforms*, *22*(3), pp.211-227.

Jansen, J.D., Fabel, D., Bishop, P., Xu, S., Schnabel, C. and Codilean, A.T., 2011. Does decreasing paraglacial sediment supply slow knickpoint retreat?. *Geology*, *39*(6), pp.543-546.

Jenny, H.J., 1941, Factors of soil formation: New York, McGraw-Hill, 281 p.

Jin, L., R. Ravella, B. Ketchum, P. R. Bierman, P. Heaney, T. White, and S. L. Brantley. 2010. Mineral weathering and elemental transport during hillslope evolution at the Susquehanna/Shale Hills Critical Zone Observatory. *Geochim. Cosmochim. Acta*, 74, 3669–3691

Kirkby, M.J., 1984, Modelling cliff development in South Wales; Savigear re-reviewed: *Zeitschrift für Geomorphologie*, v. 28p. 405-426.

Kirby, E. and Whipple, K.X., 2012. Expression of active tectonics in erosional landscapes. *Journal of Structural Geology*, *44*, pp.54-75.

Kump, L.R., Brantley, S.L. and Arthur, M.A., 2000. Chemical weathering, atmospheric CO2, and climate. *Annual Review of Earth and Planetary Sciences*, *28*(1), pp.611-667.

Lambeck, K. and Chappell, J., 2001. Sea level change through the last glacial cycle. *Science*, *292*(5517), pp.679-686.

Likens, G.E., Bormann, F.H., Johnson, N.M. and Pierce, R.S., 1967. The calcium, magnesium, potassium, and sodium budgets for a small forested ecosystem. *Ecology*, *48*(5), pp.772-785.

Milliman, J.D. and Syvitski, J.P., 1992. Geomorphic/tectonic control of sediment discharge to the ocean: the importance of small mountainous rivers. *The Journal of Geology*, pp.525-544.

McGuire, K.J., McDonnell, J.J., Weiler, M., Kendall, C., McGlynn, B.L., Welker, J.M. and Seibert, J., 2005. The role of topography on catchment-scale water residence time. *Water Resources Research*, *41*(5).

Mitchell, S.G. and Montgomery, D.R., 2006. Influence of a glacial buzzsaw on the height and morphology of the Cascade Range in central Washington State, USA. *Quaternary Research*, *65*(1), pp.96-107.

Molnar, P. and England, P., 1990. Late Cenozoic uplift of mountain ranges and global climate change: chicken or egg?. *Nature*, *346*(6279), pp.29-34.

Montgomery, D.R. 2001. Slope distributions, threshold hillslopes, and steady-state topography. *American Journal of Science*, *301*(4-5), pp.432-454.

Montgomery, D.R. and Brandon, M.T. 2002. Topographic controls on erosion rates in tectonically active mountain ranges. *Earth and Planetary Science Letters*, *201*(3), pp.481-489.

National Research Council Committee on Basic Research Opportunities in the Earth Sciences. (2001). Basic Research Opportunities in the Earth Sciences. National Academies Press, Washington, DC.

Naylor, S. and Gabet, E.J., 2007. Valley asymmetry and glacial versus nonglacial erosion in the Bitterroot Range, Montana, USA. *Geology*, *35*(4), pp.375-378.

Ouimet, W.B., Whipple, K.X. and Granger, D.E., 2009. Beyond threshold hillslopes: Channel adjustment to base-level fall in tectonically active mountain ranges. *Geology*, *37*(7), pp.579-582.

Pardee, J.T., 1910. The glacial lake Missoula. *The Journal of Geology*, *18*(4), pp.376-386.

Pardee, J.T., 1942. Unusual currents in glacial lake Missoula, Montana. *Geological Society of America Bulletin*, *53*(11), pp.1569-1600.

Pelletier, J.D. and Rasmussen, C., 2009. Quantifying the climatic and tectonic controls on hillslope steepness and erosion rate. *Lithosphere*, *1*(2), pp.73-80.

Penck, W., 1953. Morphological analysis of land forms: a contribution to physical geology. MacMillan and Company.

Rasmussen, C., S. Brantley, D. deB. Richter, A. Blum, J. Dixon, and A. F. White. 2011. Strong climate and tectonic control on plagioclase weathering in granitic terrain, *Earth Planet. Sci. Lett.*, 301, 521–530.

Riebe, C.S., Kirchner, J.W., Granger, D.E. and Finkel, R.C., 2001. Minimal climatic control on erosion rates in the Sierra Nevada, California. *Geology*, *29*(5), pp.447-450.

Riebe, C.S., Kirchner, J.W. and Finkel, R.C., 2003. Long-term rates of chemical weathering and physical erosion from cosmogenic nuclides and geochemical mass balance. *Geochimica et Cosmochimica Acta*, *67*(22), pp.4411-4427.

Riebe, C.S., Kirchner, J.W. and Finkel, R.C., 2004a. Erosional and climatic effects on long-term chemical weathering rates in granitic landscapes spanning diverse climate regimes. *Earth and Planetary Science Letters*, *224*(3), pp.547-562.

Riebe, C.S., Kirchner, J.W. and Finkel, R.C., 2004b. Sharp decrease in long-term chemical weathering rates along an altitudinal transect. *Earth and Planetary Science Letters*, *218*(3), pp.421-434.

Robl, J., Prasicek, G., Hergarten, S. and Stüwe, K., 2015. Alpine topography in the light of tectonic uplift and glaciation. *Global and Planetary Change*, *127*, pp.34-49.

Roering, J.J., Kirchner, J.W. and Dietrich, W.E., 1999. Evidence for nonlinear, diffusive sediment transport on hillslopes and implications for landscape morphology. *Water Resources Research*, *35*(3), pp.853-870.

Rohrman, M. and van der Beek, P., 1996. Cenozoic postrift domal uplift of North Atlantic margins: an asthenospheric diapirism model. *Geology*, *24*(10), pp.901-904.

Salcher, B.C., Kober, F., Kissling, E. and Willett, S.D., 2014. Glacial impact on short-wavelength topography and long-lasting effects on the denudation of a deglaciated mountain range. *Global and Planetary Change*, *115*, pp.59-70.

Saunders, A.D., Jones, S.M., Morgan, L.A., Pierce, K., Widdowson, M. and Xu, Y.G., 2007. Regional uplift associated with continental large igneous provinces: the roles of mantle plumes and the lithosphere. *Chemical Geology*, *241*(3), pp.282-318.

Schmidt, K.M. and Montgomery, D.R. 1995. Limits to relief. *Science*, *270* (5236), p.617.

Stickney, Michael. 2014. New LiDAR data reveals late Quaternary geology details in the Bitterroot Valley, Western Montana. Geological Society of America Rocky Mountain and Cordilleran Sections Joint Meeting, Session No. 27. Montana State University, Bozeman. 21 May, 2014.

Strahler, A.N., 1950. Davis' concepts of slope development viewed in the light of recent quantitative investigations. *Annals of the Association of American Geographers*, *40*(3), pp.209-213.

Sugden, D.E. and John, B.S., 1976. *Glaciers and landscape*. E. Arnold.

Summerfield, M.A. and Hulton, N.J., 1994. Natural controls of fluvial denudation rates in major world drainage basins. *JOURNAL OF GEOPHYSICAL RESEARCH-ALL SERIES-*, *99*, pp.13-871.

Taylor, A. and Blum, J.D., 1995. Relation between soil age and silicate weathering rates determined from the chemical evolution of a glacial chronosequence. *Geology*, *23*(11), pp.979-982.

West, A.J., Galy, A. and Bickle, M., 2005. Tectonic and climatic controls on silicate weathering. *Earth and Planetary Science Letters*, *235*(1), pp.211-228.

Whipple, K.X. and Tucker, G.E., 1999. Dynamics of the stream-power river incision model: Implications for height limits of mountain ranges, landscape response timescales, and research needs. *Journal of Geophysical Research: Solid Earth*, *104*(B8), pp.17661-17674.

Woolhiser, D.A., Fedors, R.W., Smith, R.E. and Stothoff, S.A., 2006. Estimating infiltration in the upper split wash watershed, Yucca Mountain, Nevada. *Journal of Hydrologic Engineering*, *11*(2), pp.123-133.

Von Blanckenburg, F., Hewawasam, T. and Kubik, P.W. 2004. Cosmogenic nuclide evidence for low weathering and denudation in the wet, tropical highlands of Sri Lanka. *Journal of Geophysical Research: Earth Surface*, *109*(F3).

CHAPTER 2

MORPHOLOGIC AND CLIMATIC CONTROLS ON SOIL EVOLUTION IN THE BITTERROOT AND SAPPHIRE MOUNTAINS

Introduction

Soil represents a dynamic interface between the Earth, atmosphere, and biosphere, and provides important substrate for terrestrial life. When soil is produced from rock, nutrients are released that power primary productivity and cascade throughout the ecosystem. Water flow patterns and chemical composition are determined in part by the shape of the landscape and the chemistry of the soil through which it flows. Trees, burrowing animals, and microorganisms act to break down and churn the soil as they utilize it for nutrients and habitat. Therefore, characterization of soil dynamics is key to understanding not only landscape evolution but also hydrologic flow regimes and ecosystem development. Mountainous landscapes present some large challenges to exploring soil formation, since soils may be patchy in these systems, and the dynamic controls on their formation difficult to quantify. Here, we explore how soil cover and weathering in mountainous systems may reflect past climates, and the morphologic legacy they leave.

Legacies of Past Climate on Landscape Morphology

While it is widely recognized that ecosystems and landforms are influenced by modern climate, which dictates temperature and moisture availability and influences fire and hydrologic regimes, the past climates may exert influence and leave a lasting legacy

as well. For example, Church and Slaymaker (1989) described the landscape of British Columbia as “imprisoned in its history” because its rivers were still responding to the last glaciation more than 10 ky later. A similar observation has been noted across many other post-glacial landscapes, since glaciers are powerful erosive agents that carve out steep valleys and characteristic topographic features that remain on the landscape thousands of years after the glaciers recede. This influence is expressed through widening and deepening of valleys through abrasion and plucking of bedrock by ice (Brocklehurst and Whipple, 2002) and can accelerate mountain erosion (Herman et al., 2013). Glaciers produce fine-grained sediments that undergo rapid weathering of carbonate and biotite (Anderson et al., 2000) and leave behind less reactive minerals so that after glacial retreat, total weathering rates may lower (Norton and von Blanckenburg, 2010). Glaciers may lead to increased mountain relief through both erosion and following isostatic compensation (Molnar and England, 1990; Champagnac et al., 2007), and fluvial export of post-glacial sediments fuels erosion (Jansen et al., 2011). The present interglacial interval, ca. 16,500 years, is likely insufficient time for rivers to achieve equilibrium, and these channel systems are likely still responding to Pleistocene glaciation (e.g., Collins and Montgomery, 2010).

To measure a landscape’s climate legacy, geomorphologists have developed a number of topographic metrics. For example, a concentration of surface area at elevations corresponding to the glacial equilibrium line altitude (ELA) is indicative of a glacial buzzsaw, where glaciers erode topography above the snowline to just below the ELA while isostatic uplift compensates by uplifting the entire landscape (Brozović et al., 1997;

Montgomery et al., 2001; Mitchell and Montgomery, 2006; Brocklehurst and Whipple, 2004). Thus hypsometry, or the frequency distribution of elevation, can be used to identify whether a landscape was shaped by fluvial or glacial processes (e.g. Brozovic et al. 1997; Kirkbride and Matthews, 1997; Montgomery et al., 2001; Brocklehurst and Whipple, 2004; Mitchell and Montgomery, 2006). Egholm et al. (2009) examined digital elevations models (DEMs) from around the world and found that regardless of tectonic setting, lithology, or uplift rate the hypsometric maximum is usually between the modern and last glacial maximum (LGM) snowlines, and that most summit elevations are not more than 1,500 m above the local snowline.

Slope-elevation distributions provide additional insight into the evolution of a landscape (Robl et al., 2015; figure 2.1). Glacial erosion erases local relief above the ELA and forms cirques, where slope gradient decreases, and can form nunataks at the summit where rock is exposed above the glacial ice with extremely steep (near vertical) slopes. Therefore, in these systems, gradients would decrease above the ELA and spike at the highest elevations, in contrast to landscapes formed by fluvial processes where gradients are generally increase smoothly with increasing elevation.

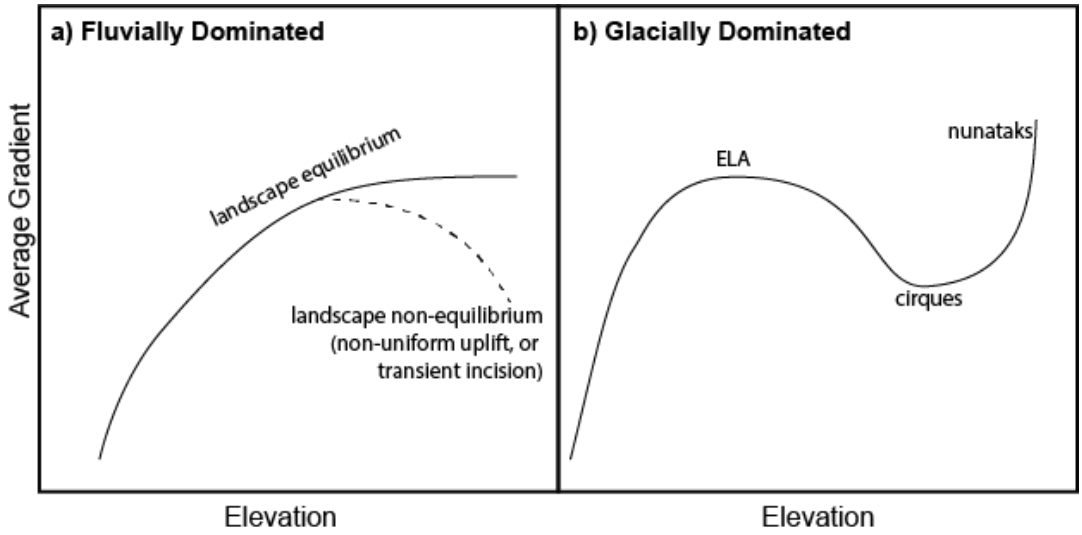

Figure 2.1. Idealized slope-elevation distributions of a single profile from headwaters to trunk stream, characteristic of a) a landscape shaped by fluvial processes, and b) a landscape shaped by glacial processes. In landscape (a), the solid line represents a landscape in equilibrium, meaning it has adapted to its present boundary conditions and the entire landscape is responding to the same forcing. The dotted line represents a landscape that is not in equilibrium, which could be either because the landscape is experiencing non-uniform uplift, or because it is experiencing transient incision, meaning a change in base level has occurred within the landscape's response time and is still being communicated across the landscape. Glacial erosion erases local relief above the ELA and forms cirques (b), where slope gradient decreases, and can form nunataks, horns, and arêtes at the summit where rock is exposed above the glacial ice with extremely steep (near vertical) slopes. Figure adapted from Robl et al. (2015).

Landscape Morphology and Soil Cover

The topographic legacy of glaciation introduces complexity to the modern understanding of hillslope dynamics, which was developed largely by G.K. Gilbert in the late 19th and early 20th century. Gilbert described a model for soil mantled hillslopes in which the two central forces behind landscape form, soil production and erosion, tend to balance each other in order to maintain a constant soil thickness and a smooth, convex hillslope shape. The rate of soil production is regulated by the thickness of the overlying soil cover, as processes that work to convert rock to soil at depth (including bioturbation,

frost cracking, and chemical weathering reactions) operate rapidly when soil is thin, and are dampened when soil cover is thicker than some optimal thickness (Gilbert, 1877; Ahnert, 1967; Carson and Kirkby, 1972; Heimsath et al., 1997; Anderson, 2002). This concept is represented concisely as a humped soil production function, where soil production rate increases at low soil depths, peaks, and declines toward zero as soil depth continues to increase (e.g., Carson and Kirkby, 1972). This formulation has been supported by numerous studies in continuously soil mantled regions, (e.g. Ahnert 1967, 1976), while soils have been demonstrated to become thinner and less extensive with increasing denudation (Heismath et al., 1997; Furbish and Fagherazzi, 2001). However, mountainous landscapes with discontinuous soil cover present a much more complex story.

Soil production and erosion are not balanced in all landscapes, as evidenced by patchy soils and exposed rock in steep mountainous landscapes (e.g. Heimsath et al., 2012, 2014). As a corollary, the exposure of bare rock is thought to signify that erosion is outpacing soil production. Research has flourished on soil-mantled terrain that conform to the classic model described by Gilbert (1909) where soil is transported primarily by creep, but steep landscapes where bedrock is exposed at the surface are less well understood. It is unclear what mechanisms allow patches of soil to persist in landscapes where landscape-scale erosion likely locally outpaces soil production rates.

At a catchment scale, hillslope gradient and topographic relief have been shown to be positively correlated with erosion rate (Dietrich et al., 1993; Rosenbloom and Anderson, 1994; Montgomery and Brandon, 2002) below some threshold, but at very

high slope gradients the relationship breaks down (e.g. Schmidt and Montgomery, 1995; Montgomery, 2001; Ouimet et al., 2009; DiBiase et al., 2010). Threshold slopes are determined by mountain-scale bedrock strength and are established and maintained by bedrock landsliding (Schmidt and Montgomery, 1995). In these settings stochastic transport events including dry ravel (Gabet, 2003) and deep-seated landslides (Selby, 1993) may remove regolith more rapidly than it is replaced by weathering of underlying rock. Channel processes help to maintain threshold slopes by removing material deposited at the base of slopes at least as rapidly as it is supplied form the above hillslope. In such systems, the relative bedrock and soil exposure would therefore reflect the regional denudation rate and the frequency and distribution of landsliding.

However, patchy soil cover and bedrock outcrops do not always reflect landsliding processes. Instead, the heterogeneity of soil cover may reflect local outpacing of soil production by erosion. Curiously, this local limit of soil production may be specific to each landscape (Dixon and von Blanckenburg, 2012) and may depend partly on rock strength and climate (Pelletier and Rasmussen, 2009). In many mountain systems the emergence of bedrock cover and the soil-bedrock transition is likely gradual and leaves a topographic signature that can be identified with high resolution topography (DiBiase et al., 2012; Milodowski et al., 2015). DiBiase et al. (2012) demonstrated that in bed rock exposure increases strongly with mean slope, and developed the Rock Exposure Index (REI) as a metric for mapping rock exposure based on a defined threshold steepness beyond which soil is not retained on the hillslope. This threshold is reflective of increasing bedrock dominance and signifies the transition from diffusive-like soil

transport processes to landslides (Heimsath et al., 2012). The critical slope for determination of REI changes from one landscape to another, depending on soil characteristics, vegetation, lithology, and climate, but is likely close to 30° (Heimsath et al., 2012; DiBiase et al., 2012), similar to the transition to landslide dominance identified across a variety of mountain ranges; (Burbank, 1996; Montgomery and Brandon, 2002). Milodowski et al. (2015) investigated the soil-mantled to bedrock transition using local variability of surface-normal vectors measured from 1 m resolution airborne LiDAR data as a roughness metric, following algorithms developed by McKean and Roering (2004). They applied surface roughness analysis to two landscapes in California and Idaho, and their results support the idea that the soil-bedrock transition is not abrupt but gradual and spatially heterogeneous. This method complements the REI developed by DiBiase et al. (2014) and is particularly useful in landscapes where rock outcrops at slopes shallower than an inferred threshold. These topographic metrics can be used to characterize the heterogeneity of soil cover in mountainous landscapes and infer changes in local mechanisms controlling hillslope evolution.

Implications of Bedrock Exposure for Chemical Weathering

The exposure of bare rock, discussed above, has important implications for chemical weathering processes. Chemical weathering rate is set by a combination of many factors, including erosion rate (Stallard and Edmond, 1983; Riebe et al., 2001c, 2003, 2004a,b; Green et al., 2006; Yoo et al., 2007; Burke et al., 2009; Dixon et al., 2009b), lithology and rock chemistry (Garrels and Mackenzie, 1971; Meybeck, 1987; Amiotte-Suchet and Probst, 1993; Bluth and Kump, 1994; Edmond et al., 1996), and

moisture availability (Dunne, 1978; Bluth and Kump, 1994; White and Blum, 1995; Dixon et al., 2016a); the relative importance of each of these influences varies with each setting. Physical erosion and chemical weathering are thought to positively feedback: erosion refreshes the supply of weatherable material from below, while weathering reactions loosen rock and make it erodible (Gilbert, 1877; Anderson, 2002), and previous studies have documented a positive correlation between erosion and chemical weathering (e.g., Riebe et al., 2001; Riebe et al., 2004; West et al., 2005; Dixon and von Blanckenburg, 2012). However, increasing erosion rate will not increase chemical weathering rate in all cases. This is because we expect that when erosion rates are very rapid, mineral residence times are reduced, such that the surface weathering reactor has insufficient time to fully alter and deplete weatherable minerals (Gabet, 2007; Ferrier and Kirchner, 2008; Gabet and Mudd, 2009). This distinction allows landscapes to be classified as belonging to one of two types: those where chemical weathering is kinetically limited and those where it is erosion-limited.

In kinetically limited landscapes, chemical erosion rate is decoupled from mineral supply rates, either because of high erosion rates, so that mineral residence times are cut short by being eroded away; or because of dry conditions, where not enough moisture is available for weathering reactions to take place (Rasmussen et al., 2011). In erosion-limited landscapes (also called supply-limited), weathering is limited only by the supply of fresh material, not by the rate of mineral dissolution (Stallard, 1995; West et al., 2005). This could be due to very low erosion rates, which allow the regolith to grow so thick that weathering processes (bioturbation, freeze-thaw, etc.) do not reach fresh rock; or it could

mean that although erosion rates are not particularly low, chemical weathering keeps pace with erosion so that a steady-state condition is maintained (Rasmussen et al., 2011).

The threshold for bedrock emergence may distinguish kinetic versus supply-limited regimes, as erosion begins to outpace soil production (Dixon and von Blanckenburg, 2012). Erosion-limited systems are ubiquitous around the globe, as evidenced by numerous studies (Riebe et al., 2001; Riebe et al., 2004; Dixon and von Blanckenburg, 2012), because erosion rates are slow to moderate at much of Earth's land surface (Dixon and von Blanckenburg, 2012; Willenbring et al., 2013). Some studies have documented kinetically limited settings (Norton and von Blanckenburg, 2010; Rasmussen et al., 2011; Dixon et al., 2012; Dixon et al., 2016b) but further exploration is required to better validate the models that describe kinetic- versus erosion-limitation (i.e., Ferrier and Kirchner, 2008; Gabet and Mudd, 2009; Hilley et al., 2010), and few studies have attempted to explore soil weathering in systems with signifcant bedrock exposure (e.g., Dixon et al., 2012). Furthermore, while previous work has suggested limits to soil cover and regolith production may determine the transition from supply to kinetic limitation (Ferrier and Kirchner, 2008; Dixon and von Blanckenburg, 2012), no work has explicitly tested this relationship. Most of the relevant stuides have instead focused on continuously soil mantled hillslopes (e.g., Riebe et al., 2004; Dixon et al., 2009), since understanding the extent of surface weathering in heterogeneous bedrock dominated landscapes requires quantifying the spatial variabilty of soil, its variable weathered state, and the complex controls on both of these things.

Distingushing when erosion rate is helping or hindering chemical weathering would also help identify where climate may influence these feedbacks. Though generally, warmer and wetter climate conditions facilitate higher weathering rate and intensity, as demonstrated in laboratory experiments (White et al., 1999; White and Brantley, 2003), Dixon et al. (2012) suggest that only when mineral supply is not limiting weathering can moisture and temperature influence chemical weathering rates.

We address the fundamental question of how soil cover, topography, and weathering relate in mountainous settings by comparing the modern soil distribution and chemical weathering extents across a previously glaciated and a nonglaciated mountain range. This work allows us to explore the transition from soil-mantled to rock-dominated hillslopes in detail and at the landscape scale, and provide added insight into how past climate legacies (such as glaciation) influence modern weathering. For this analysis we draw on the legacy left in the northern Rockies by Pleistocene glaciation, which provides an ideal natural laboratory for investigation into the controls on soil-mantled and rocky landscapes.

Study Area

Our work focuses on two mountain ranges, the Bitterroot and Sapphire Mountains, which border the Bitterroot River valley in western Montana (figure 2.2). These two systems provide important contrasts in glaciation history, topography, and soil and rock cover that provide a unique setting to explore feedbacks between climate, morphology, and weathering and erosion processes.

Tectonic History

The Bitterroot River basin, which encompasses both the Bitterroot and Sapphire Mountain Ranges, is a large (7,300 km^2 area) headwater basin of the Columbia River. The two north-south trending ranges of interest are separated by the 500-1500 m thick east-dipping Bitterroot mylonite shear zone. In broad terms, the Bitterroots are composed of granitic plutons belonging to the Bitterroot metamorphic core complex, an exposure of the middle crust of the Cordilleran Orogen. On the east of the shear zone is the Bitterroot Valley and the Sapphire Mountains, which are largely underlain by shallower Cretaceous-Eocene plutons and lower-grade Belt Supergroup strata.

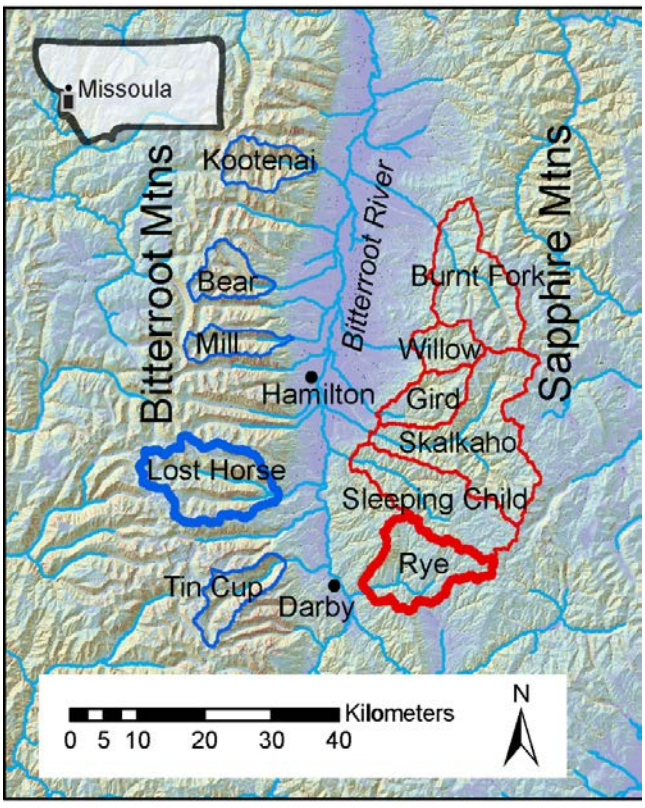

Figure 2.2. Location of the Bitterroot and Sapphire Mountains. Selected catchments for topographic analysis in the Bitterroot Mountains (blue) and Sapphire Mountains (red). All catchments drain to the Bitterroot River which runs through the valley between the two ranges. Lost Horse and Rye Creeks (bold outlines) are our detailed-study catchments.

The Bitterroot Mountains are bounded by the Montana-Idaho border to the west and the Bitterroot Valley to the east, and are comprised of a series of parallel east-draining tributaries, the northernmost of which is Lolo Creek and the southernmost the West Fork of the Bitterroot River. The Bitterroot lobe, part of the Idaho batholith, has a dome extending about 100 km north-south called the Bitterroot Dome at its eastern edge (Chase and Talbot, 1973). Early descriptions of bedrock geology in the Bitterroot Valley were made by Langton (1935), Ross (1950), and Pardee (1950). The Bitterroot Mountains are underlain by the Idaho batholith, a metamorphic core complex made up of metasedimentary rocks in the north and granitic rocks to the south (Lonn and Berg, 1996; Lewis, 1998). The quartz monzonite that makes up most of the Bitterroot Mountains displays a mineralogic composition primarily comprising quartz, orthoclase, oligoclase, and biotite, with a coarse-grained to porphyritic texture (Ross 1950). The Bitterroot Dome slopes eastward, and the Bitterroot Valley to the east controls the base level of the westward-flowing creeks in the east-west-trending valleys of the Bitterroot Range.

Immediately east of the Bitterroot Dome is the Sapphire tectonic block, a 15 km thick, 100 km long, 70 km wide tectonic block of low-grade late Precambrian Belt sedimentary rocks twice the size of Rhode Island (Hyndman, 1980). The Sapphire block is composed of Proterozoic Belt Supergroup rocks (Naylor, 2006) including greenschist and amphibolite facies as well as granitic plutons scattered throughout, more densely toward the southern end of the block (Hyndman, 1980). During the later stages of consolidation of the Idaho batholith about 75-80 Ma, the Sapphire block became detached from the roof of the Idaho batholith and moved 60 km eastward; the removal of

this weight caused the isostatic uplift of the Bitterroot Dome. Eastward movement of the Sapphire block over the Bitterroot dome is evidenced by the mylonitic shear zone that separate the Sapphire block from the Bitterroot Dome, in addition to trends in foliations, mineral streaking, and slickenslide lineations that cover the whole of the Bitterroot dome, not just one flank, and fit characteristics of many other metamorphic core complexes (such as the Shuswap metamorphic complex in British Columbia [Hyndman, 1968] and the northeastern Nevada [Misch and Hazzard, 1962; Armstrong and Hansen, 1966]) (Hyndman et al., 1980).

The Sapphire Mountains formed from the Sapphire Block, which "bulldozed" the Flint Creek Range ahead of it as it went (Hyndman, 1980). The mylonite was exposed by the Early Miocene time, according to fission-track dating along the lower easternmost extent of the Bitterroot Front (Foster and Raza, 2002). Some units of the Prichard, Ravalli, Wallace or Helena Formations, and much of the Missoula group are exposed at the surface of the Sapphire.

The ranges bordering the Bitterroot Valley are thought to be controlled by the similar modern tectonic forcings, as the massive granite assemblage underlying them is free of structural or lithologic variations (Lonn and Berg, 1996; Lewis, 1998). However, the modern tectonic activity of the region is not well constrained. The study area has been shown to have negligible ongoing rock uplift rates (Foster et al., 2008), while at the same time late Quaternary surface ruptures have been revealed along a fault parallel to the Bitterroot Front by recent ALSM data (Stickney, 2014).

Climate History

The Bitterroot Mountains experienced multiple periods of glaciation during the Pleistocene, but evidence is mixed as to how strongly the glaciers affected various parts of the range. Alden (1953) found evidence for three major glaciations in the Bitterroot Mountains correlating to Early Pleistocene, Illinoian (or Early Wisconsin), and Wisconsin ages. This was based on glacial deposits at the mouths of several canyons, and on a Pleistocene chronology Alden had already developed from work in eastern Montana (Alden, 1932). Weber (1972) built on this work by mapping three drift sequences, which he refers to as the Judd Drift (pre-Wisconsin), Charlos Drift (early Wisconsin), and Lost Horse Drift (late Wisconsin). These approximate ages are based on granite-weathering ratios, topographic position, soil development, and correlations with Glacial Lake Missoula lake stands. The Judd glaciation seems to have been the most extensive, as Judd Drift is present beyond drift of other sequences, and because Judd Drift mapped between Lost Horse and Rock Creeks indicates that the glaciers from these two creeks merged beyond the canyon mouths. Weber (1972) mapped six end moraines composed of Lost Horse Drift outside the mouth of Roaring Lion Canyon, suggesting there were at least six glacial advances within the most recent of the three main glaciations. He also noted that evidence of glaciation increases to the south because four canyons (Carlton, One Horse, Bass, and Kootenai Creeks) toward the north lacked the signature U-shape of glaciation and terminal moraine. However, reconstructions of late Pleistocene weather patterns suggest that LGM precipitation should have been similar across the Bitterroot Range with no redistribution of snow with latitude, due to the dominating influence of anticyclonic easterlies (Kutzbach and Ruddiman, 1993; Hostetler and Clark, 1997). Unlike glaciers in

nearby mountain ranges in Idaho and Montana, the glaciers in our study area on the east side of the Bitterroot Mountains escaped the containment of their valleys, growing to >10km long and leaving moraines on the axial valley floor (Foster et al., 2008).

The Bitterroots receive more modern precipitation than the Sapphires. Weather systems traveling eastward from the Pacific Ocean deposit most of their moisture on the western face of the Bitterroots, outside our study area; in fact, the western face receives nearly three times as much winter precipitation as the eastern side of the range where our research is focused (Whitlock and Bartlein, 1993). Within our study area, the upper portions of the Bitterroots receive approximately 180 cm/year annually, ranging to ~100 cm in the lower parts of the mountains. The Bitterroot Valley receives 20-40 cm/year on average, and the Sapphires tend to receive 30 cm annually on average, with a maximum of 130 cm y^{-1} (PRISM, 2014 30-year normals).

Topography and Geomorphology of the Bitterroot and Sapphire Mountains

The Bitterroots and Sapphire Mountains display key differences in morphology and erosional processes. The Bitterroots have observably steeper slopes and more exposed rock, whereas the Sapphires display less steep slope gradients and a more consistent soil mantle. Debris flows have been investigated as the primary mode of sediment transport in the Sapphires (Hyde et al., 2014; Martinez-Murillo et al., 2016). Both ranges have experienced wildfires in recent decades. In the Sapphires increasing fire severity (a measure of disturbance or removal of vegetation by wildfire) has been shown to reduce the threshold for channel incision, i.e. the location of channel heads where debris flows start following fire or intense precipitation (Hyde et al., 2014). There was a

particularly large series of wildfires in 2000 that produced post-fire debris flows (Parrett et al., 2004; Hoffman and Gabet, 2007; Gabet and Bookter, 2008; Hyde et al., 2014).

The Bitterroots have been selected for geomorphologic studies in the past because of their classically post-glacial topography. Naylor and Gabet (2007) posit that the east-west trending valleys and ridges carved by glaciers in the Bitterroots are asymmetric as a result of stronger insolation on the south-facing slopes and resulting differences in glacial erosion. They used field mapping and analysis of DEMs and aerial photography to compare north- and south-facing slopes in the Bitterroot Mountains in order to compare differing erosional regimes: due to unequal solar insolation, north-facing sides of the valleys were glaciated, while south-facing slopes were not, allowing the formation of larger cirque glaciers on north-facing slopes (Beaty, 1962; Evans and Cox, 2005). This is shown through the asymmetric ridges, as ridge-to-valley distances on north-facing slopes are ~1.5x that of south-facing slopes. Glaciated slopes are found to be less steep than non-glaciated slopes (portions of south-facing slopes that are judged to be glaciated are excluded from this analysis). This is despite equal precipitation rates and no significant redistribution of snow latitudinally, according to late Pleistocene weather reconstructions that show that anticyclonic easterlies were dominant in the northwest (Kutzbach and Ruddiman, 1993; Hostetler and Clark, 1997). The differences are also not due to lithology, as most of the range is underlain by a massive granite assemblage without discrete structural features (Lonn and Berg, 1996; Lewis, 1998). Using a spline surface fit across ridgelines to approximate the volume of material eroded (e.g. Brocklehurst and Whipple 2006), Naylor and Gabet (2007) found that glaciers have removed almost twice

as much rock as nonglacial processes. Part of this is through vertical incision but the dominant impact of glaciers is lateral erosion by headwall retreat. Naylor and Gabet (2007) concluded that glacial processes operating on north-facing slopes are more efficient at headward erosion than the nonglacial processes operating on south-facing slopes, causing ridgelines to be pushed southward. This is in accordance with the findings of Brocklehurst and Whipple (2002, 2006) that glacial erosion exceeds fluvial erosion, principally through horizontal headwall incision, based on analysis of fluvial and glacial longitudinal profiles.

Approach and Methods

To address the question of how morphology and climate may control soil formation, weathering, and erosion, our study combines topographic analysis, laboratory-based measurements of soil chemistry, and field-based analysis of soil cover and thickness to determine how soil formation varies across the study region. We explore the morphology of the previously glaciated Bitterroot Mountains and the unglaciated Sapphire Mountains by analyzing topography across eleven study catchments (figure 2.2). We quantify this glacial legacy using a variety of established topographic metrics, and compare topographic and morphologic variables using two-sample t-tests assuming unequal variances. We select two representative detailed-study catchments, Rye Creek (Sapphire Mountains) and Lost Horse Creek (Bitterroot Mountains) for further analysis. These catchments are underlain by the same unit of granodiorite bedrock and have similar elevation ranges, thus helping to isolate the role of catchment morphology on soil

formation. We measure soil distribution and chemical weathering extent across these two catchments by quantifying soil cover and thickness, and through geochemical analyses of soil and rock samples. In order to compare variation in topography and climate, for the purposes of this study we hold lithology constant between our two detail-study catchments and include lithologic heterogeneity in our broader analysis of the Sapphires (figure 2.3).

In our conceptualization, regolith is composed of both soil and saprolite following Dixon et al. (2009b). Here, soil is defined as the surface mantle of mobile material, while saprolite is the underlying weathered material still in place (physically immobile). Chemical weathering (i.e. chemical mass loss by primary mineral dissolution) and physical erosion together constitute total denudation. In the conceptual framework we adopt, chemical alteration and dissolution of bedrock at depth (possibly millimeters or tens of meters below the surface) produce saprolite, which retains its relict rock structure even as weatherable constituents are removed. Saprolite is then incorporated into the mobile soil column by mechanisms such as tree throw, bioturbation, and frost cracking, which physically disrupt underlying material, as well as further enhancing chemical weathering. In this way, a single mineral grain that starts out as part of the underlying parent rock is exhumed through the regolith column, and evolves through chemical processes within saprolite at depth, and then by chemical and physical processes in the soil profile as it is exhumed to the surface.

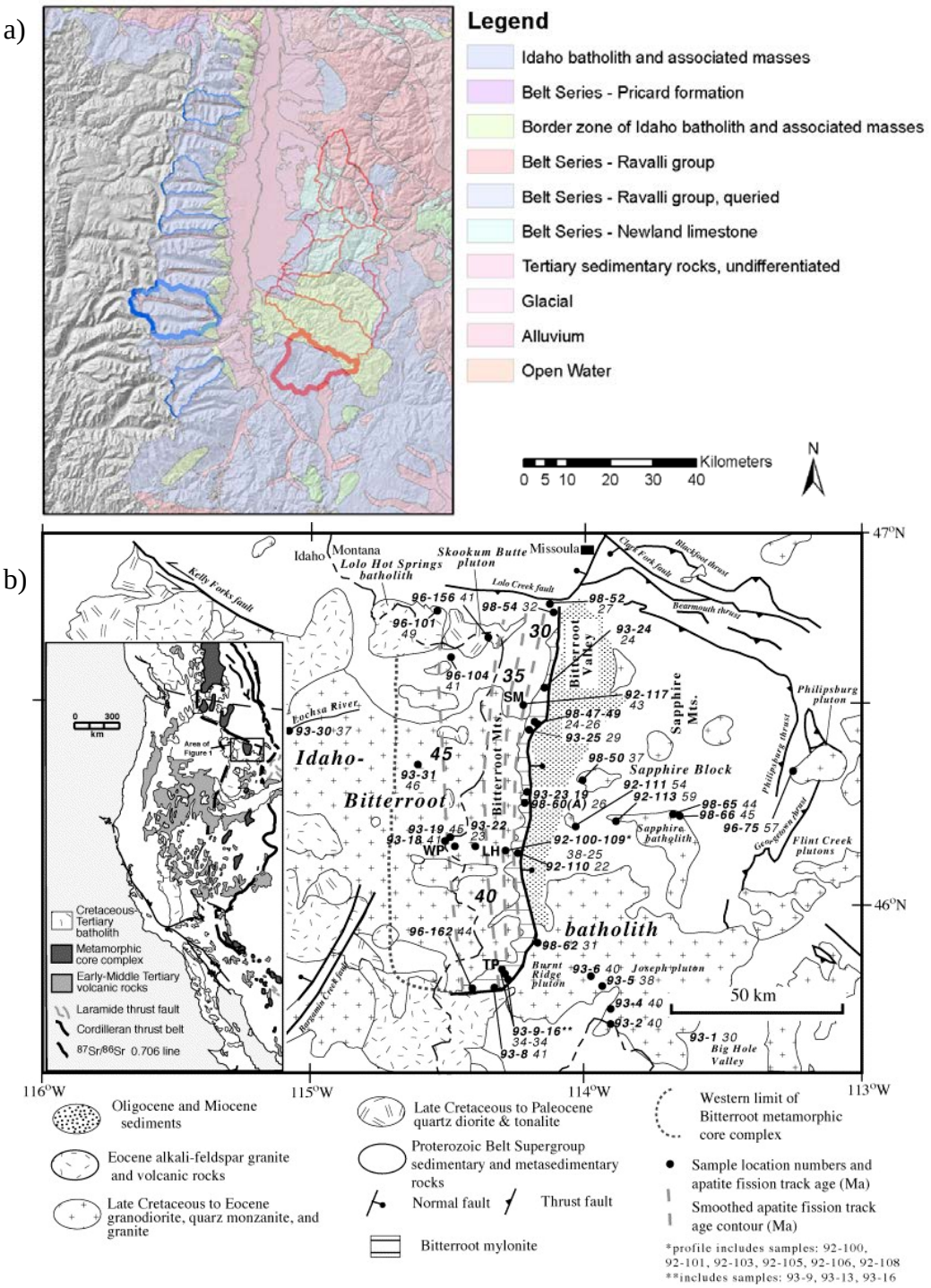

Figure 2.3. Lithologic (a) and geologic (b) maps of study site. Rye Creek (red bold outline in (a)) is almost entirely underlain by the same lithology as the Bitterroots, while other Sapphire catchments (red thin lines) show much more lithologic heterogeneity. a) from Montana Bureau of Mines and Geology 1:100k Seamless Geodatabase. b) from Foster and Raza (2002).

Topographic Analysis

We employ several metrics to explore the characteristic topography of fluvial and glacial landscapes. Our analysis relies on the USGS National Elevation Dataset 1/3 arc-second (approx. 10m) digital elevation models (DEMs). Five catchments are chosen to represent the Bitterroots and six to represent the Sapphires (figure 2.2). Terrain attributes, stream networks, and catchment extents were extracted using Spatial Analyst tools in ArcGIS. Contributing area was generated using the D-infinity algorithm from the TauDEM toolset (Tarboton, 1997). Detailed catchment data was additionally processed in Matlab to derive topographic statistics.

Hypsometry, or the frequency distribution of elevations in a given area, can be used to identify glacial versus fluvial forces acting on a landscape and to assess the evolutionary stage of a fluvial landscape (Strahler, 1952; Schumm, 1956). The hypsometric maximum, or a local maximum in the frequency distribution of elevation, represents the concentration of surface elevations within a narrow altitude interval due to some dynamic process, which may reflect tectonic, erosional, or depositional drivers (Egholm et al., 2009). We compare the hypsometry of individual catchments in the Bitterroots and Sapphires, and test correlations between the hypsometric peaks of five Bitterroot catchments to the estimated Bitterroot LGM snowline to identify the signature of the glacial buzzsaw. We measure hypsometry at the catchment scale rather than entire mountain ranges because regional-scale studies lose sight of local details that may be crucially important, such as hanging valleys (Brocklehurst and Whipple, 2004).

In addition to the frequency distribution of elevation, we examine the frequency distribution of slope in each of the 11 study catchments and regress the distribution of

slope with elevation in each catchment. Higher average slopes and the occurrence of high slopes at lower elevations have been interpreted as reflecting the glacial topographic signature (e.g., Dixon et al., 2016a). The 10 m resolution elevation datasets of each catchment were processed using the "histFreq" function in MATLAB software to create elevation and slope distribution frequency plots. We then explore the distribution of local slopes with catchment elevation by segmenting each catchment into 50 m contour elevation bins, remove values where slope equals zero, and quantifying mean and standard deviation values for slope angles within each elevation bin (following Dixon et al., 2016a).

A second tool related to hypsometry is the hypsometric integral (HI). This quantity distills the elevation frequency distribution into a single number relating the percentage of total relief to the cumulative percent of area, such that

$$\mathrm{HI} = \frac{(H_{mean} - H_{min})}{(H_{max} - H_{min})}, \qquad \text{(Equation 1)}$$

following Brocklehurst and Whipple (2004), where H is elevation. HI is used to describe the evolutionary stage of landforms (Strahler, 1952; Schumm, 1956), and has been found to be inversely correlated with total relief, drainage density, and channel gradients (Strahler, 1952). We calculate the HI of our study catchments by converting the 10 m resolution elevation rasters of all 11 catchments to points, imported them into MATLAB as arrays, and used MATLAB min, max, and mean functions on each array to follow the formula in equation 1. We additionally determine HI values at a landscape scale for the Sapphires and Bitterroots, by combining the elevation arrays of each catchment into one

Bitterroot array and one Sapphire array and calculating the min, max, and mean elevations of the combined data.

Field Methods and Sampling

All field work was conducted in the summer and fall of 2015 and 2016 and included soil sampling for chemical weathering analysis, field measurement of soil thickness, extent, and rocky cover, as well as the digging of approximately 6 soil pits for a complimentary characterization of soil attributes such as color, rockiness, and horizon depth. Because our definitions of regolith and soil are not grain size dependent, we follow Dixon et al. (2009a) by sampling bulk soils for elemental analyses, and do not sieve out coarse fractions >2mm. We deliberately include the coarse fraction in order to get an accurate snapshot of the weathered regolith (which includes variable size fractions), rather than choosing the most highly weathered (fine) material, which would overestimate the extent of weathering.

We measured the persistence and thickness of soil cover using field data across two catchments: Lost Horse Creek in the Bitterroot Mountains and Rye Creek in the Sapphire Mountains. Soil thickness was measured by hand auger to the depth of refusal at 387 points across these two catchments. A calibration of soil thickness measurement by augering 4 points within 1 m of each other show 64 ± 6.8 cm and 43.3 ± 8.4 cm in Rye, and 10.3 ± 3.9 cm and 31.25 ± 5.2 cm in Lost Horse Creek. Coefficients of variation are 15% and 27% in Rye and Lost Horse respectively, based on standard deviations of soil thickness. Because surface regolith cover included many coarse rock fragments, we estimated the spatial extent of soil cover at each sampling location by establishing a

3x3m grid at each observation site. Excluding exposed bedrock and rock fragments >5cm in length, we estimate the effective % soil cover within each of 9 squares of the grid (each 1 m^2; figure 2.4), and average them to get a single number for each sample location. We assume that the amount of rock exposed at the surface is reflective of rock fragments distributed throughout the soil column, or in other words that surface exposure reflects variability at depth. We make this assumption in order to better estimate the true amount of weathering that occurs as material is exhumed.

The 3x3m grid was also used to collect paired soil and rock samples across the two study catchments. Our rock samples are collected from the surface, assuming that their chemical composition is reflective of the underlying parent material from which surface soils were formed. We sampled the top 10 cm of soil from a point at the center of each 1x1m square within the grid (9 points), and approximately 5-10 rock samples were collected from the surface within 10 m of the grid to represent an average parent material from which its paired soil was formed. By including fragments from a variety of boulders rather than just one in a single sample, we hope to minimize the effect that one anomalous sample might have on our estimate of rock composition. To further prevent sampling bias, these rock fragments were crushed to <1 cm and powdered before subsampling for XRF analysis. For a more detailed explanation of sampling protocol, please see appendix H.

Figure 2.4. String grid used for estimating soil cover at each sample location. Soil cover excluding fragments <5 cm was estimated in each of 9 1x1 m squares, then averages and standard error calculated for each sample site. For example, at this sample site soil cover was 100%.

Analysis of Land Cover Distribution

Field measurements were restricted to low-elevation, low-slope hillslopes and valley bottoms, but in the Bitterroot Mountains it is the high-elevation, steep portions of hillslope and the ridges that separate valleys where soil is unable to persist and bare rock is exposed. Therefore, our sampling results in an unavoidable bias towards low-gradient portions of the landscape, despite our interest in landscape-scale patterns of soil weathering and cover. In order to incorporate these inaccessible domains into our landscape-scale weathering estimates, we adjust the measurements described above by remotely sensed estimate of what portion of Lost Horse Creek is soil-mantled versus rock-dominated. We assume that rock-dominated portions of the landscape are

undergoing minimal weathering, and multiply the rock-adjusted chemical depletion fraction (RACDF) of Lost Horse Creek by the percent area that is soil-mantled to produce a landscape-average RACDF. We make this landscape-scale adjustment only in postglacial Lost Horse Creek, because while Rye Creek does have some rock locally outcropping, it does not have significant rock-dominated areas (figure 1.2).

Our estimate of percent soil cover is based on the National Land Cover Database dataset (Homer et al., 2011) created by the Multi-Resolution Land Characteristics (MRLC) Consortium that characterizes land cover at 30 m resolution based primarily on a decision-tree classification of c. 2011 Landsat satellite data. We first selected NLCD categories as proxies of soil cover by comparing NLCD rasters by eye with aerial imagery base maps. The category “evergreen forest” tended to correspond to soil mantled topography, likely reflecting some soil must be present for a forest to grow. Although there is a “barren land (rock/sand/clay)” category defined by NLCD, it grossly underestimates the amount of rock in Lost Horse Creek. Instead, initial assessment suggested that an amalgamation of four NLCD categories (“perennial ice/snow”, “barren land (rock/sand/clay)”, “shrub/scrub”, and “grassland/herbaceous”) better characterizes rock cover.

To validate our use of land cover as a proxy for soil cover, we use the image analysis platform ImageJ to estimate rock cover based on the brightness of a greyscale image from Google Earth. We selected a brightness threshold by zooming in on the transition from soil to rock cover at four randomly selected portions of Lost Horse Creek of ~1 km by 1 km. We find that a minimum brightness threshold of 101 is best for a

conservative estimate of rock cover. We note that this estimate is subjective, and could always benefit from further calibration. We compare the rock and soil estimates from NLCD and ImageJ and find that while both find a similar amount of the landscape to be soil-mantled overall (59% by NLCD; 70% by ImageJ), they disagree on the value of 30% of pixels (figure 2.5). Mostly the disagreement occurs at the transition between hillslope and ridge, where vegetative cover is patchy, and on avalanche chutes which appear as bright strips on the hillslope (figure 2.5). ImageJ tends to count avalanche chutes as soil, while NLCD sometimes identifies them as rock. Additionally, ImageJ identifies parts of the rocky ridge that are in shadow as soil, raising its estimate of soil cover. (In defining a brightness threshold for rock cover in ImageJ, we chose a minimum of 101 brightness intensity, which we judge to be erring on the side of underestimating rock cover. To err on the side of overestimating rock cover, we suggest a minimum brightness intensity threshold of 68, in which case Lost Horse Creek would be identified as 27% rock and 73% soil. Under a threshold of 68, more scree slopes would be included in rock cover; however, the problem of shadows cast by cliffs being counted as soil cover persists. We experimented with several methods for validating and calibrating estimations of soil and rock cover using NLCD, including marking individual rocks by hand in Google Earth as described in Appendix A. Though our validation is not perfect, we hope this contribution will encourage more experimentation towards characterization of landscape heterogeneity.

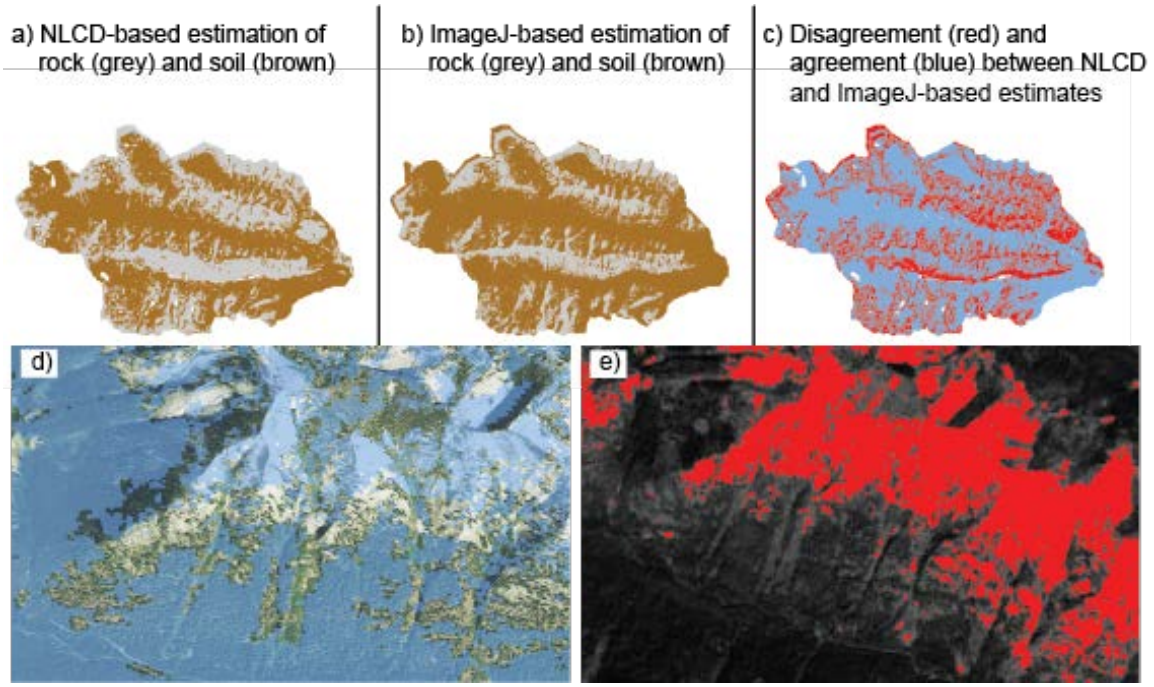

Figure 2.5. We use two different methods to estimate soil cover in Lost Horse Creek. (a) Vegetation classifications from The National Land Cover Database provide landcover at a 30 m resolution. (b) We additionally used Google Earth Imagery at a higher resolution and separated the image into soil and rock covered regions using a brightness threshold in ImageJ software (minimum brightness intensity for rock cover = 101). (c) While the two methods find similar values for total area mantled by soil (59% and 70% respectively), they disagree on the value of 30% of individual pixels, shown in red. (d) In this zoomed-in aerial photo of a Lost Horse Creek hillslope, ridge, and valley, areas where NLCD and ImageJ estimates of soil v. rock cover agree are shown in blue. Areas where they disagree have no color. Areas where they tend to disagree are avalanche chutes and the transition between soil and rock dominance where vegetation is thin and patchy. (e) The same area is shown in greyscale for ImageJ analysis, with rock cover colored red. The avalanche chutes are identified in this classification as soil-covered (non-red).

Analysis of Chemical Weathering Extent

Our geochemical analysis aims to quantify chemical weathering across multiple spatial scales and geomorphic settings. To do so, we target sample sites at a variety of topographic positions, including hillslopes and valley bottoms at a variety of slope gradients and aspects. We analyzed the bulk elemental composition of 118 soil and rock

surface samples using X-ray fluorescence spectrometry, performed by ALS Global in Reno, NV. Bulk samples were completely pulverized to <75 um. Concentrations of trace elements such as zirconium were measured by pressed pellet wavelength dispersive XRF. Major oxides were measured on a fused disk of sample mixed with a lithium borate flux. Molar concentrations were calculated from oxide percentages and all concentrations were ash-corrected to corrected for loss on ignition.

We quantify the degree of chemical weathering using calculations based on a specific refractory element (e.g., Ti). Following Riebe et al. (2001), we calculate a chemical depletion fraction (CDF), which compares the relative enrichment of an inert element in soils compared to their parent rock:

$$\text{CDF} = 1 - \left(\frac{Ti_{rock}}{Ti_{soil}}\right) . \qquad \text{(Equation 2)}$$

Here, we use titanium as the index element, assuming no chemical mobility, and Ti_{soil} and Ti_{rock} are titanium weight percent concentrations in soil and unweathered parent material, respectively. We also calculate losses of major elements (e.g., sodium, magnesium, potassium, and calcium). The element-specific index of mass loss is calculated as:

$$\tau_i = \left(\frac{i_{soil} * Ti_{rock}}{i_{rock} * Ti_{soil}}\right) - 1 . \qquad \text{(Equation 3)}$$

Here, *i* refers to the concentration of an element of interest (e.g., sodium). Values of $\tau > 0$ represent fractional mass gain in soil relative to its parent material and $\tau < 0$ represent fractional mass loss (Muir and Logan, 1982). In this analysis we assume 1) soils are derived only from underlying bedrock, and that inputs from dust or other external sources are negligible; 2) boulders on the surface have similar composition to underlying

bedrock; and 3) rock and soil contain an immobile element (Ti) that is effectively inert to chemical weathering reactions.

Several samples had anomalous Ti concentrations relative to their local pairs or regional counterparts. For example, in Rye Creek a handful of rock samples from one location had Ti values that were far outside the range of the others, and in some cases higher than their companion soil Ti value (figure 2.6). For these outlier samples, CDF was calculated using a composite parent material Ti value instead of the outlying value. This composite value was calculated by averaging Ti values of all Rye rock samples. By replacing outlying parent material values with a composite value, we assume that anomalous rock compositions result from local rock composition heterogeneity, while soils integrate across landscape rock compositions.

We develop a new "rock-adjusted" metric to account for rock fragments that exist within soil-mantled portions of the landscape. Field observations from soil pits suggest that rock fragments are mixed into the soil column as well as at the surface. In order to account for rock fragments within soil-mantled portions of the landscape, we estimate the percent soil cover at a sample site and use it to adjust our CDF and tau values, assuming that rock distribution at the surface is reflective of variability at depth. We multiply the mass transfer coefficient of a specific element or CDF by the percent soil cover estimated at the sample site using the string grid and term this the rock-adjusted mass transfer coefficient (RAτ) or rock-adjusted CDF (RACDF) value. This rock-adjusted measurement helps to quantify the weathering variability in heterogeneous and mountainous terrain by accounting for material that may travel up the soil column to the

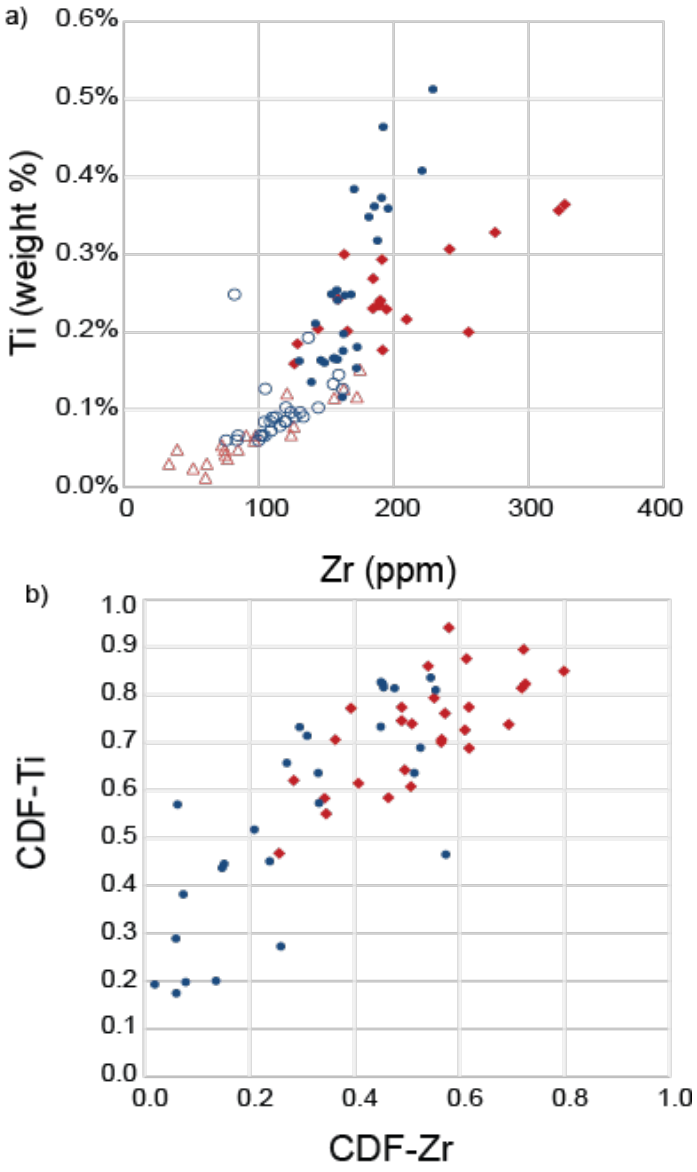

Figure 2.6. Comparison of titanium and zirconium for use as immobile element in geochemistry analysis .a)Ti and Zr concentrations of soil and rock samples: red = Sapphires; blue = Bitterroots; open symbols = rock samples; closed symbols = soil samples. Both zirconium and titanium were considered to serve as the immobile element in calculations of CDF and mass transfer coefficients. Both are present at higher concentrations in the soil than in the parent material, indicating that they are indeed remaining immobile as other elements are weathered away. However, titanium was selected because it better reflects a weathering curve rather than variations in bedrock. b) Comparison of CDF calculated with Zr and Ti. Again, red = Sapphires; blue = Bitterroots. In the Sapphires, samples whose rock samples lie outside the norm are replaced with a composite rock value averaged from all the non-outlier rock samples.

surface without getting broken down into fine soil; however, it still only applies to largely regolith-mantled portions of these systems.

Results

Topographic Variability Across Study Catchments

The Bitterroots and Sapphires exhibit several quantitative differences in morphology. Elevation distributions (i.e., hypsometry) show that the five Bitterroot catchments have similar elevation ranges, between 1,200-2,800 m, and have high mean and modal elevations (figure 2.7). Elevation distribution of Lost Horse Creek peaks at approximately 2,200 m, and in all the Bitterroot catchments we analyzed the hypsometric maximum is at roughly 2,200-2,300 m. Sapphire catchments exhibit greater variability in hypsometry (figure 2.7). For example, Skalkaho basin displays higher mean elevations than surrounding catchments, with similar hypsometries to those of the Bitterroot catchments, and a hypsometric maximum of ~2,000 m. Gird, Willow, and Burnt Fork hypsometries display greater variability in elevations, with less prominent modal elevations.

Slope gradients of the previously glaciated Bitterroot catchments tend to be steeper compared to the Sapphires (27.5° ±0.01 and 20.9° ±0.01 respectively; mean ± standard error based on analysis of ~5.4 and 11.6 million pixels across catchments in the respective ranges). Our detail-study catchment of Lost Horse Creek displays the highest proportion of low slopes (<25°) of the 5 Bitterroot catchments we analyzed (figure 2.7, table 2.1). Slope gradients of the unglaciated Sapphire catchments are generally normally

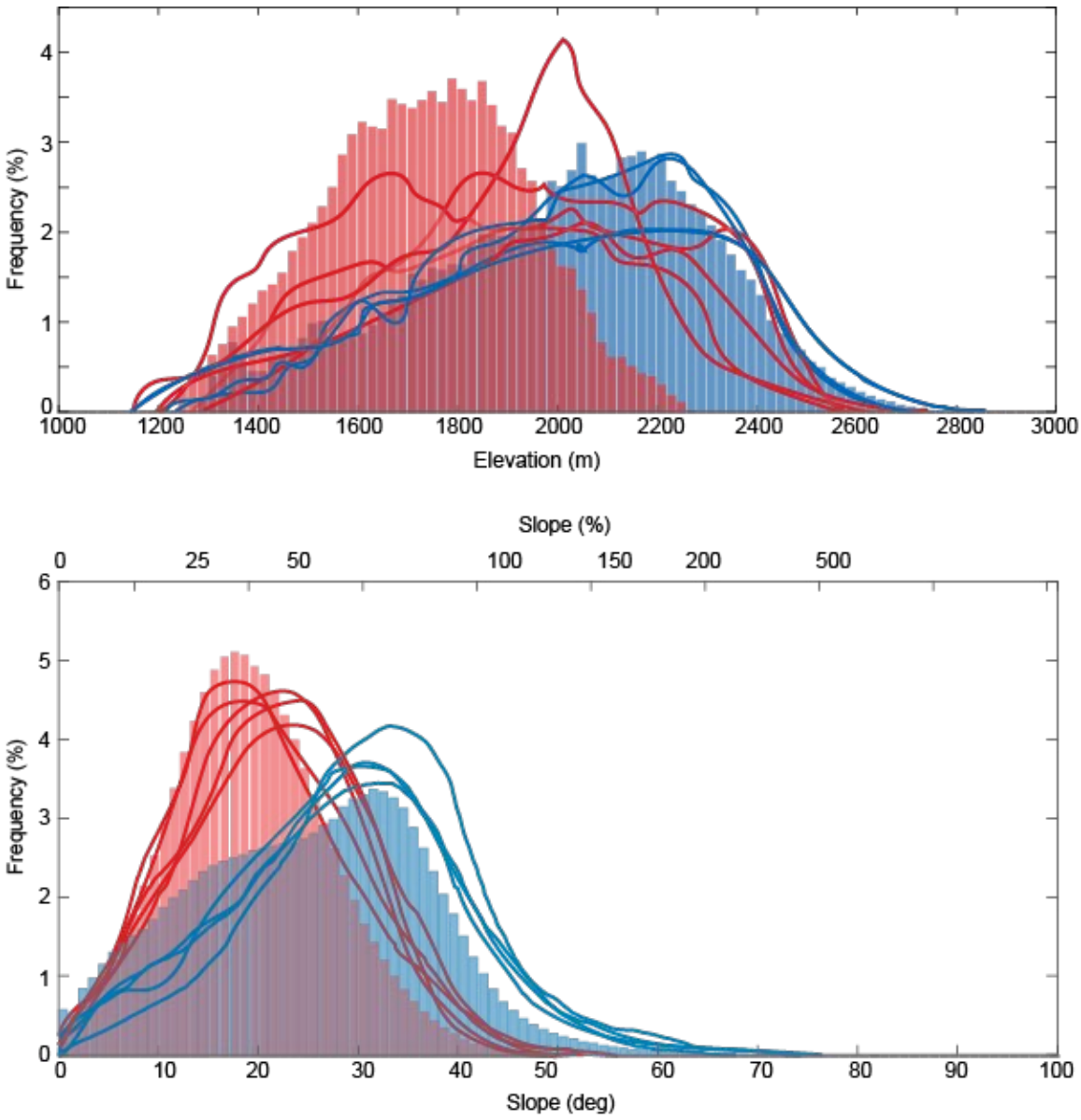

Figure 2.7. Elevation (top) and slope (bottom) distributions of eleven catchments in the Bitterroots (blue) and Sapphires (red). The shaded blue and red curves represent Lost Horse Creek and Rye Creek respectively. The elevation distributions (hypsometries) of Bitterroot catchments are generally similar, and have high modal elevations ~2300 m. Sapphire catchments exhibit greater variation in elevation distribution, with no clear general trend. Slope distributions (bottom panel) generally show similarities between catchments of each range, and Bitterroot catchments tend to have steeper slopes than those of the Sapphires.

distributed about mean slopes of ~20° (figure 2.7 and 2.8, table 2.1). Unlike frequency

distributions, hypsometric integral (HI) values are similar for all 11 catchments, making no clear distinction between Bitterroots and Sapphires (figure 2.9, table 2.2).

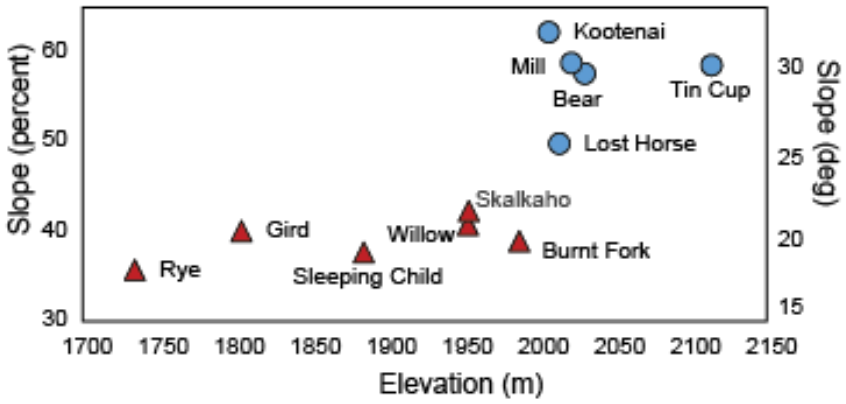

Figure 2.8. Average slope and elevation for 5 Bitterroot (blue circles) and 6 Sapphire catchments (red triangles). Bitteroot catchments tend to cluster in slope-elevation space, having have roughly similar basin average slope and elevation values. Sapphire catchments have similar mean slopes but span a wide range of mean elevations. The Bitterroot catchments are higher elevation than the Sapphire catchments (2033 ± 0.13, n = 5.4 Million pixels and 1900 ± 0.08, n = 11.6 Million pixels respectively).

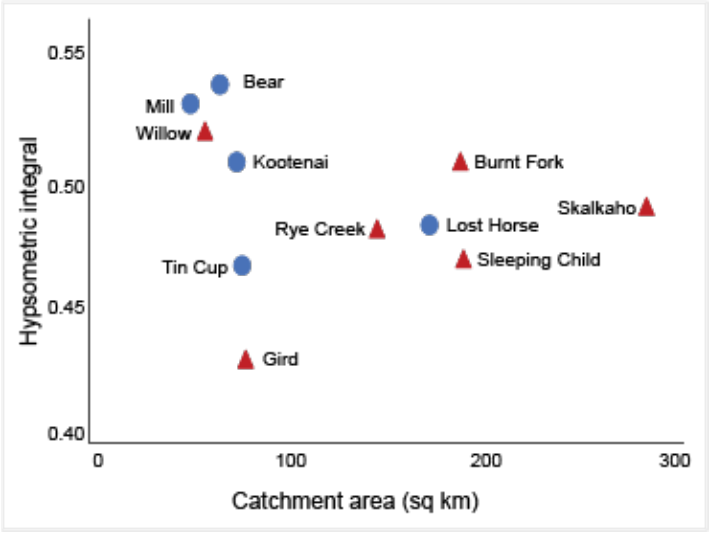

Figure 2.9. Hypsometric integral and catchment area of 11 study catchments shows no clear distinction between the Bitterroots (blue circles) and Sapphires (red triangles). Although previous studies have identified the hypsometric integral as a possible measure of the extent of glaciation on a landscape (Brocklehurst and Whipple, 2004), similar HI values in both ranges suggest that HI is not a good indicator of glacial modification at our study site. This is in keeping with results from the Alps that showed that very different valley geometries can result in similar HI values (Sternai et al., 2011).

Bitterroots	Catchment area (sq km)	Mean elevation (m)		std err	Mean slope (deg)		std err
Lost Horse	**171.8**	**2014**	**±**	**0.2**	**25**	**±**	**0.02**
Kootenai	74.5	2007	±	0.4	31	±	0.03
Bear	66.1	2030	±	0.3	28	±	0.03
Mill	51.2	2021	±	0.4	29	±	0.04
Tin Cup	77.2	2114	±	0.3	29	±	0.03
BITTERROOT AVERAGE	**440.7**	**2033**	**±**	**0.1**	**28**	**±**	**0.01**

Sapphires	Catchment area (sq km)	Mean elevation (m)		std err	Mean slope (deg)		std err
Rye	**159.9**	**1734**	**±**	**0.1**	**19**	**±**	**0.01**
Burnt Fork	187.3	1987	±	0.2	21	±	0.01
Willow	58.5	1953	±	0.4	22	±	0.03
Gird	79.0	1804	±	0.3	21	±	0.02
Skalkaho	281.2	1954	±	0.2	22	±	0.01
Sleeping Child	188.9	1885	±	0.2	20	±	0.01
SAPPHIRE AVERAGE	**940.2**	**1900**	**±**	**0.1**	**21**	**±**	**0.01**

Table 2.1. Mean elevations and slopes with standard error of study catchments in the Bitterroots and Sapphires. Catchments in the Bitterroots tend to have higher mean slopes and mean elevations than those in the Sapphires.

Bitterroot Catchments (listed north to south)	Hypsometric integral	Sapphire Catchments (listed north to south)	Hypsometric integral
Kootenai	0.506	Burnt Fork	0.506
Bear	0.535	Willow	0.518
Mill	0.528	Gird	0.432
Lost Horse	**0.482**	Skalkaho	0.489
Tin Cup	0.467	Sleeping Child	0.470
		Rye Creek	**0.481**
BITTERROOT AVERAGE	**0.504**	**SAPPHIRE AVERAGE**	**0.483**

Table 2.2. Hypsometric integrals of 11 study catchments show similar values between Bitterroots and Sapphires, and values vary similarly from north to south in both mountain ranges.

We also find noticeable differences in how slopes are distributed with elevation across our study catchments (figure 2.10). In previously glaciated catchments there is a distinctive relationship between slope and elevation, whereas patterns in nonglaciated catchments are more variable. The Bitterroot catchments all generally show a similar, with increasing slopes at high elevations, and mean slopes greater than an inferred threshold of 35° in the uppermost portion of the basin. This pattern is the least evident in Bear Creek where high elevation portions of the catchment have lower mean gradients.

The glacially sculpted catchments also show steep slopes at an elevation range below the mean, ~1,400–2,000 m. The two largest Sapphire catchments, Skalkaho and Sleeping Child, increase in slope gradient at higher elevations similar to the Bitterroot catchments. The other four (Burnt Fork, Willow, Gird, and Rye) display a humped shape, slopes first increasing in steepness and then decreasing. (Skalkaho is much larger than the other Sapphire catchments; Sleeping Child is second-largest, with Burnt Fork Creek a close third.)

Figure 2.10. (next page) Basin slopes binned by elevation. Bitterroot and Sapphire catchments are shown in the left and right columns, respectively. Elevation is binned at 50 m contours, and catchment slopes are averaged within each bin, excluding values where slope equals zero. Error bars show standard deviation. The dotted horizontal line at 35° (90%) slope represents the estimated threshold slope based on aerial photos (see Appendix A); however, NLCD data suggests a transition occurs at 25° (~46%). The LGM ELA in the Bitterroots is estimated at ~2,400 m (Foster, 2008). Lost Horse Creek slope-elevation conforms better than the other Bitterroot catchments to the idealized glaciated slope-elevation curve (figure 2.1). Skalkaho and Sleeping Child also display similar characteristics to the idealized glaciated slope-elevation curve. Sapphire catchments may show some rough similarity to the idealized curve of a fluvial system in disequilibrium (figure 2.1).

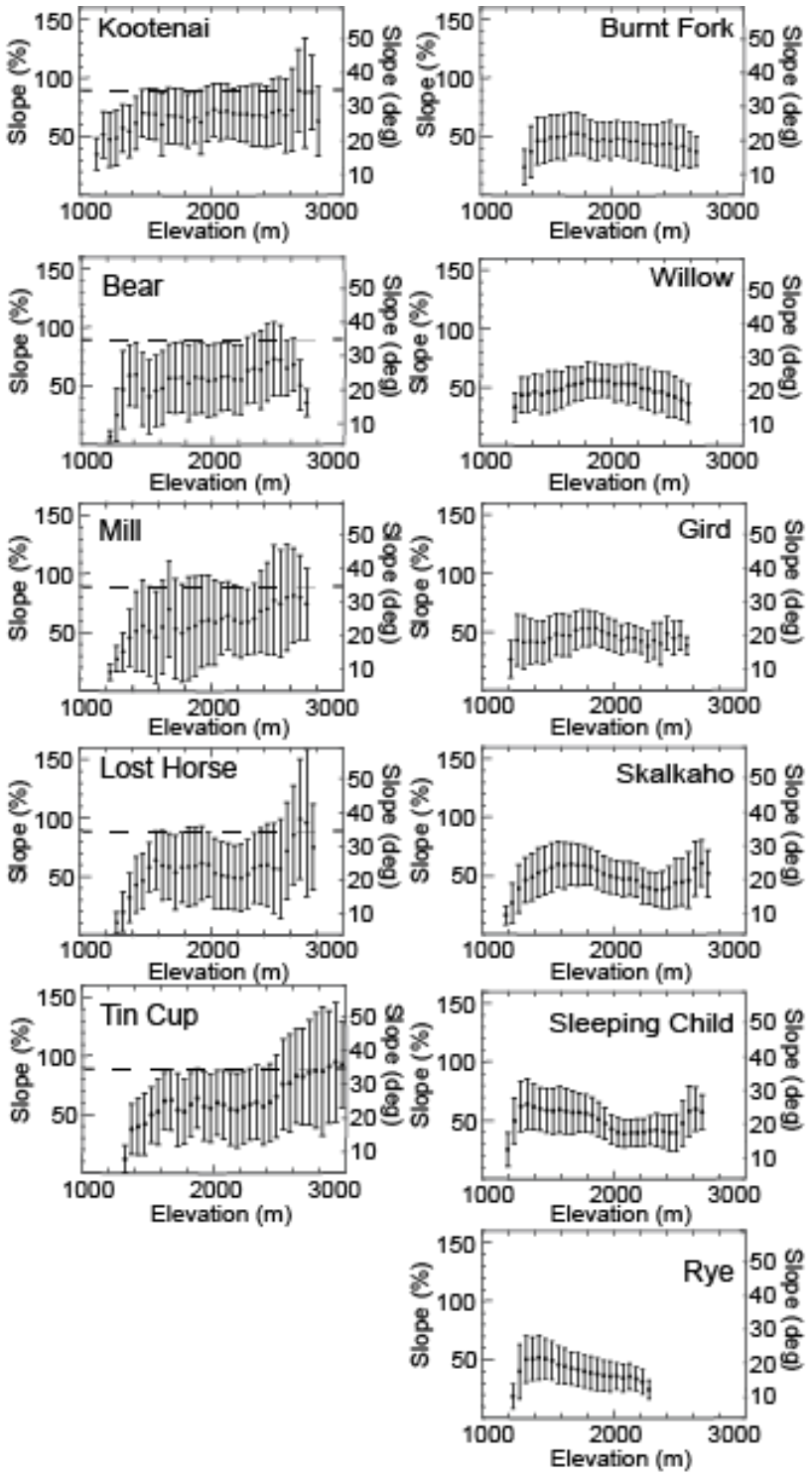
Kootenai
Burnt Fork
Bear
Willow
Mill
Gird
Lost Horse
Skalkaho
Tin Cup
Sleeping Child
Rye
Slope (%)
Slope (deg)
Elevation (m)
150
100
50
50
40
30
20
10
1000
2000
3000

Soil Cover and Thickness

Auger measurements indicate that soils are significantly different in our study catchments, with on average 80% thicker soils in Rye Creek than Lost Horse Creek (33.6 cm ± 1.3, n =200 and 17.8 cm ± 1.5, n = 186, respectively, $p<0.01$). Combining average soil thicknesses and soil cover estimates, we calculate that the soil volume in Rye is more than double that of Lost Horse (figure 2.11; 27.4 ± 3.9 cm*percent area, n=28 and 12.9 ± 2.8 cm*percent area, n = 27 respectively; $p<0.01$) when focusing on portions of each landscape estimated to be 'soil mantled' (i.e., valley bottoms and lower portions of hillslopes, but excluding rocky ridges and upper hillslopes).

Chemical Weathering Intensity

Chemical depletion fractions calculated from titanium concentrations in soils and bedrock vary between 0.17-0.84 in Lost Horse Creek (table 2.3), indicating that chemical weathering accounts for 17-84% of total denudation in these soils. In Rye Creek, CDFs range from 0.47 -0.94, indicating that chemical weathering accounts for 47 to 94% of total denudation. Importantly, these CDFs are likely too high to be taken as absolute measurements of weathering, as it is extremely unlikely that 94% of a granitic rock's mass could be removed by chemical dissolution. Though these measurements are likely complicated by variable rock chemistry, they provide useful comparison between our study catchments. CDF values suggest that soils are on average 27% more highly weathered in Rye Creek than in Lost Horse Creek (0.70 ± 0.01, n = 28 and 0.55 ± 0.04, n = 27, respectively; $p<0.01$). Mass transfer coefficients (τ) of major elements (Si, Na, and

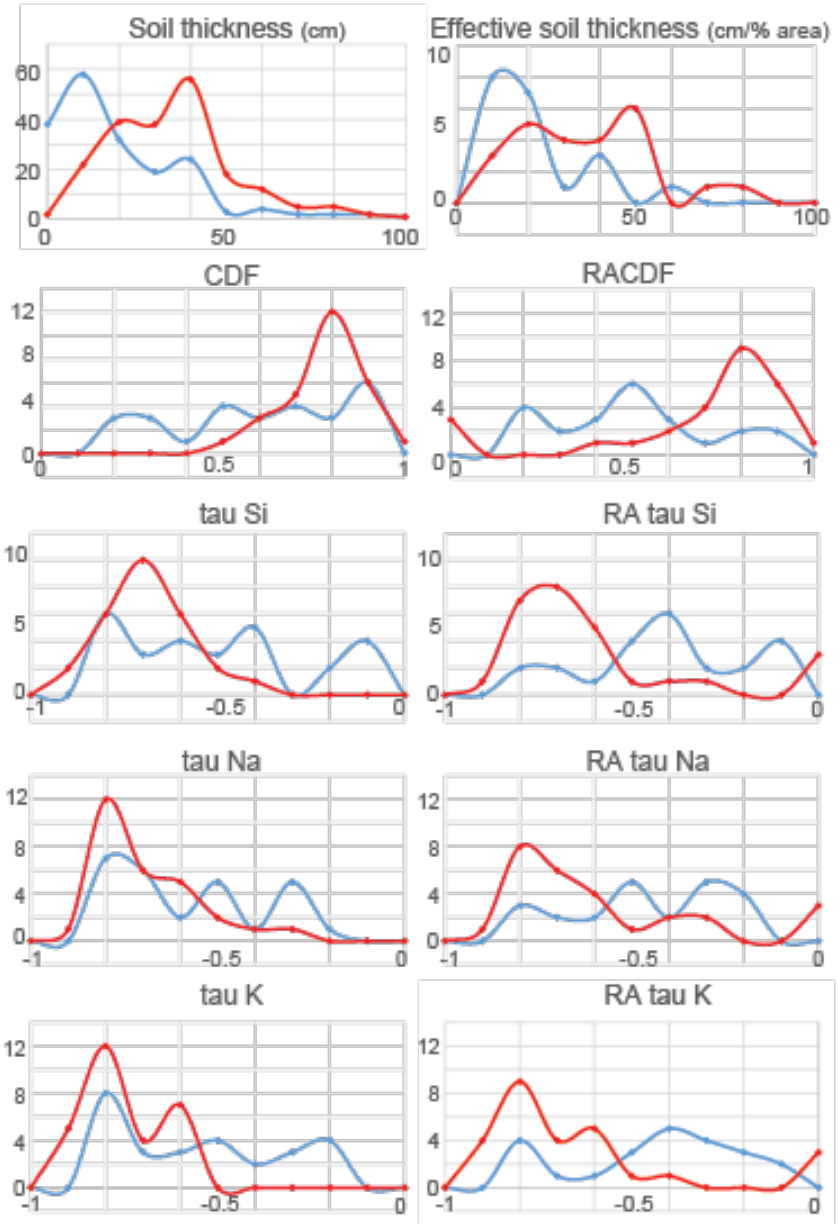

Figure 2.11. Soil thickness, soil volume, CDF, RACDF, τ, and RA τ of Si, Na, and K in Lost Horse Creek (blue) and Rye Creek (red). Values are represented as histogram, with the number of samples on the y axis. Nonglaciated Rye Creek tends to have thicker soils and higher degrees of chemical depletion as shown by higher CDF values and more strongly negative tau values.

K) also tend to be higher in Rye than Lost Horse (table 2.3). Differences between the two catchments of τSi and τK are both significant at the $p<0.01$ level, while τNa is only

significant at the $p<0.05$ level. τNa ranges from -0.26 to -0.89 in Lost Horse Creek and from -0.38 to -0.95 in Rye Creek. On average, Na losses are high in both systems (~63% in Lost Horse, ~75% in Rye), indicating strong weathering of plagioclase. The similarly large K losses (~60% in Lost Horse, ~80% in Rye) suggest intense potassium feldspar dissolution with some formation of illite clays, leading to potassium retention in soils.

Rock-adjusted CDF (RACDF) and rock-adjusted tau (RAτ) values reveal further pronounced differences in soil formation between Rye and Lost Horse catchments. RACDF is 60% higher in Rye Creek than in Lost Horse Creek (0.61 ± 0.05, $n=28$ and 0.38 ± 0.05, $n = 27$, respectively; $p<0.01$), whereas CDFs are on average 27% higher in Rye than Lost Horse. RAτ of Si, Na, and K is more negative in Rye Creek than Lost Horse Creek but adjusting for rock cover does not change the statistical results that conclude that RAτSi and RAτK are significantly different at the $p<0.01$ level while RAτNa is significant only at the $p<0.05$ level.

Despite these correlations between slope and elevation and NLCD land cover classes, field observations of soil abundance and weathered extent show no correlation with topographic metrics. CDF, RACDF, soil thickness, and soil volume show no correlation with either elevation slope, or profile or plan curvature in Lost Horse Creek or Rye Creek (in Lost Horse, the highest R-squared value for any of these correlations is 0.1; in Rye, the highest is 0.19).

	Lost Horse Creek (Bitterroots)					Rye Creek (Sapphires)				
	Average	± std err	max	min	n	Average	± std err	max	min	n
CDF	0.55	± 0.04	0.84	0.17	28	0.73	± 0.02	0.94	0.47	28
RACDF	0.38	± 4.85	81.85	0	23	0.61	± 5.34	94.09	0	27
Landscape-adjusted RACDF	0.22				23					
τ Si	-0.55	± 0.04	-0.16	-0.85	28	-0.74	± 0.02	-0.47	-0.94	28
RA τ Si	-0.38	± 4.95	0	-82.75	23	-61.95	± 5.46	0	-0.94	27
τ Al	-0.54	± 0.04	-0.2	-0.81	28	-0.67	± 0.03	-0.1	-0.94	28
RA τ Al	-0.37	± 4.68	0	-80.54	23	-56.05	± 5.51	0	-0.94	27
τ Na	-0.63	± 0.04	-0.26	-0.89	28	-0.74	± 0.02	-0.38	-0.95	28
RA τ Na	-0.44	± 5.03	0	-86.33	23	-61.68	± 5.58	0	-0.95	27
τ K	-0.6	± 0.04	-0.21	-0.9	28	-0.8	± 0.02	-0.61	-0.97	28
RA τ K	-0.42	± 5.1	0	-86.91	23	-66.64	± 5.71	0	-0.97	27
Soil thickness (cm)	33.57	± 1.29			186	17.8	± 1.48			200
Effective soil thickness (cm*percent area)	27.44	± 3.9				12.93	± 2.83			24

Table 2.3. CDF, RACDF, tau, RAτ of Si, Al, Na, and K, soil thickness, and effective soil thickness in Lost Horse Creek and Rye Creek.

	Lost Horse		Rye	
Parameters	R square	p value	R square	p value
RACDF v elevation	0.01	0.67	0.00	0.79
CDF v elevation	0.01	0.58	0.00	0.85
Soil thickness v elevation	0.09	0.15	0.02	0.48
Soil volume v elevation	0.09	0.16	0.04	0.32
Soil thickness v slope	0.03	0.40	0.15	0.05
Soil volume v slope	0.01	0.66	0.19	0.03
RACDF v slope	0.00	0.91	0.00	0.99
CDF v slope	0.05	0.28	0.00	0.90
CDF v profile curvature	0.06	0.22	0.10	0.09
RACDF v profile curvature	0.00	0.74	0.05	-0.23
Soil thickness v profile curvature	0.09	0.16	0.04	0.36
Soil volume v profile curvature	0.03	0.46	0.08	0.17
CDF v planar curvature	0.10	0.10	0.03	0.37
RACDF v planar curvature	0.02	0.53	0.02	0.52
Soil thickness v planar curvature	0.01	0.69	0.01	0.67
Soil volume v planar curvature	0.01	0.72	0.00	0.82

Table 2.4. Statistical tests for significance between soil thickness and volume, and CDF and RACDF, compared to topographic metrics in Lost Horse and Rye Creeks show no correlation between measured soil characteristics and topography.

Discussion

Assessing the Glacial Imprint on the Landscape

Our terrain analysis of 11 catchments in the Bitterroots and Sapphires used previously established metrics for distinguishing the effect of glaciation, and showed clear topographic differences across the two ranges, but presented some surprises. Hypsometric maxima correspond with the glacial ELA or snowline in many landscapes worldwide (Egholm et al., 2009). Previously-glaciated Bitterroot catchments exhibit hypsometric maxima at ~2,200-2,300 (figures 2.7 and 2.9). These elevations are similar to but slightly lower than prior estimates of equilibrium line altitudes (ELAs) during the Last Glacial Maximum (LGM) of ~2,400 m according to two estimation methods by Foster et al. (2008). The consistency of elevation maxima near ELA elevations observed here may be consistent with significant glacial erosion, especially considering the variability found across the Sapphire Range, where hypsometry is more difficult to characterize. Our findings are consistent with prior studies that indicate strong glacial imprint on the Bitterroot system. Naylor and Gabet (2006) observed that Bitterroot glaciers eroded laterally 2-4 times more efficiently than vertically due to headward erosion by cirques, and Foster et al. (2008) suggest that topographic development was efficiently contained by the glacial buzzsaw in the Beaverhead-Bitterroot region.

The variation in hypsometry between unglaciated Sapphire catchments may be due to widely differing drainage areas (Hurtrez et al., 1999) and lithologies (Lifton and Chase, 1992). Skalkaho and Sleeping Child Creeks extend into the Pintler Range to the west, which was glaciated in the past, which may explain why their elevation and slope

distributions are unlike other Sapphire catchments. Overall, hypsometric maxima are lower in the Sapphires than in the Bitterroots, consistent with a model whereby they are ultimately controlled by fluvial erosion and deposition controlled by an ocean base level (Egholm et al., 2009) while the local base level of the Bitterroots was set by glaciers.

Hypsometric integrals (HI) are similar across both ranges despite their different glacial histories, which deviates from previous observations that HI varies with glacial history (Brocklehurst and Whipple, 2004). Generally, higher HI indicates a negatively skewed distribution where modal values exceed average elevations. Low HI, where modal elevations are proportionally found lower in the catchment, is thought to be consistent with fluvial equilibrium, while higher HI values are often coincident with a higher degree of glacial modification (Brocklehurst and Whipple, 2004). Therefore, we would expect previously glaciated basins to display higher HI values than non-glaciated basins. However, understanding what HI signifies is complex, as climate, tectonics, and surface processes all play a role. HI values have been interpreted to show landscape maturity (Strahler, 1952, 1964); however, other factors such as catchment geometry (aspect ratio) and catchment size also play a role (Willgoose and Hancock, 1998). Plotting HI versus catchment area (figure 2.9), we note catchment size can likely not help clarify HI similarities (Willgoose and Hancock, 1998). Interestingly, measured HI values tend to be highest in the northernmost analyzed catchments of the two ranges (table 2.2). This observed decrease in HI southward is interesting considering inferred glacial history. Weber (1972) suggested that glaciation was strongest in the southernmost tributaries of the Bitterroots, and this southward strength of glaciation would be inconsistent with

decreasing HI. However, late Pleistocene weather reconstructions for the area that indicate that precipitation was uniform with latitude across the Bitterroots (Kutzbach and Ruddiman, 1993; Hostetler and Clark, 1997), contradicting Weber's (1972) assumption. Regardless, the similar nature of HI values between the Bitterroots and Sapphires suggests that HI is a poor indicator of glacial history across these two ranges. Instead, N-S differences may reflect a larger tectonic signal.

Despite lack of clarity provided by hypsometric analysis, slope analysis shows clear differences between the previously glaciated Bitterroots and nonglacial Sapphires (figures 2.7-2.8). All catchments in the Bitterroot range display significantly higher mean and modal slopes than those of the Sapphires (figure 2.7b). Slope-elevation distributions of the eleven catchments are partially consistent with idealized slope-elevation curves established by Robl et al. (2015)(figure 2.1). The majority of Bitterroot catchments are similar to the idealized glaciated landscape curves (figure 2.1 and 2.10). In these systems, slope gradients appear to increase markedly in uppermost portions of the catchment, consistent with near vertical cliffs and nunataks. Hillslopes in these isolated high-elevation regions exceed inferred slope thresholds. In the Sapphires, two catchments (Skalkaho and Sleeping Child) display patterns consistent with that of a glaciated landscape. This surprising inconsistent with other portions of the Sapphires can be explained by these catchments' extension into the Pintler Range to the west, which was glaciated in the past. Of specific interest is the fact that the slope-elevation curve of our study catchment, Rye Creek, is not consistent with that of a glacial landscape; instead its humped form reflects the idealized curve of a fluvial landscape in disequilibrium. The

same may be said of Burnt Fork, Willow, and Gird Creeks. This finding may question the suggestion of Foster et al. (2008), that this region has not experienced recent tectonic forcings, especially considering evidence of recent fault movement at the Bitterroot front (Stickney, 2014).

Interpretation of Soil Cover Distribution and Geochemistry

Our data consistently show that soils in the unglaciated Rye Creek are more highly weathered than post-glacial Lost Horse Creek, despite the former's drier climate. Our data higher degrees of surface weathering in the nonglacial system compared to previously glaciated hillslopes. This finding is based on CDF and τ-values of major elements derived from weatherable minerals (Si, Na, and K). CDF and tau results alone do not sufficiently reflect weathering in Rye Creek and Lost Horse Creek, because they underestimate the differences in surface weathering (high CDFs notwithstanding). CDF and tau values are based on samples and measurements taken from soil-mantled portions of each catchment, and include locations with significant rock and rock fragment cover. Adjusting for rock fragment cover at sample sites, RACDF values based on a percent of soil cover at sample sites indicate that at sample sites, ~ 38% and 61% of rock mass is lost by chemical weathering in Rye and Lost Horse systems respectively.

Additional sampling biases in these measurements must be considered. In Lost Horse Creek, sampling was restricted by accessibility to the valley bottom and low-gradient, low-elevation hillslopes. Steeper, higher elevation portions of the landscape were excluded. Because sampling was focused on primarily soil-mantled parts of the landscape, the heterogeneity of surface weathering was not fully represented, even once

adjusted locally for rock fragments. This caveat is especially important considering our study objective is to quantify the soil weathering regime of steep rock-dominated landscapes.

We derive landscape averaged surface weathering intensity can derived by multiplying the percent of the landscape that is soil-mantled by the catchment-averaged RACDF. This approximation increases differences between our study catchments, and yields a landscape-wide weathering intensity of ~ 22% in Lost Horse, compared to 61% in Rye. This derivation assumes areas of exposed bedrock have weathering rates close to zero, an assumption supported by the soil production function widely accepted by geomorphologists, but still not entirely accurate considering even bedrock dominated portions of the landscape may chemically weather over time. It also requires accurate quantification of soil mantled and bedrock dominated portions of the landscape, which we base on NLCD categories. Even with significant error, this approximation likely more accurately reflects weathering differences between the two catchments than is captured by geochemistry results alone.

Based on these data and primarily the fact that a high portion of Na and K remain in Lost Horse Creek soils, indicating that highly weatherable plagioclase persists, we infer that chemical weathering across the previously glaciated landscape is largely kinetically-limited. In a supply-limited system, the degree of weathering should be expected to be consistently high across the landscape, with significant depletion in major cations such as Na and K, having already been weathered away. The consistently high degree of weathering in nonglaciated Rye Creek fits this conceptual scenario, suggesting

that weathering may be supply-limited in Rye Creek at the catchment scale. The opposite is true in Lost Horse Creek, where weathering extent varies across the landscape and in some samples a high portion of Na and K remain in soil. Na and K are able to make their way through the soil column to the surface without being weathered away, suggesting soil residence time is short and erosion rates fast. We interpolate that weathering in Lost Horse Creek is kinetically limited. However, we find surprisingly little topographic indicators that predict weathering intensity at a local scale.

Unlike previous studies we find little correlation between soil thickness, weathering intensity, and topographic metrics. Previous work suggested curvature both reflects and is a driver of soil thickness (e.g., Dietrich et al. 1995). In this conceptualization, convergent regions collect colluvium and soil production is essentially stopped under a depth of 1m, while in divergent ridges, production rate and sediment transport compete and soil thickness may find a balance over time (possibly over 15kyr but less than 30 kyr timescales). At the spatial resolution we analyze, curvature does not appear to exert significant control on measured soil thickness in Lost Horse Creek and Rye Creek. This is to be expected in Lost Horse Creek, as the hillslope theory supported by Dietrich et al. (1995) was not meant to describe rock-dominated landscapes. Rye Creek, with its persistent and even soil mantle and its nonglaciated slopes, seems to fit the style of landscape where curvature and soil thickness are expected to be correlated. However, regressing curvature and auger measurements results in no clear link. We may also expect weathering intensities to inversely correlate with high

slope gradients, similar to findings of Dixon et al. (2012), but again, we find no clear link between weathering and slope on hillslopes of the Bitterroots or Sapphires.

There are several possible explanations for the lack of correlation between topographic indicators and soil thickness or weathering extent, some of which could be related to our data or methods and some of which could be real-world mechanisms. The discrepancy may in part result due to the poor quality of the DEM available for western Montana, which contains artefacts that complicate calculations of elevation derivatives including slope and curvature. These errors are visible in the profile curvature raster, appearing as along-contour stripes. It is also possible that a DEM with the spatial resolution of 10 m would miss many of the outcrop-scale variations in the landscape, artefacts notwithstanding. Geomorphologists have recognized the transformative improvement that comes with high resolution topographic data (e.g. Roering, 2008; Hilley and Arrowsmith, 2008; DiBiase et al., 2012).

If the lack of correlation between curvature and soil thickness is not a result of DEM artifacts but is in fact true in the landscape, we might infer a number of mechanisms that result in this decoupling of topography and weathering. The lack of correlation may result from temporal variability if Rye Creek soils are not in steady state, and are instead adjusting to disturbance. The region has been subject to logging over the last century and as recently as the 1960s, involving high road densities (McFarlane et al., 2005) and soil disturbance by machinery that is still visible as terraces carved into some hillslopes, suggesting that erosion rates in Rye Creek have been much higher in the last century than the millennial-scale rate, as is the case in other areas of high land use (e.g.

Hewawasam et al., 2003; Gellis et al., 2004). The area has also experienced forest fires including an especially large one in 2000 that affected Rye Creek and much of the surrounding region (over 360,000 forested acreage burned) (Halvorson, 2002).

The Influence of Modern Climate on Soil Evolution

Could higher precipitation rates and cooler temperatures in the Bitterroot Mountains contribute to the trends we see? Modern precipitation gradients can influence the discharge of sediment out of a basin (Biemans, 2009), the magnitude of river incision (Ferrier et al., 2013), and the landslide threshold (Gabet et al., 2004; Chleborad, 2003). Whether climate influences chemical weathering rates depends on the setting, because climate and erosion interact nonlinearly and both influence chemical weathering rate (White, 1995; Rasmussen et al., 2011). Very low erosion rates can limit weathering as regolith thickness increases above the optimal thickness for soil production and no steady state is maintained, and in wet conditions chemical weathering may be fast enough to keep pace with erosion rates even if erosion is not particularly low; thus, both these conditions can cause an erosional limitation on chemical weathering (Rasmussen et al., 2011). Conversely, in some settings, dry conditions can cause kinetic limitation, as insufficient water is present to remove weathering products (Arkley, 1963; Harden, 1990; Amundson, 2005) and water that is present may have short residence times before evapotranspiration removes water and leaves concentrated solutes (Maher, 2010).

Though we predict weathering may be enhanced by moisture availability across our system, we find no correlation between CDF and either topographic wetness index (TWI) or precipitation rates in either catchment, suggesting that modern climate plays a

minor role in influencing weathering. Soil distribution (i.e., thickness and volume) and weathering also show no correlation with hillslope aspect, further suggesting that moisture availability is not limiting weathering. The comparison of weathering indicators with precipitation may be obscured by the poor resolution of our climate data (800 m). Furthermore, in our study area, temperature and precipitation rate increase in opposite directions, which makes it difficult to disentangle the effect of modern climate on soil evolution.

Still, the finding that temperature and precipitation rate exert such little influence on chemical weathering agrees with previous studies that have found that erosion rates correlate more strongly with weathering rates than climate variables (West et al., 2005; Dixon and von Blanckenburg, 2012). Despite the fact that Lost Horse Creek has more precipitation, soils there are less weathered. This leaves open the possibility that morphology could be exerting a stronger control on soil weathering than modern climate. Thus, in the Bitterroots the climate control on chemical weathering may be overwhelmed by rapid mineral supply. We suggest that the climate history matters more to modern soil weathering than present climate conditions.

Effect of Lithology on Catchment Characteristics

Physical and chemical characteristics of rock types can drive landscape weathering and morphology and obscure other signals. For example, lithology has been observed to govern sediment supply to river channels and resultant channel morphology (Meuller and Pitlick, 2013), weaker rock strengths often correspond with low slope gradients (e.g., Norton et al., 2011) and low normalized stream steepness indices (Sternai

et al., 2012), other controls being absent. Additionally, lithology may influence chemical weathering rates through the abundance of highly weatherable minerals such as plagioclase, or through physical differences such as jointing or weak sheared zones (Norton and von Blanckenburg, 2010). We have designed our study to minimize variations in lithology and maximize those of morphology that drive differences in soil distribution and weathering extent in our study area. However, lithologic variation cannot be discounted. For their part, the Bitterroots are thought to be lithologically homogeneous, and out sampling region of Rye Creek in the Sapphires is underlain by the same bedrock unit. Though we minimize the effect of rock characteristics by choosing study sites with similar bedrock types, we are unable to account for differences in rock fabric such as facies differences and fracture spacing.

The Sapphires, which present a range of different lithologies, provide a unique additional opportunity to explore whether lithology may influence topographic metrics. The Sapphire catchments each contain between 3 to 6 geologic units (although in Rye and Sleeping Child Creeks two of these units are essentially identical, “Idaho batholith and associated masses” and “border zone of Idaho batholith and associated masses”, while the third is “alluvium”, which for our purposes is almost homogeneous). Much of Sleeping Child and the southern part of Skalkaho Creeks are composed of a unit named the border zone of the Idaho batholith and associated masses (figure 2.3). The northern part of Skalkaho Creek and the three northernmost catchments in our study (Gird, Willow, and Burnt Fork) are composed of Belt series rocks. In Burnt Fork this is mainly the Ravalli Group, and in Skalkaho, Gird, and Willow the dominant lithology is Newland

limestone, which has been used synonymously with the Wallace formation by some authors (Schweitzer, USGS Mineral Resources). When Sapphire catchments are divided by lithologic unit and mean slope of each unit is calculated, the resulting mean slopes range from ~10-28° (Table 2.5). These endmembers both occur in Willow Creek. In Willow Creek, the high variation by lithology may be due to the placement of units within the catchment. Also the geologic unit with the lowest slope (Belt Series – Ravalli group) occurs again in Sleeping Child creek where its mean slope is much higher (20° instead of 9°), which suggests there is nothing inherent to this lithology that causes a low slope gradient.

Catchment	Number of lithologic units present	Std error of slope gradient between lithologic units	% std err
Rye	3	1.31	0.00034
Gird	4	1.68	0.00044
Sleeping Child	3	0.62	0.00033
Burnt Fork	5	1.33	0.00032
Skalkaho	6	2.08	0.00025
Willow	5	2.99	0.00052

Table 2.5. Variation in slope gradient by lithologic unit in the Sapphires. For each of 6 study catchments, the number of lithologic units represented is listed. Mean slope gradient of each unit was calculated and the standard error and percent standard error between units of each catchment is listed.

Conclusions

The objective of this study was to measure the effect of a post-glacial morphology on soil chemical weathering. To do so we measured soil thickness and soil and rock

geochemistry across one glaciated and one unglaciated catchment in the neighboring Bitterroot and Sapphire Mountains in western Montana. We also compared the topography of 9 other catchments in the ranges in order to measure the glacial morphologic legacy. We select these two landscapes because they present contrasts in soil cover and morphology, providing insight into how weathering, topography, and soil cover vary in complex mountainous systems. Based on our analysis, we conclude that differences in topography between the Bitterroot and Sapphire mountains largely reflect their differing climate legacies, and that these morphologic differences drive distinct soil evolution processes in modern day. We find that the morphology formed by climate history over millennial timescales has a stronger influence on modern soil weathering than modern precipitation rates. Whereas a catchment with lower precipitation rates would normally be expected to have thinner and less developed soils, we find the opposite to be true. Furthermore, unlike previous studies, such as Dixon et al. (2012) who found that weathering intensity varied with slope gradient, we find no correlation between weathering intensity (shown by CDF or τ), soil thickness, and topographic metrics (such as curvature, slope gradient, or elevation). These relationships may be obscured by poor DEM quality and resolution, or complicated by temporal disturbances to soil cover in this fire prone and managed forest system.

While we are unable to determine the exact topographic control responsible for lower chemical weathering in the Bitterroots than the Sapphires, we have shown clear landscape-scale differences and added new insights into the heterogeneity of weathering and how to characterize it in complex bedrock-dominated landscapes. The rock-adjusted

CDF and τ metrics should be helpful for future studies seeking to quantify weathering in mountain belts.

Future work can expand on these problems by measuring topography at a finer scale. Prior work suggests high resolution (~1 m) topography is required to understand controls on local soil processes (e.g., Milodowski et al., 2015 and DiBiase et al., 2012). For some key parameters, a low-resolution DEM is sufficient; Grieve et al. (2016) analyzed the effects of grid resolution on topographic expression of geomorphic processes and found that even 30 m resolution can be enough for some analyses, and 10 m resolution data should provide insight into coarse-scale processes. However, high-resolution DEMs may help illuminate specific drivers of soil distribution and weathering in these glaciated and unglaciated landscapes.

Future research should also quantify millennial-scale erosion rates for catchments in the Bitterroots and Sapphires. We expect cosmogenic Be-10 analysis would reveal higher erosion rates in the Bitterroots, providing futher insight into erosional controls on kinetic vs supply-limited weathering regimes. Such analysis could be coupled with local soil production rates to understand to what degree topography and long term erosion or soil production are correlated.

Further work on soil weathering in mountain belts is needed to help resolve ongoing debates in geomorphology regarding an upper limit on soil production and weathering (Heimsath et al., 2012; Dixon and von Blanckenburg, 2012; Larsen et al. 2014), and whether weathering in mountain ranges occur quickly enough and on a vast enough scale to draw down enough CO_2 to regulate global climate on millennial scales.

Thus far, quantifying weathering in mountainous systems has primarily relied on riverine fluxes, which integrate across large spatial scales, but only reflect the temporal scale across the time period of sampling. Understanding how mountain belts weather and the tectonic, glacial, or climatic controls on these processes requires better quantification of long-term weathering extents and rates and improved characterization of the heterogeneity of the surface weathering environment.

References Cited

Ahnert, F. 1967. The role of the equilibrium concept in the interpretation of landforms of fluvial erosion and deposition.

Ahnert, F., 1970. Functional relationship between denudation, relief, and uplift in large mid-latitude drainage basins. *Am. J. Sci*. 268, 243–263.

Alden, W.C., 1932. Physiography and glacial geology of eastern Montana and adjacent areas (No. 174). US Government Printing Office.

Alden, W.C., 1953, Physiography and glacial geology of western Montana and adjacent areas: U.S. Geological Survey Professional Paper 231, pp. 200.

Amiotte-Suchet, P., Probst, J.L., 1993. Flux de CO_2 atmosphérique consommé par altération chimique continentale. Influence de la nature de la roche. C.R. Acad. Sci. Paris 317, 615–622, Serie II.

Amundson, R., Richter, D.D., Humphreys, G.S., Jobbágy, E.G. and Gaillardet, J., 2007. Coupling between biota and earth materials in the critical zone. *Elements*, *3*(5), pp.327-332.

Amundson, R, Heimsath, A., Owen, J., Yoo, K., and Dietrich, WE. 2015. Hillslope soils and vegetation: A review. *Geomorphology*, 234: 122-132.

Anderson, S.P., Drever, J.I., Frost, C.D. and Holden, P., 2000. Chemical weathering in the foreland of a retreating glacier. *Geochimica et Cosmochimica Acta*, *64*(7), pp.1173-1189.

Anderson SP, von Blanckenburg F, White AF. 2007. Physical and chemical controls on the Critical Zone. *Elements* **3** : 315–319.

Anderson SP, Dietrich WE, Brimhall GH Jr. 2002. Weathering profiles, mass-balance analysis, and rates of solute loss: Linkages between weathering and erosion in a small, steep catchment. *Geological Society of America, Bulletin* **114** : 1143–1158.

Arkley, R.J., 1963. CALCULATION OF CARBONATE AND WATER MOVEMENT IN SOIL FROM CLIMATIC DATA. *Soil Science*, *96*(4), pp.239-248.

Armstrong, R.L. and Hansen, E., 1966. Cordilleran infrastructure in the eastern Great Basin. *American Journal of Science*, *264*(2), pp.112-127.

Bern CR, Chadwick OA, Hartshorn AS, Khomo LM, Chorover J. 2011. A mass-balance model to separate and quantify colloidal and solute redistributions in soil. *Chemical Geology* **282** : 113–119.

Berner, R.A., Lasaga, A.C., Garrels, R.M., 1983. The carbonate-silicate geochemical cycle and its effect on atmospheric carbon dioxide over the past 100 million years. *Am. J. Sci.* 283, 641–683.

Biemans, H., Hutjes, R.W.A., Kabat, P., Strengers, B.J., Gerten, D. and Rost, S., 2009. Effects of precipitation uncertainty on discharge calculations for main river basins. *Journal of Hydrometeorology*, *10*(4), pp.1011-1025.

Bluth, G.J.S., Kump, L.R., 1994. Lithological and climatological controls of river chemistry. *Geochim. Cosmochim. Acta* 58, 2341–2359.

Brantley SL, White AF., 2009. Approaches to modeling weathered regolith. *Reviews in Mineralogy and Geochemistry* **70** : 435–484.

Brimhall, G. H., and W. E. Dietrich., 1987. Constitutive mass balance relations between chemical composition, volume, density, porosity, and strain in metasomatic hydrochemical systems: Results on weathering and pedogenesis, *Geochim. Cosmochim. Acta*, 51(3), 567–587.

Brocklehurst, S.H. and Whipple, K.X., 2002. Glacial erosion and relief production in the Eastern Sierra Nevada, California. *Geomorphology*, *42*(1), pp.1-24.

Brocklehurst, S.H. and Whipple, K.X., 2004. Hypsometry of glaciated landscapes. *Earth Surface Processes and Landforms*, *29*(7), pp.907-926.

Brocklehurst, S.H. and Whipple, K.X., 2006. Assessing the relative efficiency of fluvial and glacial erosion through simulation of fluvial landscapes. *Geomorphology*, *75*(3), pp.283-299.

Brozović, N., Burbank, D.W. and Meigs, A.J., 1997. Climatic limits on landscape development in the northwestern Himalaya. *Science*, *276*(5312), pp.571-574.

Burke BC, Heimsath AM, Dixon JL, Chappell J, Yoo K. 2009. Weathering the escarpment: chemical and physical rates and processes, south-eastern Australia. *Earth Surface Processes and Landforms* **34** : 768–785.

Burke BC, Heimsath AM, White AF. 2007. Coupling chemical weathering with soil production across soil-mantled landscapes. *Earth Surface Processes and Landforms* **32** : 853–873.

Carson MA, Kirkby MJ. 1972. *Hillslope Form and Process*. Cambridge University Press: London. Chadwick OA, Roering JJ, Heimsath AM, Levick SR, Asner GP, Khomo

L. 2013. Shaping post-orogenic landscapes by climate and chemical weathering. *Geology* **41** : 1171–1174.

Champagnac, J.D., Molnar, P., Anderson, R.S., Sue, C. and Delacou, B., 2007. Quaternary erosion-induced isostatic rebound in the western Alps. *Geology*, *35*(3), pp.195-198.

Chase, R.B. and Talbot, J.L., 1973. Structural evolution of the northeastern border zone of the Idaho batholith, western Montana. In *Geological Society of America Abstracts with Programs* (Vol. 5, pp. 470-471).

Chleborad, A.F., 2003. Preliminary evaluation of a precipitation threshold for anticipating the occurrence of landslides in the Seattle, Washington, Area (No. 2003-463).

Church, M. and Slaymaker, O., 1989. Disequilibrium of Holocene sediment yield in glaciated British Columbia. *Nature*, *337*(6206), pp.452-454.

Collins, B.D. and Montgomery, D.R., 2011. The legacy of Pleistocene glaciation and the organization of lowland alluvial process domains in the Puget Sound region. *Geomorphology*, *126*(1), pp.174-185.

Culling WEH., 1960. Analytical theory of erosion. *Journal of Geology* **68** : 336–344.

Culling WEH., 1963. Soil creep and the development of hillside slopes. *Journal of Geology* **71** : 127–161.

DiBiase, R.A., Whipple, K.X., Heimsath, A.M. and Ouimet, W.B., 2010. Landscape form and millennial erosion rates in the San Gabriel Mountains, CA. *Earth and Planetary Science Letters*, *289*(1), pp.134-144.

DiBiase, R.A., Heimsath, A.M. and Whipple, K.X., 2012. Hillslope response to tectonic forcing in threshold landscapes. *Earth Surface Processes and Landforms*, *37*(8), pp.855-865.

Dietrich WE, Bellugi DG, Sklar LS, Stock JD, Heimsath AM, Roering JJ. 2003. Geomorphic Transport Laws for Predicting Landscape Form and Dynamics. In *Prediction in Geomorphology, Geophysical Monograph Series 135*, Wilcock PR and Iverson RM (eds). American Geophysical Union: Washington, DC; 103–132.

Dietrich WE, Reiss R, Hsu ML, Montgomery DR. 1995. A process-based model for colluvial soil depth and shallow landsliding using digital elevation data. *Hydrological Processes* **9** : 383–400.

Dixon JL, Blanckenburg von F. 2012. Soils as pacemakers and limiters of global silicate weathering. *Comptes Rendus Geoscience* **344** : 597–609.

Dixon JL, Heimsath AM, Amundson RC. 2009. The critical role of climate and saprolite weathering in landscape evolution. *Earth Surface Processes and Landforms* **34** : 1507–1521.

Dixon, J.L., Heimsath, A.M., Kaste, J.M., Amundson, R., 2009. Climate driven processes of hillslope weathering. *Geology*.

Dixon, J.L., Hartshorn, A.S., Heimsath, A.M., DiBiase, R.A. and Whipple, K.X., 2012. Chemical weathering response to tectonic forcing: A soils perspective from the San Gabriel Mountains, California. *Earth and Planetary Science Letters*, *323*, pp.40-49.

Dixon J.L., Riebe CS. 2014. Tracing and pacing soil across slopes. *Elements* **10** : 363–368.

Dixon, J.L.., von Blanckenburg, F, Stuwe, K., and Christl, M., 2016a. Glaciation's topographic control on Holocene erosion at the eastern edge of the Alps. *Earth Surf. Dynam. Discuss.,* doi:10.5194/esurf-2016-29

Dixon, J.L., Chadwick, O.A., Vitousek, P.M., 2016b. Climate-driven thresholds for chemical weathering in postglacial soils of New Zealand. *JGR-Earth Surface,* doi: 10.1002/2016JF003864

Edmond, J.M. et al., 1994. Fluvial geochemistry and denudation rate of Guyana Shield. Geochim. Cosmochim. Acta 59, 3301– 3325.

Edmond, J.M., Palmer, M.R., Measures, C.I., Brown, E.T., Huh, Y., 1996. Fluvial geochemistry of the northeastern Andes and its fordeep in the drainage of the Orinoco in Columbia and Venezuela. Geochim. Cosmochim. Acta 60 16 , 2949–2976.

Egholm, D.L., Nielsen, S.B., Pedersen, V.K. and Lesemann, J.E., 2009. Glacial effects limiting mountain height. *Nature*, *460*(7257), pp.884-887.

Evans, I.S., and Cox, N.J., 2005, Global variations in local asymmetry in glacier altitude: Separation of north-south and east-west components: *Journal of Glaciology*, v. **51** pp. 469-482.

Ferrier KL, Kirchner JW. 2008. Effects of physical erosion on chemical denudation rates: A numerical modeling study of soil-mantled hillslopes. *Earth and Planetary Science Letters* **272** : 591–599.

Ferrier KL, Kirchner JW, Finkel RC. 2011. Estimating millennial-scale rates of dust incorporation into eroding hillslope regolith using cosmogenic nuclides and immobile weathering tracers. *Journal of Geophysical Research* **116** : 1–11.

Ferrier KL, Kirchner JW, Riebe CS, Finkel RC. 2010. Mineral-specific chemical weathering rates over millennial timescales: Measurements at Rio Icacos, Puerto Rico. *Chemical Geology* **277** : 101–114.

Ferrier, K.L., Huppert, K.L. and Perron, J.T., 2013. Climatic control of bedrock river incision. *Nature*, *496*(7444), pp.206-209.

Ferrier KL, Riebe CS, Hahm WJ. 2016. Testing for supply-limited and kinetic-limited chemical erosion in field measurements of regolith production and chemical depletion. *Geochemistry, Geophysics, Geosystems* **17** : 2270–2285.

Foster, D., Brocklehurst, S.H., Gawthorpe, R.L., 2008. Small valley glaciers and the effectiveness of the glacial buzzsaw in the northern Basin and Range, USA. Geomorphology 102, 624-639.

Foster, D.A. and Raza, A., 2002. Low-temperature thermochronological record of exhumation of the Bitterroot metamorphic core complex, northern Cordilleran Orogen. *Tectonophysics*, *349*(1), pp.23-36.

Gabet, E.J., 2003. Sediment transport by dry ravel. *Journal of Geophysical Research: Solid Earth*, *108*(B1).

Gabet, E.J., Burbank, D.W., Putkonen, J.K., Pratt-Sitaula, B.A., Ojha, T., 2004. Rainfall thresholds for landsliding in the Himalayas of Nepal. Geomorphology 63, 131-143.

Gabet, E.J. and Bookter, A., 2008. A morphometric analysis of gullies scoured by post-fire progressively bulked debris flows in southwest Montana, USA. *Geomorphology*, *96*(3), pp.298-309.

Garrels, R.M., Mackenzie, F.T., 1971. Evolution of Sedimentary Rocks. Norton, New York.

Gellis, A.C., Pavich, M.J., Bierman, P.R., Clapp, E.M., Ellevein, A. and Aby, S., 2004. Modern sediment yield compared to geologic rates of sediment production in a semi-arid basin, New Mexico: assessing the human impact. *Earth Surface Processes and Landforms*, *29*(11), pp.1359-1372.

Gilbert GK. 1877. *Report on the Geology of the Henry Mountains*. Department of the Interior: Washington, DC.

Gilbert GK. 1909. The convexity of hilltops. *Journal of Geology* **17** : 344–350.

Granger DE, Kirchner JW, Finkel RC. 1996. Spatially averaged long-term erosion rates measured from in situ-produced cosmogenic nuclides in alluvial sediment. *Journal of Geology* **104** : 249–257.

Granger DE, Riebe CS. 2014. Cosmogenic Nuclides in Erosion and Weathering. In *Treatise on Geochemistry*, Drever JI (ed). Elsevier: Oxford; 401-436.

Green, E.G., Dietrich, W.E., Banfield, J.F., 2006. Quantification of chemical weathering rates across an actively eroding hillslope. Earth Planet. Sci. Lett. 242, 155–169.

Grieve, S.W., Mudd, S.M., Milodowski, D.T., Clubb, F.J. and Furbish, D.J., How does grid-resolution modulate the topographic expression of geomorphic processes?.

Hack JT, Goodlett JC. 1960. Geomorphology and forest ecology of a mountain region in the central Appalachians. US Geological Survey Professional Paper 347, US Department of the Interior; Washington, DC: 1–66.

Hack JT. 1960. Interpretation of erosional topography in humid temperate regions. *American Journal of Science* **258** : 80–97.

Hahm WJ, Riebe CS, Lukens CE, Araki S. 2014. Bedrock composition regulates mountain ecosystems and landscape evolution. *Proceedings of the National Academy of Sciences* **111** : 3338–3343.

Halvorson, S.J., 2002. The fires of 2000: Community response and recovery in the Bitter Root Valley, Western Montana. Natural Hazards Research and Applications Information Center.

Harden, J.W., 1990. Soil development on stable landforms and implications for landscape studies. *Geomorphology*, *3*(3-4), pp.391-398.

Heimsath AM, Chappell J, Dietrich WE, Nishiizumi K, Finkel RC. 2000. Soil production on a retreating escarpment in southeastern Australia. *Geology* **28** : 787–790.

Heimsath AM, DiBiase RA, Whipple KX. 2012. Soil production limits and the transition to bedrock-dominated landscapes. *Nature Geoscience* **5** : 210–214.

Heimsath AM, Dietrich WE, Nishiizumi K, Finkel RC. 1997. The soil production function and landscape equilibrium. *Nature* **388** : 358–361.

Heimsath AM, Dietrich WE, Nishiizumi K, Finkel RC. 1999. Cosmogenic nuclides, topography, and the spatial variation of soil depth. *Geomorphology* **27** : 151–172.

Heimsath AM, Furbish DJ, Dietrich WE. 2005. The illusion of diffusion: Field evidence for depth-dependent sediment transport. *Geology* **33** : 949–952.

Herman, F., Seward, D., Valla, P.G., Carter, A, Kohn, B., Willett, S.D. and Ehlers, T.A., 2013. Worldwide acceleration of mountain erosion under a cooling climate. Nature, 504, 423–426.

Hewawasam, T., von Blanckenburg, F., Schaller, M. and Kubik, P., 2003. Increase of human over natural erosion rates in tropical highlands constrained by cosmogenic nuclides. *Geology*, *31*(7), pp.597-600.

Hilley, G.E. and Arrowsmith, J.R., 2008. Geomorphic response to uplift along the Dragon's Back pressure ridge, Carrizo Plain, California. *Geology*, *36*(5), pp.367-370.

Hilley, G.E., Porder, S., 2008. A framework for predicting global silicate weathering and CO2 drawdown rates over geologic time-scales. Proc. Natl. Acad. Sci. 105, 16855–16859

Homer, C.G., Dewitz, J.A., Yang, L., Jin, S., Danielson, P., Xian, G., Coulston, J., Herold, N.D., Wickham, J.D., and Megown, K., 2015, Completion of the 2011 National Land Cover Database for the conterminous United States-Representing a decade of land cover change information. *Photogrammetric Engineering and Remote Sensing*, v. 81, no. 5, p. 345-354

Hostetler, S.W., and Clark, P.U., 1997, Climatic controls of western U.S. glaciers at the Last Glacial Maximum: *Quaternary Science Reviews,* v. **16** pp. 505-511 doi: 10.1016/S0277-3791 (96)00116-3.

Hurst MD, Mudd SM, Walcott R, Attal M, Yoo K. 2012. Using hilltop curvature to derive the spatial distribution of erosion rates. *Journal of Geophysical Research* **117** : 1–19.

Hoffman, D.F. and Gabet, E.J., 2007. Effects of sediment pulses on channel morphology in a gravel-bed river. *Geological Society of America Bulletin*, *119*(1-2), pp.116-125.

Hyde, K.D., Wilcox, A.C., Jencso, K. and Woods, S., 2014. Effects of vegetation disturbance by fire on channel initiation thresholds. *Geomorphology*, *214*, pp.84-96.

Hyndman, D.W., 1980. Bitterroot dome-Sapphire tectonic block, an example of a plutonic-core gneiss-dome complex with its detached suprastructure. *Geological Society of America Memoirs*, *153*, pp.427-444.

Jansen, J.D., Fabel, D., Bishop, P., Xu, S., Schnabel, C. and Codilean, A.T., 2011. Does decreasing paraglacial sediment supply slow knickpoint retreat?. *Geology*, *39*(6), pp.543-546.

Kirkbride, M. and Matthews, D., 1997. The role of fluvial and glacial erosion in landscape evolution: the Ben Ohau Range, New Zealand. *Earth Surface Processes and Landforms*, *22*(3), pp.317-327.

Kump, Lee R., Susan L. Brantley, and Michael A. Arthur. 2000. Chemical weathering, atmospheric CO2, and climate. *Annual Review of Earth and Planetary Sciences* 28.1: 611-667.

Kutzbach, J.E. and Ruddiman, W.F., 1993. Model description, external forcing, and surface boundary conditions. *Global climates since the last glacial maximum*, pp.12-23.

Langton, C.M., 1935. Geology of the northeastern part of the Idaho batholith and adjacent region in Montana. *The Journal of Geology*, pp.27-60.

Larsen, I. J., P. C. Almond, A. Eger, J. O. Stone, D. R. Montgomery, and B. Malcolm (2014), Rapid soil production and weathering in the Southern Alps, New Zealand, *Science*, **343**(6171), 637–640.

Lebedeva MI, Brantley SL. 2013. Exploring geochemical controls on weathering and erosion of convex hillslopes: Beyond the empirical regolith production function. *Earth Surface Processes and Landforms* **38** : 1793–1807.

Lewis, R.S., 1998, Geologic map of the Montana part of the Missoula West 30′ × 60′ quadrangle: Montana Bureau of Mines Open-File Report 373, scale 1:100,000.

Lindgren, Waldemar, 1904, A geological recon- naissance across the Bitterroot Range and Clear- water Mountains in Montana and Idaho: U.S. Geol. Survey Prof. Paper 27, 222 p.

Lonn, J.D., and Berg, R.B., 1996, Preliminary geologic map of the Bitterroot Valley, Montana: Montana Bureau of Mines Open-File Report 340, scale 1:100,000.

Lukens CE, Riebe CS, Sklar LS, Shuster DL. 2016. Grain-size bias in cosmogenic nuclide studies of catchment-wide erosion. *Journal of Geophysical Research, Earth Surface* **121** : 978–999.

Maher, K., 2010. The dependence of chemical weathering rates on fluid residence time. *Earth and Planetary Science Letters*, *294*(1), pp.101-110.

Martínez-Murillo, J.F., Neris, J., Hyde, K. and Keizer, J.J., 2016. Advances towards an Integrated Assessment of Fire Effects on Soils, Vegetation and Geomorphological Processes. *Land Degradation & Development*, *27*(5), pp.1314-1318.

Merrill GP. 1897. *A Treatise on Rocks, Rock-Weathering and Soils*. Macmillan Company: New York.

Mueller, E.R. and Pitlick, J., 2013. Sediment supply and channel morphology in mountain river systems: 1. Relative importance of lithology, topography, and climate. *Journal of Geophysical Research: Earth Surface*, *118*(4), pp.2325-2342.

Meybeck, M., 1987. Global chemical weathering of surficial rocks estimated from river dissolved loads. *Am. J. Sci.* 287, 401–428.

Milodowski, D.T., Mudd, S.M. and Mitchard, E.T.A., 2015. Topographic roughness as a signature of the emergence of bedrock in eroding landscapes. *Earth Surface Dynamics*, *3*(4), p.483.

Mitchell, S.G. and Montgomery, D.R., 2006. Influence of a glacial buzzsaw on the height and morphology of the Cascade Range in central Washington State, USA. *Quaternary Research*, *65*(1), pp.96-107.

Misch, P. and Hazzard, J.C., 1962. Stratigraphy and metamorphism of Late Precambrian rocks in central northeastern Nevada and adjacent Utah. *AAPG Bulletin*, *46*(3), pp.289-343.

Molnar, P. and England, P., 1990. Late Cenozoic uplift of mountain ranges and global climate change: chicken or egg?. *Nature*, *346*(6279), pp.29-34.

Montgomery, D.R. 2001. Slope distributions, threshold hillslopes, and steady-state topography. *American Journal of Science*, *301*(4-5), pp.432-454.

Moon S, Chamberlain CP, Blisniuk K, Levine N, Rood DH, Hilley GE. 2011. Climatic control of denudation in the deglaciated landscape of the Washington Cascades. *Nature Geoscience* **4** : 469–473.

Naylor, S., 2006. The influence of glacial erosion on landscape evolution and basin morphology in the Bitterroot Mountains Montana.

Naylor, S. and Gabet, E.J., 2007. Valley asymmetry and glacial versus nonglacial erosion in the Bitterroot Range, Montana, USA. *Geology*, *35*(4), pp.375-378.

Norton, K.P., von Blanckenburg, F., DiBiase, R., Schlunegger, F. and Kubik, P.W., 2011. Cosmogenic 10Be-derived denudation rates of the Eastern and Southern European Alps. *International Journal of Earth Sciences*, *100*(5), pp.1163-1179.

Norton, K.P. and Von Blanckenburg, F., 2010. Silicate weathering of soil-mantled slopes in an active Alpine landscape. *Geochimica et Cosmochimica Acta*, *74*(18), pp.5243-5258.

Pardee, J.T., 1950. Late Cenozoic block faulting in western Montana. *Geological Society of America Bulletin*, *61*(4), pp.359-406.

Parrett, C., Cannon, S.H. and Pierce, K.L., 2004. *Wildfire-related floods and debris flows in Montana in 2000 and 2001* (No. 3-4319). US Geological Survey.

PRISM Climate Group, Oregon State University, http://prism.oregonstate.edu, created 4 Feb 2004.

Rasmussen, C., S. Brantley, D. deB. Richter, A. Blum, J. Dixon, and A. F. White. 2011. Strong climate and tectonic control on plagioclase weathering in granitic terrain, *Earth Planet. Sci. Lett.*, 301, 521–530.

Riebe CS, Kirchner JW, Granger DE. 2001a. Quantifying quartz enrichment and its consequences for cosmogenic measurements of erosion rates from alluvial sediment and regolith. *Geomorphology* **40** : 15–19.

Riebe, C.S., Kirchner, J.W., Granger, D.E., Finkel, R.C., 2001b. Minimal climatic control on erosion rates in the Sierra Nevada, California. Geology 29, 447–450.

Riebe, C.S., Kirchner, J.W., Granger, D.E., Finkel, R.C., 2001c. Strong tectonic and weak climatic control of long-term chemical weathering rates. Geology 26, 511–514.

Riebe, C.S., Kirchner, J.W., Finkel, R.C., 2003. Long-term rates of chemical weathering and physical erosion from cosmogenic nuclides and geochemical mass balance. Geochim. Cosmochim. Acta 67, 4411–4427.

Riebe, C.S., Kirchner, J.W., Finkel, R.C., 2004a. Erosional and climatic effects on longterm chemical weathering rates in granitic landscapes spanning diverse climate regimes. Earth Planet. Sci. Lett. 224, 547–562.

Riebe, C.S., Kirchner, J.W., Finkel, R.C., 2004b. Sharp decrease in long-term chemical weathering rates along an altitudinal transect. Earth Planet. Sci. Lett. 218, 421–434

Riggins SG, Anderson RS, Anderson SP, Tye AM. 2011. Solving a conundrum of a steadystate hilltop with variable soil depths and production rates, Bodmin Moor, UK. *Geomorphology* **128** : 73–84.

Robl, J., Prasicek, G., Hergarten, S. and Stüwe, K., 2015. Alpine topography in the light of tectonic uplift and glaciation. *Global and Planetary Change*, *127*, pp.34-49.

Roering JJ. 2008. How well can hillslope evolution models "explain" topography? Simulating soil transport and production with high-resolution topographic data. Geological Society of America Bulletin 120: 1248–1262. DOI. 10.1130/b26283.1

Roering JJ, Kirchner JW, Dietrich WE. 1999. Evidence for nonlinear, diffusive sediment transport on hillslopes and implications for landscape morphology. *Water Resources Research* **35** : 853–870.

Ross, C. P., 1950, The eastern front of the Bitterroot Range, Montana: U.S. Geol. Survey Bull. 974-E, p. 135-174.

Schweitzer, Peter. USGS Mineral Resources Online Spatial Data. Newland limestone. http://mrdata.usgs.gov/geology/state/sgmc-unit.php?unit=MTpCAn%3B0

Schumm, S.A., 1956. Evolution of drainage systems and slopes in badlands at Perth Amboy, New Jersey. *Geological society of America bulletin*, *67*(5), pp.597-646.

Small EE, Anderson RS, Hancock GS. 1999. Estimates of the rate of regolith production using Be-10 and Al-26 from an alpine hillslope. *Geomorphology* **27** : 131–150.

Stallard RF. 1985. River Chemistry, Geology, Geomorphology, and Soils in the Amazon and Orinoco Basins. In *The Chemistry of Weathering*, Drever JI (ed). D. Reidel Publishing Company: Dordrecht; 293–316.

Stallard, R.F., Edmond, J.M., 1983. Geochemistry of the Amazon 2. The influence of geology and weathering environment on the dissolved load. J. Geophys. Res. 88, 9671–9688.

Sternai, P., Herman, F., Champagnac, J.D., Fox, M., Salcher, B. and Willett, S.D., 2012. Pre-glacial topography of the European Alps. *Geology*, *40*(12), pp.1067-1070.

Strahler, A.N., 1950. Davis' concepts of slope development viewed in the light of recent quantitative investigations. *Annals of the Association of American Geographers*, *40*(3), pp.209-213.

Strahler, A.N., 1952. Hypsometric (area-altitude) analysis of erosional topography. *Geological Society of America Bulletin*, *63*(11), pp.1117-1142.

Strahler, A.N., 1954. Statistical analysis in geomorphic research. *The Journal of Geology*, pp.1-25.

Stickney, Michael. 2014. New LiDAR data reveals late Quaternary geology details in the Bitterroot Valley, Western Montana. Geological Society of America Rocky Mountain and Cordilleran Sections Joint Meeting, Session No. 27. Montana State University, Bozeman. 21 May, 2014.

Walker JCG, Hays PB, Kasting JF. 1981. A negative feedback mechanism for the long-term stabilization of the Earth's surface temperature. *Journal of Geophysical Research* **86** : 9776–9782.

Weber, W.M., 1972, Correlation of Pleistocene glaciation in the Bitterroot Range, Montana, with fluctuations of Glacial Lake Missoula, Montana: Bureau of Mines and Geology Memoir 42p. 44 p.

West AJ, Galy A, Bickle MJ. 2005. Tectonic and climatic controls on silicate weathering. *Earth and Planetary Science Letters* **235** : 211–228.

West AJ. 2012. Thickness of the chemical weathering zone and implications for erosional and climatic drivers of weathering and for carbon-cycle feedbacks. *Geology* **40** : 811–814.

Whipple KX. 2004. Bedrock rivers and the geomorphology of active orogens. *Annual Review of Earth and Planetary Sciences* **32** : 151–185.

White AF. 1995. Chemical weathering rates of silicate minerals in soils. *Reviews in Mineralogy and Geochemistry* **31** : 407–461.

White AF. 2002. Determining mineral weathering rates based on solid and solute weathering gradients and velocities: application to biotite weathering in saprolites. *Chemical Geology* **190** : 69–89.

White AF, Blum AE. 1995. Effects of climate on chemical weathering in watersheds. *Geochimica et Cosmochimica Acta* **59** : 1729–1747.

Whitlock, C. and Bartlein, P.J., 1993. Spatial variations of Holocene climatic change in the Yellowstone region. *Quaternary Research*, *39*(2), pp.231-238.

Willgoose, G. and Hancock, G., 1998. Revisiting the hypsometric curve as an indicator of form and process in transport-limited catchment. *Earth Surface Processes and Landforms, 23*(7), pp.611-623.

Willenbring JK, von Blanckenburg F. 2010. Meteoric cosmogenic Beryllium-10 adsorbed to river sediment and soil: Applications for Earth-surface dynamics. *Earth-Science Reviews* **98** : 105–122.

Yoo, K., Amundson, R., Heimsath, A.M., Dietrich, W.E., Briimhall, G.H., 2007. Integration of geochemical mass balance with sediment transport to calculate rates of soil chemical weathering and transport on hillslopes. J. Geophys. Res. 112, F02013.

CHAPTER 3

SUMMARY

Soil chemical weathering and erosion are tied in complex ways to topography and climate. In this study we examine two landscapes that are near to each other in space but which have experienced very different climatic forcings. Sculpting by glaciers carved steep-walled, U-shaped valleys in the Bitterroots that cause soil to be eroded downslope when it has reached a lower degree of weathering than soils in the unglaciated Sapphires, where soils may have longer residence times. We add to a growing body of literature that examines the differences between soil-mantled and rock-dominated landscapes. Rock-dominated landscapes disobey many of the geomorphic transport laws that soil-mantled landscapes adhere to, such as a linear relationship between erosion rate and slope gradient. Our results show differences in soil abundance and extent of soil chemical weathering in our two study catchments. Soil cover is more extensive and thicker in unglaciated Rye Creek than glaciated Lost Horse Creek, as shown in the higher average soil thickness and soil volume in Rye Creek. Despite there being more soil to weather, Rye Creek soils are also more highly weathered than Lost Horse Creek soils, as shown in the higher CDF and lower mass transfer coefficient (tau) values. This is despite higher precipitation rates in the Bitterroots, which indicates that the glacial history of the Bitterroots exerts stronger influence on chemical weathering than modern climate. Although glaciers reset the weathering clock in Lost Horse Creek and not in Rye Creek, we believe that soils have turned over multiple times since the end of glaciation in Rye Creek and that soils simply being older in Rye Creek is not the cause of the higher degree

of weathering there. For example, based on measurements in similar systems, Rye Creek might be estimated to be eroding at an average of 50 mm/ky; on a hillslope with soil thickness of 25 cm, soil residence time would be ~5000 yr, so that we would be measuring the third or fourth generation of soil since glaciers left Lost Horse Creek. Our quantification of these differences and variability in soil extent and chemistry significant improves on past work that has focused solely on continuously soil mantled hillslopes, and we develop new metrics for such landscapes including rock-adjusted CDFs. While we see some landscape-scale differences in weathering, we are unable to identify specific local landscape drivers that may control variability in soil weathering. Such variability in soil thickness may reflect either spatial or temporal heterogeneity, and more research is needed to close in on the drivers that control chemical weathering in such mountainous landscapes.

We add important new data to the collection of measurements on the relationship between climate and weathering, and between soil characteristics and local topography. Our field samples are complemented by remotely sensed land cover data, which help to provide insight into landscape-scale weathering, including steep ridges out of reach of field investigation. Our rock-adjusted metric for soil volume and weathering extent helps to account for the true amount of soil and rock present in soil-mantled areas and we hope it will be useful in further research in the Bitterroots and Sapphires and in other mountain belts around the world.

APPENDICES

APPENDIX A

CALIBRATION OF THE ROCK EXPOSURE INDEX

In order to better understand the transition from a soil-mantled to rock-dominated system, it would be helpful to have an estimate of the slope at which the transition occurs. This will be different in each landscape. In order to determine a threshold slope value in our two systems, we selected three 100m x 100m regions within each of our detailed sample catchments for aerial mapping of bedrock exposure using Google Earth imagery. Patches were chosen to span a variety of soil- and rock-dominated surfaces and a variety of slope gradients and hillslope positions. Following the example of DiBiase et al. (2012), we selected 3 patches in Rye Creek and 3 patches in Lost Horse Creek of approximately 100 x 100 m and identified exposed rock in Google Earth and compare this to slope gradient using our 10m DEM in ArcGIS in order to identify a slope threshold for rock exposure (S*).

In Rye Creek, one patch had no exposed rock. The other two patches had 0.47% and 0.61% rock. In Lost Horse, the patches were found to have 9.57%, 19.16%, and 14.20% rock exposed on their surface. The rest of the surface is mantled by soil. The maximum slope in Rye was 31.4 deg in patch 3; the maximum slope in Lost Horse was 38.7 deg in patch 2. We compared the amount of exposed rock with possible S* of 15 deg (Rye only), 20 deg, 25 deg, 30 deg, and 35 deg.

Our results show that S* = 35 deg has the highest agreement with rock exposure in Lost Horse, the highest threshold we could test ($R^2 = 0.77$). In Rye, slope gradient does not show itself to be a useful metric for predicting rock exposure; at S*=15 deg, $R^2=0.41$, but for all S* above that (20, 25, and 30 deg) R^2 stayed the same at 0.44 ($p=0.54$).

The analysis is displayed below.

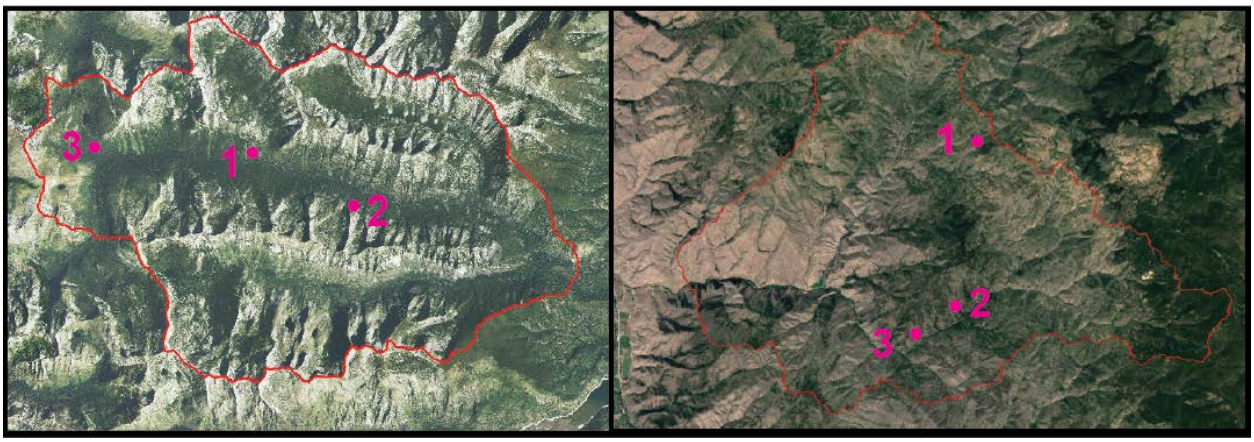

Fig A1. Location of selected patches in a) Lost Horse Creek and b) Rye Creek.

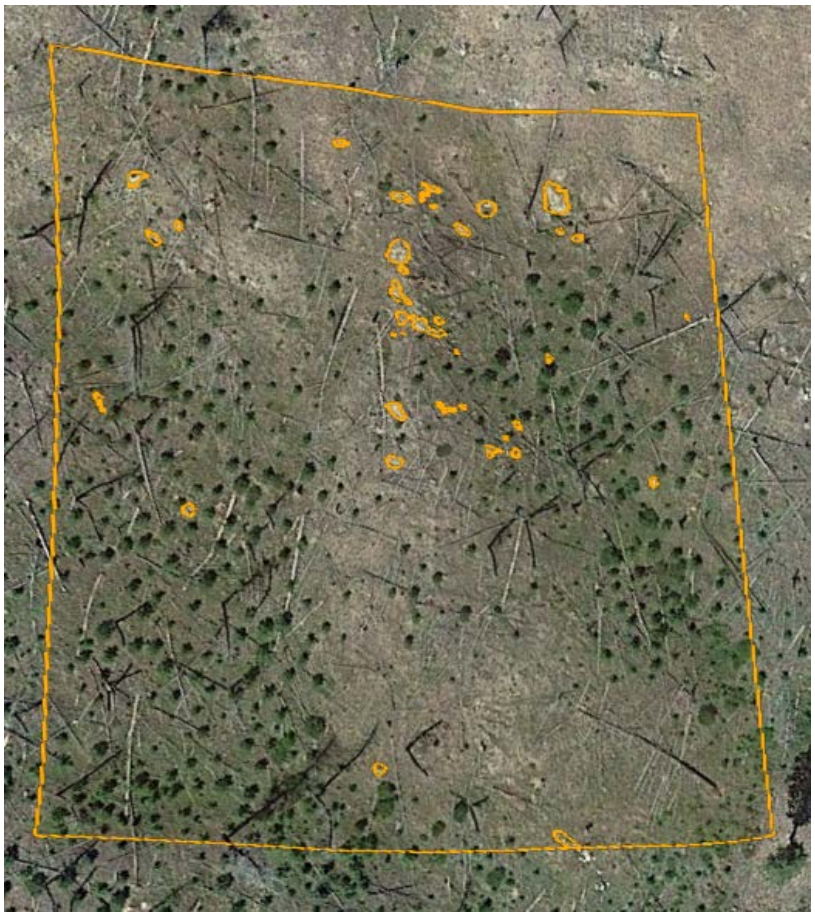

Fig. A2. Rye Patch 3, for example. Rock exposure is circled.

	Lost Horse Creek			Rye Creek		
	Patch 1	Patch 2	Patch 3	Patch 1	Patch 2	Patch 3
Total points	138	128	119	126	112	157
Points <10 deg	0	0	0	20	16	0
Points <15	0	0	0	80	69	5
Points < 20	0	0	9	123	109	49
Points < 25	6	1	98	126	112	126
Points <30	100	67	119	0	0	154
Points <35	138	116	0	0	0	157
Points <40	0	128	0	0	0	0
Percent area <10 deg	0	0	0	16	14	0
Percent area < 15	0	0	0	63	62	3
Percent area <20	0	0	8	98	97	31
Percent area <25	4	1	82	100	100	80
Percent area <30	72	52	100	100	100	98
Percent area <35	100	91	100	100	100	100
Percent area <40	100	100	100	100	100	100
% Rock (aerial photo)	9.57	19.16	14.20	0.48	0.00	0.61

Table A1. Slope and landcover distributions for three 100 x 100 m^2 patches in Lost Horse and Rye Creeks. The number of points above each slope threshold is determined for each patch. This is converted to a percent of patch area. % rock mapped is judged from Google Earth.

	Lost Horse		Rye	
S*	**R squared**	**p-value**	**R squared**	**p-value**
15 deg			0.41	0.55
20 deg	0.00	0.99	0.44	0.54
25 deg	0.00	0.96	0.44	0.54
30 deg	0.19	0.71	0.44	0.54
35 deg	0.77	0.32	1.00	
40 deg	1.00			

Table A2. Correlations between potential S* values and rock exposure

APPENDIX B

SAMPLE FIELD DATA

Lost Horse Creek

Soil Sample ID	Rock Sample ID	Latitude	Longitude	Soil Depth	Soil Cover Estimate		Soil volume
				(cm)	% soil	SE (n=9)	
LST22	LST23	46.14	-114.39	10	76.67	5.27	767
LST24	LST25	46.14	-114.39	40	91.67	1.18	3667
LST26	LST27	46.14	-114.39	10	88.89	1.82	889
LST30	LST31	46.13	-114.43		100.00	0.00	0
LST32	LST33	46.13	-114.43	10	95.00		950
LST37	LST38	46.16	-114.50	12	94.44	2.42	1133
LST40	LST41	46.16	-114.49	40	97.44	0.67	3898
LST43	LST44	46.16	-114.49	2			0
LST45	LST46	46.16	-114.49	10	77.44	5.04	774
LST47	LST48	46.16	-114.49	10	67.78	8.78	678
LST49	LST50	46.14	-114.44	12	86.44	9.20	1037
LST51	LST52	46.15	-114.44	5	73.33	6.01	367
LST54	LST55	46.15	-114.44	15	71.11	8.89	1067
LST56	LST57	46.11	-114.28	40	85.67	3.70	3427
LST59	LST60	46.11	-114.28	34	77.78	7.55	2644
LST62	LST63	46.15	-114.48	15	99.33	0.44	1490
LST64	LST65	46.15	-114.48	22	61.67	4.25	1357
LST66	LST68	46.14	-114.47	105			0
LST70	LST71	46.14	-114.47	30			0
LST72	LST73	46.14	-114.47	15			0
LST77	LST78	46.14	-114.50	10	100	0	1000
LST79	LST80	46.10	-114.28	2	68	4	136
LST81	LST82	46.13	-114.37	60	99	1	5940
LST103	LST104	46.11	-114.29		100	0	0
LST110	LST111	46.14	-114.48	20	86	10	1720
LST112	LST113	46.14	-114.48	20	99	0	1980
LST114	LST115	46.14	-114.47		100	0	0

Rye Creek

Soil Sample ID	Rock Sample ID	Latitude	Longitude	Soil Depth	Soil Cover Estimate		Soil volume
				(cm)	% soil	SE (n=9)	
RYE48	RYE49	46.01	-113.97	45	100	0	4500
RYE55	RYE56	46.01	-113.97	50	98	1	4900
RYE57	RYE58	46.00	-113.97	50	100	0	5000
RYE59	RYE60	46.01	-113.90	50	100	0	5000
RYE63	RYE64	46.02	-113.92	35	100	0	3500
RYE68	RYE69	45.98	-113.88	30	100	0	3000
RYE72	RYE73	46.01	-113.96	45	100	0	4500
RYE74	RYE75	46.00	-113.95	30	98	1	2940
RYE76	RYE77	46.00	-113.95	19	88	5	1672
RYE78	RYE79	45.99	-113.95	20	100	0	2000
RYE80	RYE81	46.01	-113.96	75	100	0	7500
RYE82	RYE83	46.00	-113.96	35	97	0	3395
RYE84	RYE85	46.01	-113.96	66	100	0	6600
RYE86	RYE87	46.00	-113.96	35			0
RYE88	RYE89	46.00	-113.97	35	100	0	3500
RYE102	RYE103	45.99	-113.95	12	99	1	1188
RYE104	RYE105	45.99	-113.95	10	100	0	1000
RYE106	RYE107	45.99	-113.95	21	100	0	2100
RYE110	RYE111	45.99	-113.88	12	99	1	1188
RYE112	RYE113	45.96	-113.99	20	100	0	2000
RYE26	RYE27	46.00	-113.99				0
RYE28	RYE29	46.01	-113.99				0
RYE38	RYE39	46.00	-113.99	45	100	0	4500
RYE44	RYE45	46.01	-113.99	70			0
RYE61	RYE62	46.02	-113.89	10	53	9	530
RYE70	RYE71	46.01	-113.96	35	100	0	3500
RYE100	RYE101	45.99	-113.96	25	97	2	2425
RYE108	RYE109	45.99	-113.88	4	99	1	396

APPENDIX C

SAMPLE GIS-DERIVED DATA

Lost Horse Creek

Soil Sample ID	Rock Sample ID	Elev (m)	Slope (deg)	Aspect	Total curvature	Profile curvature	Planar curvature	NLCD classification Code	NLCD classification Name
LST22	LST23	2028.91	31.33	158.96	-0.57	0.11	-0.46	71	grass/herb
LST24	LST25	1917.10	33.83	157.13	0.63	-0.09	0.54	42	forest
LST26	LST27	1794.50	28.75	178.02	1.16	-0.48	0.68	42	forest
LST30	LST31	1798.08	21.63	5.46	0.29	-0.30	-0.01	42	forest
LST32	LST33	1868.38	19.01	22.03	0.05	-0.31	-0.26	42	forest
LST37	LST38	2036.62	13.48	221.90	-0.01	0.05	0.04	42	forest
LST40	LST41	2094.20	22.75	235.78	-0.06	0.22	0.16	42	forest
LST43	LST44	2289.33	16.48	234.30	0.14	-0.04	0.09	42	forest
LST45	LST46	2219.52	22.48	245.86	0.03	0.07	0.10	42	forest
LST47	LST48	2098.23	25.71	238.32	-0.46	0.08	-0.38	42	forest
LST49	LST50	1669.98	3.25	186.69	0.03	-0.10	-0.07	52	shrub/scrub
LST51	LST52	1810.76	22.58	207.55	0.55	-0.06	0.49	42	forest
LST54	LST55	1880.84	28.70	191.08	0.21	0.04	0.25	42	forest
LST56	LST57	1325.31	42.38	178.55	-1.29	1.24	-0.05	42	forest
LST59	LST60	1371.44	15.89	230.35	-0.39	0.41	0.02	42	forest
LST62	LST63	1863.89	26.68	159.24	1.12	-0.45	0.66	52	shrub/scrub
LST64	LST65	1891.26	24.04	155.75	-2.38	0.91	-1.47	42	forest
LST66	LST68	1733.77	7.65	347.17	-0.47	0.24	-0.23	42	forest
LST70	LST71	1769.34	17.04	352.25	-0.15	0.42	0.27	42	forest
LST72	LST73	1785.87	20.27	351.15	-0.42	0.25	-0.17	42	forest
LST77	LST78	2018.33	11.46	25.40	0.08	0.10	0.18	42	forest
LST79	LST80	1322.14	11.25	99.37	0.13	0.10	0.22	42	forest
LST81	LST82	1503.87	4.20	215.07	0.07	0.00	0.07	42	forest
LST103	LST104	1319.94	4.19	173.89	0.24	-0.20	0.04	42	forest
LST110	LST111	1783.19	13.31	176.72	-0.17	0.13	-0.04	42	forest
LST112	LST113	1785.74	19.53	153.00	-0.24	-0.08	-0.32	42	forest
LST114	LST115	1737.05	7.05	157.08	-0.27	0.19	-0.08	42	forest

Soil Sample ID	Rock Sample ID	Contributing area (D-infinity) (sq m)	January precip (mm/yr)	July precip (mm/yr)	January max temp	July max temp	January min temp	July min temp	January mean temp	July mean temp
					(deg C)					
LST22	LST23	189.2	150.4	40.98	-1.3	22.25	-9.55	6.36	-5.4	14.6
LST24	LST25	161.6	150.4	40.98	-1.3	22.25	-9.55	6.36	-5.4	14.6
LST26	LST27	187.5	150.4	40.98	-1.3	22.25	-9.55	6.36	-5.4	14.6
LST30	LST31	5973.6	147.8	40	-0.6	23.24	-9.82	5.62	-5.2	14.7
LST32	LST33	2592.8	147.8	40	-0.6	23.24	-9.82	5.62	-5.2	14.7
LST37	LST38	749.1	226.4	52.81	-2.7	20.58	-10.33	7.35	-6.5	14.2
LST40	LST41	474.3	226.4	52.81	-2.7	20.58	-10.33	7.35	-6.5	14.2
LST43	LST44	207.1	226.4	52.81	-2.7	20.58	-10.33	7.35	-6.5	14.2
LST45	LST46	338.4	237.4	54.24	-1.7	21.08	-9.73	6.85	-5.7	14.3
LST47	LST48	859.4	237.4	54.24	-1.7	21.08	-9.73	6.85	-5.7	14.3
LST49	LST50	1449.6	139.3	38.42	0.0	24.01	-9.38	5.58	-4.7	15.0
LST51	LST52	190.9	139.3	38.42	0.0	24.01	-9.38	5.58	-4.7	15.0
LST54	LST55	484.2	172.1	44.69	-1.8	20.68	-9.98	6.74	-5.9	14.0
LST56	LST57	219.2	80.1	34.2	1.3	27.39	-8.45	7.67	-3.6	17.8
LST59	LST60	197.4	80.1	34.2	1.3	27.39	-8.45	7.67	-3.6	17.8
LST62	LST63	190.3	191.3	50.16	-1.4	21.12	-9.71	6.74	-5.6	14.2
LST64	LST65	2117.5	199.1	50.26	-1.8	20.85	-9.89	7.15	-5.8	14.3
LST66	LST68	1214.1	156.5	41.61	-0.4	23.82	-9.47	5.64	-4.9	15.0
LST70	LST71	708.8	156.5	41.61	-0.4	23.82	-9.47	5.64	-4.9	15.0
LST72	LST73	846.5	156.5	41.61	-0.4	23.82	-9.47	5.64	-4.9	15.0
LST77	LST78	113.3	210.02	49.81	-1.05	21.86	-9.28	6.37	-5.2	14.4
LST79	LST80	60.6	75.4	33.8	1.5	27.36	-8.48	7.68	-3.5	17.8
LST81	LST82	107.3	142.0	40.01	1.2	25.48	-8.63	6.43	-3.7	16.2
LST103	LST104	817.7	80.1	34.2	1.3	27.39	-8.45	7.67	-3.6	17.8
LST110	LST111	535.4	162.3	42.98	-0.5	23.72	-9.56	5.62	-5.0	14.9
LST112	LST113	735.7	170.08	44.66	-0.62	23.56	-9.61	5.70	-5.1	14.9
LST114	LST115	1007.6	156.5	41.61	-0.4	23.82	-9.47	5.64	-4.9	15.0

Notes: Precip and temperature values are 30-year normals, 1981-2010 (PRISM Climate Group)

Rye Creek

Soil Sample ID	Rock Sample ID	Elev	Slope	Aspect	Total curvature	Profile curvature	Planar curvature	NLCD classification	
		(m)	(deg)					Code	Name
RYE48	RYE49	1987.91	9.37	146.46	-0.71	0.27	-0.43	42	forest
RYE55	RYE56	1900.26	17.88	115.28	1.95	-0.89	1.05	52	shrub/scrub
RYE57	RYE58	1872.36	15.83	74.98	-0.18	-0.11	-0.29	42	forest
RYE59	RYE60	2052.91	7.92	42.62	0.14	-0.13	0.01	42	forest
RYE63	RYE64	2026.38	21.14	219.68	-0.05	0.25	0.20	42	forest
RYE68	RYE69	2054.19	16.10	315.79	0.04	0.31	0.35	42	forest
RYE72	RYE73	1866.44	27.90	89.10	-1.62	0.89	-0.73	52	shrub/scrub
RYE74	RYE75	1672.62	24.98	100.35	-3.00	1.56	-1.45	52	shrub/scrub
RYE76	RYE77	1636.57	24.93	265.05	-3.57	3.61	0.04	42	forest
RYE78	RYE79	1724.45	16.62	166.99	0.62	-0.17	0.45	52	shrub/scrub
RYE80	RYE81	1868.20	8.63	195.16	0.89	-0.43	0.46	52	shrub/scrub
RYE82	RYE83	1851.18	19.04	207.85	0.22	0.09	0.30	52	shrub/scrub
RYE84	RYE85	1891.79	9.89	217.11	0.40	-0.33	0.07	52	shrub/scrub
RYE86	RYE87	1857.16	11.21	48.33	0.63	-0.21	0.42	42	forest
RYE88	RYE89	1882.28	12.71	80.12	-0.15	0.14	-0.01	42	forest
RYE102	RYE103	1678.68	29.84	348.46	-0.20	0.24	0.04	42	forest
RYE104	RYE105	1802.29	25.87	343.55	0.65	-0.61	0.04	42	forest
RYE106	RYE107	1781.82	17.20	305.54	1.31	-0.69	0.62	42	forest
RYE110	RYE111	1989.36	16.63	356.53	-0.36	0.18	-0.17	42	forest
RYE112	RYE113	1476.53	23.24	28.60	-1.05	0.72	-0.33	52	shrub/scrub
RYE26	RYE27	1817.86	8.36	317.99	1.45	-0.58	0.88	42	forest
RYE28	RYE29	1781.47	18.00	328.91	-1.74	1.63	-0.11	42	forest
RYE38	RYE39	1826.41	10.28	320.20	0.43	0.11	0.53	42	forest
RYE44	RYE45	1773.09	24.85	17.84	-1.56	0.97	-0.59	42	forest
RYE61	RYE62	2040.29	17.87	149.67	-0.78	1.15	0.37	42	forest
RYE70	RYE71	1949.00	12.18	151.08	0.74	-0.29	0.44	42	forest
RYE100	RYE101	1599.90	38.13	327.59	-0.78	0.92	0.13	42	forest
RYE108	RYE109	2032.73	15.17	12.68	0.68	-0.24	0.45	42	forest

Soil Sample ID	Rock Sample ID	Contributing area (D-infinity)	January precip	July precip	January max temp	July max temp	January min temp	July min temp	January mean temp	July mean temp
		(sq m)	(mm/yr)	(mm/yr)			(deg C)			
RYE48	RYE49	183.1	46.5	37.01	-1.5	23.31	-9.64	7.04	-5.6	15.3
RYE55	RYE56	21.1	46.5	37.01	-1.5	23.31	-9.64	7.04	-5.6	15.3
RYE57	RYE58	165.4	41.3	36.49	-1.7	23.83	-9.94	7.70	-5.8	15.9
RYE59	RYE60	122.0	70.6	38.92	-2.3	22.38	-10.36	5.98	-6.3	14.3
RYE63	RYE64	85.3	63.4	38.3	-1.9	22.25	-9.82	6.73	-5.9	14.6
RYE68	RYE69	82.5	70.2	39.57	-2.2	22.60	-10.36	6.31	-6.3	14.6
RYE72	RYE73	109.9	46.7	36.96	-1.9	23.58	-10.18	7.45	-6.0	15.6
RYE74	RYE75	264.5	41.8	35.85	-0.7	24.86	-9.49	6.39	-5.1	15.8
RYE76	RYE77	70.3	39.3	35.41	-0.5	25.38	-9.20	6.30	-4.8	16.0
RYE78	RYE79	33.5	39.3	35.41	-0.5	25.38	-9.20	6.30	-4.8	16.0
RYE80	RYE81	17.6	46.7	36.96	-1.9	23.58	-10.18	7.45	-6.0	15.6
RYE82	RYE83	59.5	46.5	37.01	-1.5	23.31	-9.64	7.04	-5.6	15.3
RYE84	RYE85	36.1	46.5	37.01	-1.5	23.31	-9.64	7.04	-5.6	15.3
RYE86	RYE87	41.8	46.5	37.01	-1.5	23.31	-9.64	7.04	-5.6	15.3
RYE88	RYE89	70.4	46.5	37.01	-1.5	23.31	-9.64	7.04	-5.6	15.3
RYE102	RYE103	54.6	37.8	35.8	-0.7	25.09	-9.35	6.51	-5.1	15.9
RYE104	RYE105	127.6	37.6	35.38	-1.5	24.12	-9.97	7.12	-5.7	15.7
RYE106	RYE107	86.7	37.6	35.38	-1.5	24.12	-9.97	7.12	-5.7	15.7
RYE110	RYE111	284.9	81.8	39.91	-2.2	22.58	-10.53	5.80	-6.4	14.3
RYE112	RYE113	154.9	33.2	33.53	0.3	26.60	-9.79	7.07	-4.7	17.0
RYE26	RYE27	26.7	39.5	35.97	-1.6	24.44	-9.78	7.18	-5.7	15.9
RYE28	RYE29	68.9	39.5	35.97	-1.6	24.44	-9.78	7.18	-5.7	15.9
RYE38	RYE39	27.4	39.5	35.97	-1.6	24.44	-9.78	7.18	-5.7	15.9
RYE44	RYE45	67.9	39.5	35.97	-1.6	24.44	-9.78	7.18	-5.7	15.9
RYE61	RYE62	114.5	77.0	39.11	-2.3	22.39	-10.45	5.90	-6.4	14.3
RYE70	RYE71	23.4	46.5	37.01	-1.5	23.31	-9.64	7.04	-5.6	15.3
RYE100	RYE101	102.5	37.8	35.8	-0.7	25.09	-9.35	6.51	-5.1	15.9
RYE108	RYE109	61.6	81.8	39.91	-2.2	22.58	-10.53	5.80	-6.4	14.3

Notes: Precip and temperature values are 30-year normals, 1981-2010 (PRISM Climate Group)

APPENDIX D

ELEMENTAL COMPOSITION OF FIELD SAMPLES FROM X-RAY FLUORESCENCE SPECTROSCOPY

Soil Samples

Method Code	WEI-21	ME-XRF06	ME-XRF06	ME-XRF06	ME-XRF06	ME-XRF06	ME-XRF06	ME-XRF06	ME-XRF06	ME-XRF06	ME-XRF06	ME-XRF06	ME-XRF06	ME-XRF06	ME-XRF06	ME-XRF06	ME-XRF06	ME-XRF06	ME-XRF05	ME-XRF05
SAMPLE	Recvd Wt.	SiO2	Al2O3	Fe2O3	CaO	MgO	Na2O	K2O	Cr2O3	TiO2	MnO	P2O5	SrO	BaO	LOI	Total	Y	Zr		
DESCRIPTION	kg	%	%	%	%	%	%	%	%	%	%	%	%	%	%	%	ppm	ppm		
LST22	0.04	61.36	13.5	2.4	1.8	0.5	3.24	2.74	<0.01	0.26	0.08	0.13	0.08	0.18	12.7	98.97	7	149		
LST24	0.04	64.66	13.67	2.03	1.99	0.4	3.64	2.87	<0.01	0.23	0.07	0.078	0.1	0.18	9.19	99.09	6	155		
LST26	0.04	65.68	13.74	2.16	1.79	0.36	3.71	2.92	<0.01	0.25	0.07	0.068	0.1	0.17	7.46	98.47	6	144		
LST30	0.04	53.29	13.52	3.27	1.62	1	2.48	2.1	<0.01	0.5	0.04	0.081	0.04	0.1	21.6	99.64	11	133		
LST32	0.03	43.21	11.09	3.39	1.46	1.01	1.89	1.58	<0.01	0.5	0.14	0.17	0.03	0.08	33.6	98.15	12	124		
LST37	0.04	65.64	12.53	1.99	1.3	0.31	3.02	3.14	<0.01	0.24	0.08	0.071	0.06	0.15	10.45	98.98	8	115		
LST39	0.04	71.34	14.19	1.91	1.25	0.34	3.35	3.63	<0.01	0.2	0.02	0.035	0.07	0.16	2.96	99.44	10	117		
LST40	0.04	67.81	13.93	2.34	1.22	0.31	3.26	3.49	<0.01	0.21	0.04	0.066	0.07	0.16	6.85	99.75	9	129		
LST43	0.04	54.28	13.45	4.31	1.24	0.74	2.35	2.09	<0.01	0.68	0.09	0.168	0.03	0.09	20.5	100	14	182		
LST45	0.03	56.84	12.67	2.76	1.1	0.51	2.59	2.58	<0.01	0.33	0.05	0.089	0.04	0.11	19.5	99.17	9	134		
LST47	0.04	31.73	7.9	1.87	1.13	0.47	1.38	1.29	<0.01	0.29	0.29	0.188	0.02	0.07	52.6	99.24	11	89		
LST49	0.04	61.44	12.5	2.03	1.52	0.42	3.12	2.6	<0.01	0.23	0.05	0.204	0.07	0.14	14.8	99.11	8	123		
LST51	0.03	54.93	10.78	1.62	1.39	0.29	2.76	2.33	<0.01	0.2	0.11	0.085	0.06	0.13	23.7	98.37	6	111		
LST54	0.04	55.47	11.86	2.4	1.4	0.4	2.73	2.28	<0.01	0.31	0.05	0.063	0.06	0.12	22	99.15	7	122		
LST56	0.04	66.85	14.66	2.36	1.64	0.7	3.37	3.6	<0.01	0.26	0.07	0.148	0.07	0.15	5.67	99.54	11	146		
LST58	0.04	70.13	14.66	2.83	1.56	0.5	3.8	3.21	<0.01	0.25	0.04	0.051	0.08	0.16	2.59	99.85	9	161		
LST59	0.04	65.27	14.25	2.43	1.66	0.55	3.14	2.81	<0.01	0.3	0.15	0.154	0.06	0.15	8.79	99.72	10	148		
LST62	0.05	59.04	12.12	2.58	1.44	0.45	2.83	2.69	<0.01	0.34	0.13	0.125	0.05	0.13	17.75	99.66	10	126		
LST64	0.04	55.11	12.24	2.95	1.34	0.59	2.57	2.39	<0.01	0.33	0.15	0.145	0.04	0.11	22	99.97	10	123		
LST66	0.04	53.7	12.53	2.36	1.24	0.67	2.18	1.62	<0.01	0.45	0.04	0.226	0.03	0.08	24.7	99.82	16	147		
LST70	0.04	59.88	15.54	3.7	1.58	0.79	3.02	2.44	<0.01	0.53	0.08	0.107	0.05	0.11	11.65	99.49	13	163		
LST72	0.04	56.68	12.4	2.43	1.62	0.52	2.92	2.44	<0.01	0.28	0.08	0.083	0.05	0.12	19.45	99.09	8	113		
LST74	0.04	66.58	13.39	2.9	1.37	0.51	3.08	2.87	<0.01	0.4	0.03	0.075	0.06	0.13	8.6	100	12	172		
LST77	0.03	58.15	13.86	3.88	1.35	0.59	2.86	2.27	<0.01	0.57	0.03	0.08	0.04	0.1	15.8	99.57	12	185		
LST79	0.04	58.74	12.62	2.18	1.75	0.48	3	2.43	<0.01	0.24	0.16	0.157	0.05	0.13	16.4	98.34	10	133		
LST81	0.03	65.2	12.66	1.14	1.73	0.18	3.63	2.63	<0.01	0.17	0.07	0.07	0.08	0.15	12.2	99.9	5	142		
LST103	0.05	67.72	14.82	1.91	1.59	0.36	3.64	2.83	<0.01	0.26	0.11	0.403	0.07	0.15	5.78	99.64	7	146		
LST110	0.04	49.52	11.61	2.16	1.14	0.47	2.49	2.15	<0.01	0.29	0.17	0.206	0.04	0.09	28.6	98.94	11	115		
LST112	0.04	49.19	11.27	3.08	1.37	0.6	2.24	1.96	<0.01	0.41	0.19	0.132	0.03	0.09	27.7	98.27	10	128		
LST114	0.03	45.36	11.42	2.6	1.13	0.64	2.09	1.91	<0.01	0.35	0.11	0.28	0.03	0.08	33	99.02	11	124		
RYE26	0.04	71.36	12.31	2.48	1.05	0.56	2.44	2.66	<0.01	0.35	0.17	0.113	0.02	0.09	5.36	98.96	16	210		
RYE28	0.04	68.73	13.61	2.16	1.27	0.4	2.87	3.35	<0.01	0.25	0.09	0.079	0.03	0.13	5.83	98.81	15	138		
RYE38	0.04	70.87	11.51	2.46	1.05	0.54	1.95	2.64	<0.01	0.35	0.12	0.094	0.02	0.09	8.16	99.86	19	206		
RYE44	0.03	65.95	14.07	3.1	1.25	0.69	2.47	2.87	<0.01	0.43	0.16	0.451	0.03	0.11	7.34	98.91	17	209		
RYE48	0.04	68.22	14.01	2.36	1.57	0.47	2.87	3.19	<0.01	0.37	0.09	0.109	0.04	0.15	6.23	99.71	13	177		
RYE55	0.04	66.75	13.45	3.92	1.37	1.2	2.07	2.02	0.01	0.56	0.2	0.477	0.02	0.09	7.84	99.99	21	301		
RYE57	0.05	67.01	14.26	2.25	1.34	0.49	2.77	3.33	<0.01	0.31	0.24	0.312	0.03	0.13	7.39	99.86	13	153		
RYE59	0.04	64.26	13.97	3.66	1.25	0.88	2.28	2.18	<0.01	0.49	0.09	0.291	0.02	0.09	10.2	99.67	18	246		
RYE61	0.04	72.05	12.25	2.43	1.05	0.76	2.93	2.55	<0.01	0.34	0.07	0.076	0.02	0.13	5.24	99.91	15	242		
RYE63	0.03	65.73	14.08	3.35	1.63	0.65	2.7	3.06	<0.01	0.36	0.14	0.281	0.03	0.14	7.78	99.93	12	174		
RYE68	0.04	66.51	12.96	2.81	1.45	0.67	2.62	2.2	<0.01	0.46	0.05	0.088	0.03	0.09	9.12	99.08	17	217		
RYE70	0.05	68.36	13.6	2.11	1.21	0.35	2.53	3.51	<0.01	0.29	0.24	0.09	0.04	0.21	5.99	98.54	9	179		
RYE72	0.04	65.7	14.3	2.74	1.44	0.52	2.46	3.28	<0.01	0.35	0.18	0.32	0.03	0.21	8.37	99.9	12	178		
RYE74	0.04	67.29	13.81	3.33	1.96	0.77	2.79	3.02	<0.01	0.36	0.18	0.116	0.03	0.11	6.3	100.05	14	173		
RYE76	0.04	62.45	12.2	2.67	1.86	0.54	2.67	2.73	<0.01	0.31	0.14	0.169	0.04	0.14	13.6	99.52	13	180		
RYE78	0.05	69.12	13.74	2.58	1.59	0.73	2.56	2.87	<0.01	0.32	0.19	0.09	0.03	0.12	5.89	99.84	10	135		
RYE80	0.04	68.69	14.43	2.4	1.53	0.46	3.06	3.66	<0.01	0.28	0.13	0.088	0.04	0.23	4.9	99.89	8	182		
RYE82	0.05	68.99	14.24	3.27	2.23	0.94	2.98	3.09	<0.01	0.39	0.11	0.072	0.04	0.1	3.43	99.89	15	153		
RYE84	0.04	70.18	13.96	2.54	1.53	0.42	3.24	3.23	<0.01	0.32	0.18	0.063	0.06	0.2	4.02	99.96	9	245		
RYE86	0.04	63.01	14.18	3.63	1.55	0.89	2.55	2.93	<0.01	0.44	0.2	0.382	0.03	0.14	9.22	99.15	16	172		
RYE88	0.04	65.55	14.22	3.52	1.49	0.89	2.32	2.77	<0.01	0.46	0.32	0.234	0.03	0.11	7.19	99.1	14	150		
RYE100	0.04	67.57	14.24	2.78	1.34	0.62	2.74	2.93	<0.01	0.4	0.09	0.178	0.03	0.12	6.65	99.7	15	185		
RYE102	0.04	65.97	14.34	2.69	1.78	0.64	2.98	2.93	<0.01	0.37	0.16	0.12	0.04	0.13	7.9	100.05	13	175		
RYE104	0.04	69.96	13.03	2.48	1.44	0.62	2.34	3.57	<0.01	0.29	0.2	0.082	0.03	0.14	5.68	99.87	10	121		
RYE106	0.04	69.97	12.96	2.31	1.45	0.5	2.51	3.83	<0.01	0.25	0.18	0.069	0.04	0.15	5.7	99.92	11	119		
RYE108	0.04	62.94	16.05	4.65	2.72	1.09	3.2	1.4	<0.01	0.59	0.08	0.229	0.04	0.13	6.68	99.8	12	331		
RYE110	0.04	60.63	15.72	4.5	1.65	0.75	2.79	2.1	<0.01	0.53	0.08	0.21	0.03	0.09	10.05	99.12	17	287		
RYE112	0.04	67.78	13.56	3.05	2.07	0.89	2.96	2.38	0.01	0.42	0.27	0.163	0.03	0.12	6.35	100.05	16	173		

Rock Samples																				
Method Code	WEI-21	ME-XRF06	ME-XRF06	ME-XRF06	ME-XRF06	ME-XRF06	ME-XRF06	ME-XRF06	ME-XRF06	ME-XRF06	ME-XRF06	ME-XRF06	ME-XRF06	ME-XRF06	ME-XRF06	ME-XRF06	ME-XRF06	ME-XRF06	ME-XRF05	ME-XRF05
SAMPLE	Recvd Wt.	SiO2	Al2O3	Fe2O3	CaO	MgO	Na2O	K2O	Cr2O3	TiO2	MnO	P2O5	SrO	BaO	LOI	Total	Y	Zr		
DESCRIPTION	kg	%	%	%	%	%	%	%	%	%	%	%	%	%	%	%	ppm	ppm		
LST23	0.04	70.67	15.52	1.9	2.01	0.45	4.34	3.7	<0.01	0.24	0.02	0.058	0.13	0.25	0.35	99.62	4	158		
LST25	0.05	70.17	16.05	1.88	2.17	0.4	4.81	3.32	<0.01	0.21	0.02	0.06	0.13	0.21	0.24	99.66	5	161		
LST27	0.05	71	15.29	1.96	1.92	0.42	4.44	3.62	0.01	0.22	0.02	0.081	0.11	0.19	0.17	99.44	5	154		
LST31	0.06	72.5	14.94	1.47	1.55	0.32	4.28	3.58	<0.01	0.17	0.02	0.056	0.08	0.16	0.59	99.72	6	119		
LST33	0.06	62.06	12.72	5.16	6.75	5.97	3.26	2.31	0.02	0.41	0.09	0.049	0.07	0.11	0.59	99.57	10	81		
LST34	0.04	73.62	13.5	1.57	1.28	0.26	3.58	4.06	<0.01	0.15	0.02	0.052	0.05	0.11	1.17	99.42	3	78		
LST38	0.06	72.87	15.04	1.49	1.7	0.3	4.41	3.57	<0.01	0.15	0.02	0.031	0.08	0.16	0.38	100.2	4	110		
LST41	0.05	73.06	14.77	1.51	1.56	0.31	4.11	3.76	<0.01	0.16	0.02	0.047	0.09	0.19	0.67	100.25	5	130		
LST42	0.05	71.9	15.27	1.5	1.56	0.33	4.18	3.85	<0.01	0.17	0.03	0.036	0.09	0.18	0.69	99.78	4	114		
LST44	0.04	73.57	14.7	1.46	1.59	0.26	4.25	3.66	<0.01	0.14	0.02	0.03	0.09	0.17	0.4	100.35	3	104		
LST46	0.06	73.09	14.78	1.4	1.55	0.31	4.29	3.62	<0.01	0.15	0.03	0.031	0.09	0.17	0.3	99.8	6	112		
LST48	0.05	76.19	13.19	1.19	1.29	0.22	3.64	3.69	<0.01	0.11	0.02	0.026	0.08	0.17	0.54	100.35	4	104		
LST50	0.06	72.67	14.71	1.29	1.92	0.27	4.4	3.09	<0.01	0.13	0.02	0.041	0.11	0.16	0.55	99.35	4	114		
LST52	0.06	72.45	14.98	1.54	1.69	0.31	4.18	3.8	<0.01	0.15	0.02	0.056	0.1	0.22	0.37	99.87	4	126		
LST53	0.06	71.88	15.12	1.47	1.64	0.31	4.28	3.95	<0.01	0.16	0.02	0.041	0.1	0.2	0.67	99.84	6	125		
LST55	0.06	69.42	16.02	2.76	2.18	0.67	4.72	3.09	<0.01	0.32	0.03	0.105	0.11	0.15	0.48	100.05	8	136		
LST57	0.06	71.87	15.63	1.02	1.48	0.21	4.45	4.16	<0.01	0.1	0.02	0.048	0.09	0.18	0.56	99.81	5	75		
LST60	0.04	72.76	14.93	1.41	1.71	0.29	4.51	3.36	<0.01	0.14	0.02	0.05	0.09	0.16	0.24	99.67	5	108		
LST61	0.06	71.78	15.37	1.45	1.69	0.29	4.49	3.79	<0.01	0.16	0.02	0.046	0.1	0.18	0.97	100.35	4	116		
LST63	0.04	73.49	14.57	1.29	1.24	0.21	4.25	3.86	<0.01	0.11	0.02	0.035	0.08	0.16	0.42	99.73	5	84		
LST65	0.06	72.54	15.08	1.3	1.55	0.24	4.31	3.76	<0.01	0.12	0.02	0.028	0.08	0.15	0.53	99.71	5	108		
LST68	0.04	73.46	13.97	1.23	1.47	0.42	3.8	3.83	<0.01	0.11	0.02	0.044	0.07	0.17	0.7	99.28	6	101		
LST71	0.05	74.06	14.18	1.15	1.4	0.25	4.39	3.18	<0.01	0.11	0.02	0.024	0.07	0.13	0.47	99.45	4	100		
LST73	0.04	71.72	15.32	1.63	1.93	0.34	4.65	3.2	<0.01	0.15	0.02	0.029	0.1	0.16	0.39	99.62	4	132		
LST76	0.05	73.71	13.15	2.4	1.24	0.94	3.14	3.39	<0.01	0.26	0.03	0.028	0.06	0.12	0.71	99.18	9	161		
LST78	0.06	69.2	16.35	1.94	1.59	0.5	4.85	4.37	<0.01	0.21	0.03	0.05	0.08	0.19	0.55	99.9	10	104		
LST80	0.05	72.27	15.09	1.6	1.57	0.3	4.39	3.77	<0.01	0.16	0.02	0.07	0.09	0.18	0.32	99.83	6	123		
LST82	0.05	72.48	14.86	1.47	1.78	0.32	4.31	3.56	<0.01	0.14	0.02	0.051	0.1	0.19	0.29	99.58	5	119		
LST104	0.05	74.55	13.44	1.9	1.52	0.37	3.96	3.04	<0.01	0.17	0.03	0.069	0.08	0.14	0.43	99.69	8	143		
LST111	0.06	71.58	15.32	1.54	1.64	0.29	4.48	3.75	<0.01	0.14	0.02	0.032	0.08	0.16	0.49	99.52	5	118		
LST113	0.05	73.11	14.74	1.28	1.5	0.27	4.27	3.8	<0.01	0.1	0.02	0.03	0.08	0.16	0.37	99.73	4	99		
LST115	0.05	73.89	14.32	1.11	1.33	0.16	3.88	4.17	<0.01	0.1	0.02	0.044	0.05	0.11	0.68	99.87	4	83		
RYE27	0.04	85.11	6.27	2.82	0.11	0.73	0.75	3.12	<0.01	0.31	0.05	0.037	0.01	0.06	0.52	99.89	20	246		
RYE29	0.05	76.25	12.31	1.93	0.64	0.35	2.86	4.71	<0.01	0.3	0.02	0.023	0.01	0.04	0.62	100.05	19	171		
RYE39	0.05	80.02	9.38	3.83	0.07	0.95	0.49	2.86	<0.01	0.58	0.05	0.027	<0.01	0.05	0.84	99.16	21	293		
RYE45	0.05	84.63	5.93	3.05	0.13	0.78	0.83	3.11	<0.01	0.46	0.04	0.025	<0.01	0.05	0.4	99.44	11	511		
RYE49	0.04	74.25	14.1	1.22	1.2	0.15	3.56	4.55	<0.01	0.1	0.03	0.036	0.04	0.18	0.63	100.05	6	96		
RYE56	0.05	79.67	10	2.19	0.77	0.88	2.41	2.6	<0.01	0.25	0.02	0.048	0.02	0.08	0.72	99.65	14	173		
RYE58	0.04	75.36	13.66	0.84	0.68	0.07	3.51	4.97	<0.01	0.05	0.02	0.031	0.01	0.03	0.63	99.85	15	33		
RYE60	0.06	85.13	6.64	1.82	0.26	1.31	1.58	2.39	<0.01	0.21	0.01	0.059	<0.01	0.02	0.43	99.87	11	162		
RYE62	0.06	75.34	7.32	8.01	0.19	1.54	1.08	3.22	0.01	1.95	0.03	0.048	0.01	0.06	0.55	99.36	41	>4000		
RYE64	0.04	74.23	13.86	1.2	1.15	0.18	3.37	4.91	<0.01	0.08	0.02	0.033	0.04	0.16	0.41	99.63	12	84		
RYE69	0.04	78.89	10.21	1.75	0.49	1.18	2.09	2.99	<0.01	0.19	0.03	0.035	0.01	0.05	0.88	98.8	11	169		
RYE71	0.04	70.52	14.57	2.52	0.86	0.45	2.57	6.72	<0.01	0.28	0.03	0.108	0.06	0.59	0.55	99.83	11	229		
RYE73	0.05	72.04	13.94	1.57	1.38	0.24	3.64	4.52	<0.01	0.11	0.03	0.045	0.03	0.21	0.39	98.14	8	121		
RYE75	0.05	75.08	13.72	0.88	0.65	0.06	3.04	5.82	<0.01	0.04	0.02	0.019	0.03	0.15	0.49	99.98	6	51		
RYE77	0.05	71.75	14.64	1.89	1.57	0.44	3.61	4.42	<0.01	0.19	0.02	0.073	0.05	0.24	0.53	99.42	9	154		
RYE79	0.04	74.97	13.8	0.79	0.89	0.07	3.25	5.38	<0.01	0.02	0.05	0.023	0.03	0.09	0.5	99.86	12	60		
RYE81	0.04	74.51	13.87	1.19	1.18	0.16	3.54	4.38	<0.01	0.08	0.04	0.032	0.04	0.18	0.54	99.75	7	74		
RYE83	0.04	74.74	13.72	0.98	0.75	0.07	3.35	5.6	<0.01	0.05	0.02	0.023	0.02	0.06	0.33	99.7	38	61		
RYE85	0.05	73.98	13.75	1.74	1.3	0.22	3.27	4.58	<0.01	0.13	0.03	0.063	0.05	0.24	0.43	99.79	7	125		
RYE87	0.04	72.77	15.02	1.61	1.67	0.24	4.35	3.4	<0.01	0.11	0.03	0.047	0.06	0.12	0.43	99.87	10	97		
RYE89	0.04	87.69	6.23	1.21	0.25	0.22	1.13	3.04	<0.01	0.07	0.01	0.026	0.01	0.07	0.16	100.1	18	75		
RYE101	0.05	78.13	11.72	1.78	1.11	0.4	3.7	2.19	<0.01	0.24	0.04	0.052	0.04	0.08	0.52	100	13	235		
RYE103	0.06	74.44	13.95	1.33	1.02	0.15	3.73	4.41	<0.01	0.09	0.02	0.036	0.04	0.1	0.54	99.86	9	72		
RYE105	0.05	73.78	13.95	1.33	0.96	0.14	3.26	5.37	<0.01	0.08	0.02	0.022	0.04	0.13	0.56	99.64	6	39		
RYE107	0.05	74.84	13.53	1.22	0.9	0.1	3.22	5.14	<0.01	0.06	0.02	0.023	0.03	0.13	0.5	99.71	6	76		
RYE109	0.05	69.82	15.46	3.16	3.37	0.86	3.83	2.23	0.01	0.33	0.04	0.124	0.06	0.17	0.48	99.95	12	225		
RYE111	0.06	73.49	14.39	1.57	0.96	0.22	3.87	4.58	<0.01	0.11	0.02	0.048	0.03	0.08	0.68	100.05	16	90		
RYE113	0.04	72.16	14.78	2.17	1.37	0.62	4.11	3.75	<0.01	0.2	0.03	0.054	0.03	0.09	0.62	99.98	24	120		

APPENDIX E

CALCULATED CHEMICAL DEPLETION FRACTIONS AND MASS TRANSFER COEFFICIENTS

Rye Creek

Soil Sample ID	Rock Sample ID	CDF	τSi	τAl	τFe	τCa	τMg	τNa	τK	τMn	τP	τSr	τBa
RYE48	RYE49	0.75	-0.75	-0.73	-0.48	-0.65	-0.15	-0.78	-0.81	-0.19	-0.18	-0.73	-0.77
RYE55	RYE56	0.58	-0.63	-0.40	-0.20	-0.21	-0.39	-0.62	-0.65	3.46	3.44	-0.55	-0.50
RYE57	RYE58	0.85	-0.86	-0.83	-0.57	-0.68	0.13	-0.87	-0.89	0.94	0.62	-0.52	-0.30
RYE59	RYE60	0.61	-0.68	-0.10	-0.14	1.06	-0.71	-0.38	-0.61	2.86	1.11	0.00	0.93
RYE63	RYE64	0.79	-0.80	-0.77	-0.38	-0.69	-0.20	-0.82	-0.86	0.56	0.89	-0.83	-0.81
RYE68	RYE69	0.62	-0.65	-0.48	-0.34	0.22	-0.77	-0.48	-0.70	-0.31	0.04	0.24	-0.26
RYE72	RYE73	0.71	-0.71	-0.68	-0.45	-0.67	-0.32	-0.79	-0.77	0.89	1.23	-0.69	-0.69
RYE74	RYE75	0.90	-0.90	-0.89	-0.58	-0.66	0.43	-0.90	-0.94	0.00	-0.32	-0.89	-0.92
RYE76	RYE77	0.47	-0.47	-0.49	-0.13	-0.27	-0.25	-0.55	-0.62	3.29	0.42	-0.51	-0.64
RYE78	RYE79	0.94	-0.94	-0.94	-0.80	-0.89	-0.35	-0.95	-0.97	-0.76	-0.76	-0.94	-0.92
RYE80	RYE81	0.73	-0.74	-0.70	-0.42	-0.63	-0.18	-0.75	-0.76	-0.07	-0.21	-0.71	-0.63
RYE82	RYE83	0.88	-0.88	-0.87	-0.57	-0.62	0.72	-0.89	-0.93	-0.29	-0.60	-0.74	-0.79
RYE84	RYE85	0.61	-0.61	-0.59	-0.41	-0.52	-0.22	-0.60	-0.71	1.44	-0.59	-0.51	-0.66
RYE86	RYE87	0.77	-0.78	-0.76	-0.44	-0.77	-0.07	-0.85	-0.78	0.67	1.03	-0.88	-0.71
RYE88	RYE89	0.86	-0.89	-0.65	-0.56	-0.09	-0.38	-0.69	-0.86	3.87	0.37	-0.54	-0.76
RYE102	RYE103	0.77	-0.78	-0.75	-0.51	-0.58	0.04	-0.81	-0.84	0.95	-0.19	-0.76	-0.68
RYE104	RYE105	0.74	-0.74	-0.74	-0.49	-0.59	0.22	-0.80	-0.82	1.76	0.03	-0.79	-0.70
RYE106	RYE107	0.77	-0.78	-0.77	-0.55	-0.61	0.20	-0.81	-0.82	1.16	-0.28	-0.68	-0.72
RYE110	RYE111	0.81	-0.83	-0.77	-0.41	-0.64	-0.29	-0.85	-0.90	-0.17	-0.09	-0.79	-0.77
RYE112	RYE113	0.55	-0.55	-0.56	-0.33	-0.28	-0.32	-0.66	-0.70	3.29	0.44	-0.52	-0.37
RYE26	RYE27*	0.70	-0.70	-0.70	-0.45	-0.66	-0.47	-0.76	-0.81	1.20	-0.08	-0.79	-0.76
RYE28	RYE29*	0.58	-0.60	-0.53	-0.33	-0.42	-0.47	-0.60	-0.66	0.63	-0.10	-0.56	-0.52
RYE38	RYE39*	0.71	-0.70	-0.72	-0.45	-0.66	-0.49	-0.81	-0.81	0.55	-0.23	-0.79	-0.76
RYE44	RYE45*	0.76	-0.77	-0.72	-0.44	-0.67	-0.47	-0.80	-0.83	0.69	2.00	-0.75	-0.76
RYE61	RYE62*	0.69	-0.69	-0.69	-0.44	-0.65	-0.26	-0.70	-0.81	-0.07	-0.36	-0.79	-0.65
RYE70	RYE71*	0.64	-0.65	-0.60	-0.43	-0.52	-0.60	-0.70	-0.69	2.75	-0.11	-0.50	-0.33
RYE100	RYE101*	0.74	-0.75	-0.69	-0.46	-0.62	-0.49	-0.76	-0.81	0.02	0.27	-0.73	-0.72
RYE108	RYE109*	0.82	-0.84	-0.77	-0.39	-0.47	-0.39	-0.81	-0.94	-0.39	0.11	-0.75	-0.80

* Weathering calculations were made using a composite rock value for these samples because their rock sample Zr value was unreliable. The composite rock value is the average of all the non-outlying Rye rock values.

Lost Horse Creek

Soil Sample ID	Rock Sample ID	CDF	τSi	τAl	τFe	τCa	τMg	τNa	τK	τMn	τP	τSr	τBa
LST22	LST23	0.20	-0.20	-0.20	0.17	-0.17	0.03	-0.31	-0.32	2.69	1.07	-0.43	-0.34
LST24	LST25	0.17	-0.16	-0.22	-0.01	-0.16	-0.09	-0.31	-0.21	2.20	0.19	-0.30	-0.22
LST26	LST27	0.19	-0.19	-0.21	-0.03	-0.18	-0.25	-0.26	-0.29	2.08	-0.26	-0.20	-0.21
LST30	LST31	0.73	-0.75	-0.69	-0.24	-0.64	0.06	-0.80	-0.80	-0.32	-0.51	-0.83	-0.79
LST32	LST33	0.47	-0.43	-0.29	-0.46	-0.82	-0.86	-0.52	-0.44	0.28	1.84	-0.65	-0.40
LST37	LST38	0.45	-0.44	-0.48	-0.17	-0.52	-0.35	-0.57	-0.45	1.50	0.43	-0.53	-0.41
LST40	LST41	0.29	-0.29	-0.28	0.18	-0.40	-0.24	-0.40	-0.29	0.52	0.07	-0.41	-0.36
LST43	LST44	0.84	-0.85	-0.81	-0.39	-0.84	-0.41	-0.89	-0.88	-0.07	0.15	-0.93	-0.89
LST45	LST46	0.64	-0.65	-0.61	-0.10	-0.68	-0.25	-0.73	-0.68	-0.24	0.30	-0.80	-0.71
LST47	LST48	0.82	-0.84	-0.77	-0.40	-0.67	-0.19	-0.86	-0.87	4.50	1.74	-0.91	-0.84
LST49	LST50	0.52	-0.52	-0.52	-0.11	-0.55	-0.12	-0.60	-0.52	0.41	1.81	-0.64	-0.51
LST51	LST52	0.44	-0.43	-0.46	-0.21	-0.38	-0.30	-0.50	-0.54	3.13	0.14	-0.55	-0.56
LST54	LST55	0.20	-0.18	-0.24	-0.10	-0.34	-0.38	-0.40	-0.24	0.72	-0.38	-0.44	-0.17
LST56	LST57	0.64	-0.64	-0.64	-0.11	-0.57	0.28	-0.71	-0.67	0.35	0.19	-0.70	-0.68
LST59	LST60	0.57	-0.58	-0.55	-0.20	-0.55	-0.11	-0.68	-0.61	2.50	0.44	-0.69	-0.56
LST62	LST63	0.73	-0.74	-0.73	-0.35	-0.62	-0.31	-0.78	-0.77	1.10	0.16	-0.80	-0.74
LST64	LST65	0.71	-0.72	-0.70	-0.17	-0.69	-0.11	-0.78	-0.77	1.73	0.88	-0.82	-0.73
LST66	LST68	0.81	-0.82	-0.78	-0.53	-0.79	-0.61	-0.86	-0.90	-0.51	0.26	-0.90	-0.88
LST70	LST71	0.82	-0.83	-0.77	-0.33	-0.77	-0.34	-0.86	-0.84	-0.17	-0.07	-0.85	-0.82
LST72	LST73	0.57	-0.58	-0.57	-0.20	-0.55	-0.18	-0.66	-0.59	1.14	0.53	-0.73	-0.60
LST77	LST78	0.69	-0.69	-0.69	-0.26	-0.69	-0.57	-0.78	-0.81	-0.63	-0.41	-0.82	-0.81
LST79	LST80	0.45	-0.46	-0.44	-0.09	-0.26	0.07	-0.54	-0.57	4.33	0.50	-0.63	-0.52
LST81	LST82	0.27	-0.26	-0.30	-0.36	-0.20	-0.54	-0.31	-0.39	1.88	0.13	-0.34	-0.35
LST103	LST104	0.38	-0.41	-0.28	-0.34	-0.32	-0.36	-0.40	-0.39	1.40	2.82	-0.43	-0.30
LST110	LST111	0.66	-0.67	-0.63	-0.32	-0.66	-0.22	-0.73	-0.72	3.10	2.11	-0.76	-0.73
LST112	LST113	0.83	-0.84	-0.81	-0.41	-0.78	-0.46	-0.87	-0.87	1.32	0.07	-0.91	-0.86
LST114	LST115	0.81	-0.82	-0.77	-0.33	-0.76	0.14	-0.85	-0.87	0.57	0.82	-0.83	-0.79

APPENDIX F

NOTES ON THE UTILIZATION OF COSMOGENIC NUCLIDES FOR THE STUDY OF LANDSCAPE EVOLUTION

Cosmogenic nuclides are an essential tool for modern studies of landscape evolution (Granger and Riebe, 2014; Dixon and Riebe, 2014). They measure average erosion rates (total denudation D) over the time required to erode the portion of the surface that receives cosmic rays, which can be 1-2m of soil, depending on soil density. They have revolutionized geomorphology since they were first developed in the 1980s, when accelerator mass spectrometry (AMS) was developed and the measurement of nuclides ^{3}He, ^{10}Be, ^{26}Al, and ^{36}Cl were detected in soil and rock (Pavich et al., 1985; Kurz, 1986; Nishiizumi et al., 1986; Phillips et al., 1986; Elmore and Phillips, 1987). Cosmogenic nuclides are produced in the atmosphere and in minerals at Earth's surface when cosmic ray particles interact with Earth's atmosphere. Today they can be used to measure exposure ages of rocks and the speed at which soil is produced and eroded (von Blanckenburg and Willenbring, 2014). The underlying principle is that since cosmogenic nuclides are produced in rock only when they are exposed at earth's surface, the quantity of cosmogenic nuclides present in a rock can tell us the time that has passed since exhumation. Cosmic rays were first detected in the early 1900s, but it was not until much later that scientists developed methods to quantify amounts of cosmogenic nuclides present in rocks and only recently that earth scientists applied cosmogenic nuclides to problems of landscape evolution. The basis for using cosmogenic nuclides in earth science was laid by Lal and Peters (1967), who first estimated production rates of cosmogenic nuclides and how those rates are affected by latitude and longitude. Lal (1991) showed how the mechanics of cosmogenic nuclide production could be applied to

geomorphology, using the accumulation of cosmogenic nuclides to measure the rate of change of a landscape.

Dunai and Lifton (2014) describe the mechanics of cosmogenic nuclide production including the types of cosmic ray particles, the effect of altitude, latitude, and time on cosmogenic radionuclide (CRN) production rates, and methods for calculating production rates. Most cosmic rays are produced by supernova explosions, which have been occurring at an approximately constant rate of once every 50 years for the last 10 my. They are composed of particles; mainly protons (87%) and alpha particles (12%), accompanied by some heavier nuclei (~1%) (Dunai and Lifton, 2014). These enter Earth's atmosphere and interact with atmospheric atoms to produce secondary cosmic rays, which contain neutrons and muons that produce CRNs in the atmosphere (atmospheric or metoric CRNs) and in rocks at the surface (in situ). The most important type of reaction to using CRNs to measure landscape change is spallation, where high-energy nucleons collide with atomic nuclei, knocking some protons and neutrons off and converting that atom to a new product (Dunai and Lifton, 2014), most importantly converting ^{16}O to ^{10}Be. In addition to spallation, CRNs can also be produced through neutron capture and two types of muon reactions. In situ CRN concentrations can be experimentally established at sites where age is independently determined and with well-constrained exposure histories, such as moraines or lava flows where no significant erosion, burial, or prior exposure has occurred. Then scaling factors must be applied in order to account for spatial variation in cosmic ray flux due to altitude, latitude, variations in geomagnetic field strength, and changes in solar activity.

There are two varieties of ^{10}Be: in situ and meteoric. In situ ^{10}Be is produced in mineral grains, whereas meteoric ^{10}Be is produced in the atmosphere (mostly by spallation) and attach to reactive surfaces in the regolith. Meteoric ^{10}Be is still being calibrated as a tool in landscape evolution studies, but in situ ^{10}Be has already been utilized in a number of crucial areas.

In situ ^{10}Be accumulates as deep as ~50-60cm in rock (Nishiizumi et al., 1993) or 3m in soil. Its half-life is 1.6 My, and it is used for calculating millennial-scale ages (Nishiizumi et al., 1986). The soil model that is used when applying cosmogenic nuclides to soils is based on a soil column with bedrock underlying and regolith on top, described succinctly by Dixon and Riebe (2014). The regolith is composed of saprolite, a chemically weathered but physically immobile layer of material, with soil on top. The soil is chemically altered and physically mobile. The erosion rate describes the rate at which soil is removed from the top of the column and moved downslope, and the soil production rate describes the rate at which bedrock is weathered into regolith.

Spatial variations in sediment size produced on slopes (Lukens et al., 2016) and preferential chemical erosion of more soluble minerals, which biases interpretation of CRNs from quartz in soils and sediment (Small et al., 1999) can complicate CRN analysis. It is necessary to account for these issues following Riebe et al., 2015 for sediment size and Riebe et al., 2001a for chemical erosion bias.

Six samples of river sand from catchment outlets in the Bitterroots and Sapphires have been prepared for cosmogenic nuclide analysis. These are Lost Horse, Bear, Mill, and Kootenai Creeks in the Bitterroots, and Rye Creek and East Fork Bitterroot River in

the Sapphires. In the near future we hope that these samples may reveal catchment-wide millennial-scale erosion rates that will complement the topographic analysis in this study. Erosion rate will be compared with catchment mean slope and relief, and in Lost Horse and Rye Creeks total denudation from CRN can be combined with mass balance geochemistry to quantify the chemical and physical components of denudation.

References Cited

Dixon JL, Riebe CS. 2014. Tracing and pacing soil across slopes. *Elements* **10** : 363–368.

Dunai, T.J. and Lifton, N.A., 2014. The nuts and bolts of cosmogenic nuclide production. *Elements*, *10*(5), pp.347-350.

Elmore, D. and Phillips, F.M., 1987. Accelerator mass spectrometry for measurement of long-lived radioisotopes. *Science*, *236*(4801), pp.543-550.

Granger DE, Riebe CS. 2014. Cosmogenic Nuclides in Erosion and Weathering. In *Treatise on Geochemistry*, Drever JI (ed). Elsevier: Oxford; 401-436.

Kurz, M.D., 1986. In situ production of terrestrial cosmogenic helium and some applications to geochronology. *Geochimica et Cosmochimica Acta*, *50*(12), pp.2855-2862.

Lal, D., 1991. Cosmic ray labeling of erosion surfaces: in situ nuclide production rates and erosion models. Earth and Planetary Science Letters 104:424–439

Lal, D. and Peters, B., 1967, Cosmic ray produced radioactivity on the Earth. Handbuch der Physik 46:551-612.

Lukens, C., Riebe, C.S., Sklar, L.S., and Shuster, D.L., 2016. Grain-size bias in cosmogenic nuclide studies of stream sediment in steep terrain: Grain-size bias in average erosion rates. Journal of Geophysical Research: Earth Surface 121(5).

Nishiizumi, K., Kohl, C.P., Arnold, J.R., Dorn, R., Klein, I., Fink, D., Middleton, R. and Lal, D., 1993. Role of in situ cosmogenic nuclides 10Be and 26Al in the study of diverse geomorphic processes. *Earth Surface Processes and Landforms*, *18*(5), pp.407-425.

Nishiizumi, K., Lal, D., Klein, J., Middleton, R. and Arnold, J.R., 1986. Production of 10Be and ^{26}Al by cosmic rays in terrestrial quartz in situ and implications for erosion rates.

Pavich, M.J., Brown, L., Valette-Silver, N., Klein, J., Middleton, R., 1985. ^{10}Be analysis of a Quaternary weathering profile in the Virginia Piedmont. Geology. 13:39-41.

Phillips, F.M., Leavy, B.D., Jannik, N.O., Elmore, D. and Kubik, P.W., 1986. The accumulation of cosmogenic chlorine-36 in rocks: A method for surface exposure dating. *Science*, *231*(4733), pp.41-43.

Riebe CS, Kirchner JW, Granger DE. 2001a. Quantifying quartz enrichment and its consequences for cosmogenic measurements of erosion rates from alluvial sediment and regolith. *Geomorphology* **40** : 15–19.

Riebe, C.S., Sklar, L.S., Lukens, C.E. and Shuster, D.L., 2015. Climate and topography control the size and flux of sediment produced on steep mountain slopes. *Proceedings of the National Academy of Sciences*, *112*(51), pp.15574-15579.

Small, E.E., Anderson, R.S. and Hancock, G.S., 1999. Estimates of the rate of regolith production using 10Be and 26Al from an alpine hillslope. *Geomorphology*, *27*(1), pp.131-150.

von Blanckenburg, Friedhelm, and Jane K. Willenbring. "Cosmogenic nuclides: Dates and rates of Earth-surface change." *Elements* 10.5 (2014): 341-346.

APPENDIX G

LITERATURE REVIEW

Hillslope Dynamics

Many hilly and mountainous portions of Earth's surface bear a soil mantle. This soil mantle is produced primarily from underlying bedrock, as well as eolian, fluvial, and glacial deposition in some settings. The balance between soil production and transport determines whether soil is present and how thick it is at any given location (e.g. Ahnert, 1967; Dietrich et al., 1995; Heimsath et al., 1997). Recent developments in analytical techniques, especially the use of cosmogenic nuclides for quantifying soil production rates as well as remote sensing and geospatial analysis, have enabled the quantitative testing of the soil production hypothesis proposed by G.K. Gilbert, who developed much of his thinking while studying Utah's Henry Mountains for the USGS in the late 1800s and early 1900s. Gilbert noticed that some amount of soil is necessary to facilitate weathering of underlying rock but too much soil is detrimental, so that the soil production rate first increases with increasing soil thickness and decreases after some optimal thickness (Gilbert, 1877). He also noticed that convex drainage divides are ubiquitous and that this topographic form may be maintained if soil is moved downslope by creep and the flux of eroded regolith increases downslope, as each point on a slope transports all the material originating above itself in addition to the material produced in situ from underlying rock. In this way, topographic curvature is both the cause and the result of sediment flux downslope in dynamic equilibrium. These ideas laid the foundation for more recent concepts concerning dynamic equilibrium (Hack, 1960), geomorphic transport laws (Culling, 1960; Dietrich et al., 2003), and the soil production function (Ahnert, 1967; Carson and Kirkby, 1972).

Soil thickness on slopes reflects the balance between production of soil from underlying bedrock and erosion, or the divergence of soil flux. Soil production occurs through the physical disruption of underlying bedrock or saprolite, where it begins its journey through the soil column (figure 2.1). Erosion takes place through a variety of mechanisms that move particles downslope in a diffusive-like way (Fernandes and Dietrich, 1997; Roering et al., 1999; Heimsath et al., 2005). Geomorphologists use the term soil to refer to the mobile portion of the weathering profile. This is different from saprolite, which still retains the fabric of its parent rock and is immobile. Other disciplines may use soil to refer to mobile and immobile portions of the weathering profile, and what geomorphologists call soil others may call the A horizon or the biologically mixed portion of a soil profile.

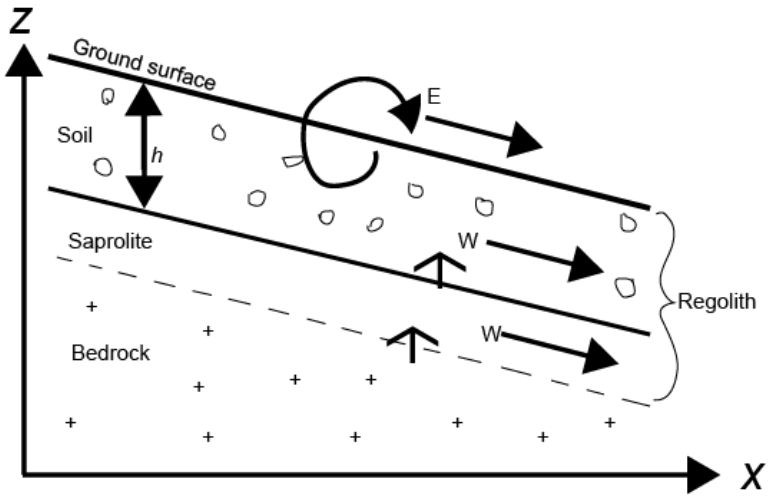

Figure A3. *A hillslope cross section displays bedrock conversion to saprolite, and saprolite conversion to soil (upward arrows). Saprolite undergoes chemical weathering (W), while soil undergoes both chemical weathering (W) and physical erosion (E) and mixing. Soil and saprolite together comprise the regolith. Soil thickness is termed h.*

The change in soil thickness can be calculated as the soil production minus erosion:

$$\frac{dH}{dt} = P_s - E \quad , \qquad \text{(Equation 1)}$$

where dH/dt represents the change in soil thickness over time, P_s is the soil production rate, and E is soil erosion. When local soil depth is constant over time, dH/dt equals zero such that P_s and E are balanced. If soil thicknesses are constant in space and time, a landscape is considered to be in dynamic equilibrium. Numerous studies, beginning with Heimsath et al. (1997) have measured ^{10}Be concentrations in saprolite or soils to test the variability of soil production rates. Many have found inverse relationships between soil thickness and soil production rates (Heimsath et al., 1997; Small et al., 1999; Heimsath et al., 2000, 2001a,b; Wilkinson, 2005; Wilkinson et al., 2005).

The rate at which soil is produced from underlying rock is often theoretically described by the soil production function (Heimsath et al., 1997), which defines the rate of bedrock conversion to soil in relation to the thickness of the overlying soil cover. There are two common forms of a soil production function (SPF), which describes the production and erosion of soils. One is the soil thickness-dependent SPF (Heimsath et al., 1997):

$$P_s = P_0 e^{-aH} \quad , \qquad \text{(Equation 2)}$$

where P_0 is the maximum soil production at a site (L/T), and α is a constant with dimensions 1/L. The other is a humped SPF, where maximum soil production rate occurs at some shallow soil thickness, as predicted by Gilbert (1877):

$$P_s = P_0 e^{(-bH)}(1 + cH), \qquad \text{(Equation 3)}$$

where b (L^{-1}) is the scaling factor for the decrease in soil production with depth and c (L^{-1}) determines the thickness at which soil production is maximized for a given value of b. If $c/b > 1$, the relationship is humped and P_s reaches a maximum at thickness $(c - b) / bc$. The two functions are similar to each other if soil thickness at the peak production value is small, less than approximately 10 cm, and if in equation 3 c = 0, they will be identical. However, under the humped production scenario, exposed bedrock will shed particles much more slowly than when buried by any soil. The humped model (equation 3) leads to an unstable system at shallow soil thicknesses, with a bimodal landscape of soil and bare rock (Carson and Kirkby, 1972; Dietrich et al., 1995; D'Odorico, 2000; Norton et al., 2014). Observational evidence is inconclusive as to which equation may dominate in any particular setting, and although the humped function has been found (Riggins et al., 2011), whether the humped SPF exists extensively in nature is debated (Heimsath et al., 2009). An exponential decline in soil production rate with increasing thickness has been measured in many landscapes (Heimsath et al., 1999, 2000).

Measurements of the exponential relationship between soil thickness and production rate suggest a self-sustaining system in which thickening or thinning of soil cause an adjustment in soil production so that steady state values are maintained (Heimsath et al., 1997, 2005). A flat soil production rate has also been observed (Wilkinson et al., 2005; Dixon et al., 2009). There is also a more recently developed soil production formula based on an Arrhenius formula (Norton et al., 2014):

$$SPR_{max} = a_o \, Pe^{\frac{-E_a}{R}(\frac{1}{T}-\frac{1}{T_0})} \ , \qquad \text{(Equation 4)}$$

where SPR_{max} = maximum soil production (L/t), a_0 = a factor to scale precipitation (P) rate (L/t) to soil production function, E_a = activation energy for silicate weathering (kJ mol^{-1}), R is the gas constant, T = MAT (K) and T_0 is a reference temperature (278 K). In this model, chemical alteration that frees up particles is the main control on the maximum soil production rate.

Using new advances in cosmogenic nuclide techniques, Heimsath et al. (1997, 1999, 2000, 2001, 2005, 2006) found soil production rates to vary locally across several distinct landscapes, suggesting that these studied systems are not in dynamic equilibrium, as was suggested by Gilbert (1877, 1909) and Hack (1960). Instead, upland landscapes are evolving locally through time both physically and chemically, likely reflecting the also varying climatic (e.g., Porder et al., 2007; Dixon et al., 2009a; Ferrier et al., 2012) and

tectonic (e.g., Riebe et al., 2001b; West et al., 2005; Dixon et al., 2012; Hurst et al., 2012) forces that influence the evolution of landscapes.

Actively eroding landscapes often exhibit ridge and valley topography with a thin, sometimes rocky colluvial soil mantle that is produced from in-place bedrock and transported by mechanical processes including tree throw, animal burrowing, and freeze-thaw and shrink-swell cycles (Lutz and Griswold, 1939; Lutz, 1960; Hole, 1981; Mitchell, 1988; Matsuoka, 1990; Schaetzl and Follmer, 1990; Norman et al., 1995; Paton et al., 1995). Mechanical processes are able to produce soil from bedrock regardless of its weathered state, but they work faster in tandem with chemical weathering (e.g. Dixon et al., 2012; Heimsath et al., 2012). When fluvial landscapes are rapidly uplifting, slope should be expected to increase with elevation until a critical slope threshold is reached, above which rock strength prohibits slopes from steepening further (Strahler, 1950; Montgomery, 2001). This critical slope threshold will vary depending on lithology according to the rock's resistance to erosion.

Sediment transport has been classically thought to be dependent on slope, and erosion laws based on theories of Gilbert et al. (1898) assume soil flux (Qs) is linearly dependent on the local slope (S), such that:

$$Q_s = KS. \qquad \text{(Equation 5)}$$

However, the sediment transport rate may only be a function of slope in certain settings. In steep terrain where landsliding becomes the dominant sediment transport mechanism, Dietrich and Montgomery (1998) argued that linear flux applies only on gentle slopes near ridge crests. Roering et al., (1999) proposed a different transport law to describe steep terrain where transport becomes nonlinear as slopes steepen to a critical gradient (S_c) in the Oregon Coast Range:

$$Q_s = \frac{KS}{1-(\frac{S}{S_c})^2} \quad . \qquad \text{(Equation 6)}$$

This equation can be adapted to other landscapes by including a background erosion rate (E_0) that is specific to each landscape:

$$E = E_0 + \frac{KS}{1-(\frac{S}{S_c})^2}. \qquad \text{(Equation 7)}$$

Equation 7 was first calibrated in a real landscape (Roering et al., 1999) and was later validated by numerical modeling and laboratory studies (Roering et al., 2001a, b). Taken together, these studies present a strong case that on slopes above some critical steepness, sediment transport is strongly nonlinear, and that hillslope relief and slope are not valid indicators of erosion rate. Additionally, the timescale of morphologic adjustment to changing boundary conditions will be faster under nonlinear transport than for linear transport.

Insights into chemical weathering and its ties to vegetation, climate, lithology, and topography hinge on measuring the elemental composition of soil and its parent rock to calculate mass gain or loss. The method of calculating mass loss in a soil using the enrichment of insoluble elements in soil compared to its parent rock originated with Merrill (1897) and was later developed further (Brimhall et al., 1985, 1988, 1991, 1992; Brimhall and Dietrich, 1987; Chadwick et al., 1990). Paired measurement of immobile elements in parent material and soil are similarly used to calculate a chemical depletion fraction (CDF; Riebe et al., 2003). This quantity represents the fraction of total denudation removed by chemical dissolution rather than physical erosion at a given location (Riebe et al., 2003). It is defined as:

$$CDF = 1 - \frac{C_{i,p}}{C_{i,s}} = W/D, \qquad \text{(Equation 8)}$$

where $C_{i,p}$ and $C_{i,s}$ = immobile element concentration in parent material and soil, respectively (for example, titanium); W = chemical weathering flux; D = total denudation flux. Mass loss for individual elements is often calculated as a mass transfer coefficient, or tau (τ), which represents the fractional loss or gain of a mobile element or all mobile elements from a soil (Brimhall et al., 1992).

While similar to each other and derived from the same equation, CDF and tau each have their strengths. CDF is best used as a single value to quantify depletion of bulk soil, while tau is best for quantifying more detailed variations in depletion with depth (Brantley and Lebedeva, 2011). Tau is useful for calculating element- or mineral-specific chemical erosion rates (White, 2002; Ferrier et al., 2010), measuring the importance of saprolite weathering (White et al., 1998; Dixon et al., 2009), and quantifying the airborne dust contribution to soil (Ferrier et al., 2011). These tools are not perfect. They assume complete immobility of the index element, but even high field strength elements such as Zr, Ti, and Nb have some degree of mobility (Sudom and St. Arnaud, 1971; Colin et al., 1993; Cornu et al., 1999; Kurtz et al., 2000; Taboada et al., 2006; Jin et al., 2010).

The above tools lay the groundwork for quantifying and linking topography and rates of chemical weathering and erosion, which can then be related to other influences such as climate. Climate controls chemical weathering and erosion via temperature and moisture availability. Riebe et al. (2001b) measured long-term erosion rates across seven unglaciated granitic Sierra Nevada sites spanning a temperature and precipitation gradient (4-15° C in average temperature and 22-178 cm/year in annual precipitation) and found that long-term erosion rates from cosmogenic nuclides varied by a factor of only 2.5, and showed no correlation with temperature and precipitation ($r < 0.17$, $p > 0.5$). This seems to indicate that long-term average climatic regimes have little effect on mountain erosion rates. Additionally, Kirchner et al. (2001) found that 5 catchments that were glaciated in the Pleistocene had similar long-term and short-term erosion rates to 25 unglaciated catchments in central Idaho. However, in kinetically limited systems, climatic setting

may influence sediment transport mechanisms and resulting catchment morphology. For example, a study of a climate gradient across a granitic, slowly-eroding landscape in South Africa found that wetter climate conditions favored hillslope processes over valley-forming processes, meaning that in dry sites overland events were infrequent and short-lived while the wetter sites experience a hydrologic regime dominated by throughflow and enhanced bioturbation (Chadwick et al., 2013). Hill-valley spacing and local relief were found to increase with annual rainfall. This was not the case in a study of the Washington Cascades, however. There, Moon et al. (2011) found that modern erosion rates are controlled by both glacial conditioning and precipitation-driven landslides. This may be because the precipitation gradient, slope distributions are more uniform, and the area of homogeneous lithology is smaller in the Cascades than in the Alps region studied by Schlunegger and Norton (2013). Von Blanckenburg (2006) found that climate has very weak effects on catchment erosion rates. Amundson et al. (2015) found that an aridity index represented by the ratio of mean annual precipitation to mean annual temperature was a strong indicator of maximum soil production rate. Specifically, in this study, SPR_{max} values are generally similar to measured P_0 values as a function of the aridity index.

Climate has been found to influence soil evolution in some landscapes and not others partly because of linkages to erosion rate and topography (Dixon et al., 2016). There exists a threshold below which chemical denudation and erosion rates are coupled, and above which further increase in erosion rate leads to decreasing chemical weathering rate. These two systems are referred to as supply-limited or kinetically limited regimes. In threshold landscapes, the strength of bedrock is not enough to allow the hillslope to steepen any further, and mean hillslope angle becomes decoupled from erosion rate. This prevents hillslopes from being steeper than approximately 35-40° (Carson and Petley, 1970; Schmidt and Montgomery, 1995; Burbank et al., 1996; Montgomery and Brandon, 2002). Several studies have found support for a process transition from soil creep at low slopes to landsliding above a slope threshold, above which erosion is so rapid that the surface is unable to maintain a continuous soil cover (e.g., DiBiase et al. 2010).

Chemical weathering may be controlled by inherently different mechanisms above and below the soil-mantled to rock-dominated transition. Chemical weathering rates and erosion rates are positively correlated, as each provides fresh material for the other to work on (Stallard and Edmond, 1983; Riebe et al., 2004; West et al., 2005; Dixon et al., 2009). The decoupling of chemical weathering and erosion above some threshold is supported by Anderson et al. (2002), who predicted that chemical denudation rates and erosion rates would both increase only while the landscape remains mantled by soil, and corroborated by Dixon et al. (2012), who found that at high erosion rates, erosion outpaces weathering and regolith residence time is decreased so much that minerals do not have time to decompose. This means that erosion rate, via its control on regolith residence time, influences the degree to which climate can control chemical weathering.

In kinetically limited landscapes, weathering intensity is low because chemical weathering reactions are not allowed to act on weatherable materials completely. This could be due to high erosion rates, where mineral residence times are cut short by being eroded away, or dry conditions, where not enough moisture is available for weathering reactions to take place (Rasmussen et al., 2011). In erosion-limited landscapes (also called supply-limited), weathering intensity is high and weathering is limited only by the supply of fresh material, not by the rate of mineral dissolution (Stallard, 1995; West et al., 2005). This could be due to very low erosion rates, which allow the regolith to grow so thick that weathering processes (bioturbation, freeze-thaw, etc.) do not reach fresh rock; or it could mean that although erosion rates are not particularly low, chemical weathering keeps pace with erosion so that a steady-state condition is maintained (Rasmussen et al., 2011).

While supply-limited systems are ubiquitous and well-documented around the globe, kinetically limited landscapes are less well understood. One that has been observed is the San Gabriel Mountains in California, a transient landscape where some regions are low-relief and soil-mantled, while others are high-relief and dominated by bedrock, with an intermediate transient landscape (Dixon et al., 2012). Soil residence times and water availability determine the extent to which soils are able to weather, reflected in their CDF and tau values. This is indicative of a kinetically limited system because minerals in this setting are not allowed sufficient time to fully weather, whereas in a transport-limited system all soils would have their weatherable components removed and display a similar degree of weathering regardless of slope, water availability, or dust deposition. Between the supply-limited and kinetically limited portions of the landscape, weathering rates increase because of the increase in mineral supply. Within the kinetically limited portion of the landscape, the chemical weathering rate reaches a peak and then decreases as the mineral residence time becomes so short that it outweighs the benefits of having fresh mineral supply.

The threshold for kinetically limited weathering may be coincident with another threshold below which hillslope gradient and topographic relief are positively correlated with erosion rate (Ahnert, 1970; Montgomery and Brandon, 2002) and above which, at very high slope gradients, the relationship breaks down (e.g. Schmidt and Montgomery, 1995; Montgomery, 2001; Ouimet et al., 2009; DiBiase et al., 2010). Steep landscapes erode quickly partly because of tectonic forcings, as rock uplift can lower a region's relative base level and drive river incision, raising landscape-scale erosion rates (Howard et al., 1994; Whipple and Tucker, 1999). Hillslopes are not as quick as river channels in adjusting their base level by increasing erosion rate (Fernandes and Dietrich, 1997; Mudd and Furbish, 2007). The change in erosion rate is directly related to channel steepness, a metric of topographic relief, as observed by Ouimet et al. (2009) in the Tibetan Plateau and by DiBiase et al. (2010) in the San Gabriel Mountains in California, both of whom

measured erosion rates using ^{10}Be from stream sediments. Tectonic uplift can cause fractures and jointing in rock that contributes to erosion (Molnar et al., 2007).

Glacial Signature on Topography

Glacial erosion is extremely important in shaping mountain topography (e.g. Penck, 1905) and increasing erosion rates (Zhang et al., 2001; Molnar, 2004; Herman, 2013). It also has implications for chemical weathering, which will be discussed later. The abrasion and plucking of ice widens and deepens bedrock valleys (Brocklehurst and Whipple, 2002) and increases local relief by carving into existing valleys rather than summits (Anderson et al., 2006), meaning that total relief increases even as the whole region may be uplifted isostatically (Small and Anderson, 1996).

The effort to evaluate the linkages between glacial history and topography has gone through three phases. Early work sought to compare the erosional efficiency of glaciers and rivers by measuring sediment yield (Hicks et al., 1990; Hallet et al., 1996); Koppes and Hallet (2002) pointed out that sediment budgets in recently deglaciated fjords are representing only a small, recent timescale and that long-term rates are much lower (e.g. ~37 mm/yr recently vs. ~7 mm/yr long-term for the Muir Glacier). Sediment yield has not been a useful tool to understand the impact of glaciers on the landscape or the atmosphere. Although they are rare and brief, episodic erosion events dominate the long-term sediment yield. Kirchner et al. (2001) compared long-term erosion rates with cosmogenic ^{10}Be on the scale of 5-27 ky and compared with short-term sediment yields through conventional sediment-trapping and sediment-gauging that measures sediment yields over the scale of decades (average 24 years), and found that the sediment yield estimates were so wildly different that 70-97% of sediment delivery must be occurring in catastrophic events that are too infrequent to be detected by conventional sediment-yield methods. Because sediment yield is likely to measure only a short period between major erosional events, this is not a good method for measuring the erosional impact of glaciation. Instead, it is more useful to examine topography.

A second method used for detecting the glacial signature on landscape is the examination of river channel organization and steepness. Glacial topography has been found to control channel organization and river profiles in mountain basins of British Columbia (Brardinoni and Hassan, 2006, 2007) and in Puget Sound (Collins and Montgomery, 2010), where channel concavity was utilized to show that landscapes in the Puget Sound region are still responding to Pleistocene glaciation. Profile concavity was found to vary systematically between valleys created by subglacial fluvial erosion versus those eroded by post-glacial incision, with rivers either aggrading or degrading in response to glacially imposed topography. This would indicate that the present interglacial interval, ca. 16,500 years, is less than the time required for rivers to achieve equilibrium. Drainage density also may be distinct between glacially and nonglacially developed landscapes. For

example, Salcher et al. (2014) investigated the relationship between drainage density and denudation and found two different rules, one for fluvially-dominated landscapes and another for glacially-eroded landscapes. In fluvially dominated landscapes at low elevations, drainage density was found to increase with increasing erosion rate, while a negative correlation was found in high-elevation, glacially eroded basins. The authors attribute this change to glacial processes dominating above the lowest extent of the Quaternary ELA and working to bulldoze short-wavelength topography, effectively lengthening hillslopes and increasing mass transfer and denudation (Salcher et al., 2014). Howard (1997) and Tucker and Bras (1998) predicted that in threshold landscapes, slopes will lengthen with increasing relief because while channels steepen with increasing erosion rate, threshold hillslopes do not, so that the position where channels reach the threshold slope shifts downstream. This would result in a decreasing drainage density, as hillslope length is inversely related to drainage density. DiBiase et al. (2012) found this to be only partly true; they differentiate between fluvial channels, which obey Flint's law so that slope decreases as a power law with drainage area, versus colluvial channels, where slope is independent of drainage area. Generally colluvial channels occupy the headwaters and transition to fluvial channels downstream. When the authors compared drainage density with erosion rate, they found that *fluvial* drainage density did decrease with increasing erosion rate as predicted by Howard (1997) and Tucker and Bras (1998), but that this was balanced out by an increase in *colluvial* drainage density, so that total drainage density was similar across the landscape regardless of erosion rate (DiBiase et al., 2012). Therefore, how glaciation might change drainage density if at all is a topic for further research.

A third method for detecting the glacial signature on a landscape is to focus on the landscape's elevation distribution. This method is derived from the glacial buzzsaw hypothesis, where glaciers erode topography above the snowline. A concentration of surface area at elevations corresponding to the glacial equilibrium line altitude (ELA) supports the idea of a glacial buzzsaw because glacial processes are reducing higher peaks to just below the ELA. Thus hypsometry, or the frequency distribution of elevation, can be used to analyze glaciated landscapes (e.g. Brozović et al. 1997, Kirkbride and Matthews, 1997; Montgomery et al., 2001; Mitchell and Montgomery, 2006). Egholm et al. (2009) examined DEMs around the world and found that regardless of tectonic setting, lithology, or uplift rate the hypsometric maximum is usually between the modern and LGM snowlines. Also, most summit elevations are not more than 1,500 m above the local snowline, again suggesting that glacial erosion controls the maximum height of mountains. Brocklehurst and Whipple (2002) demonstrated a close correlation between mean Quaternary ELA (halfway between modern and LGM ELA; Porter, 1989) and the elevation of glacial modification of the landscape in the Sierra Nevada. This is due to cirque floor development flattening the valley. Brocklehurst and Whipple (2004) identified a characteristic hypsometry of glaciated landscapes using the concentration of glacial erosion around the ELA. Pederson et al. (2010) found that fraction of topography

above snowline altitude depends on rate of rock column uplift and time elapsed since cessation of tectonic activity. They used a length scale indicating how rapidly the portion of surface area decays with elevation above snowline altitude and the maximum above-snowline relief at a variety of sites around the globe. In all cases the proportion of topography decays rapidly above the snowline, but at different rates. Based on these rates, the authors divide the global sites into three groups: active, recently active (the Rockies are in this group), and inactive.

In addition to hypsometry, slope-elevation plots can be used in evaluating fluvial or glacial landscapes. For example, Dixon et al. (2016) found that in nonglaciated catchments, the steepest slopes occur at high elevations, whereas in previously-glaciated catchments, the highest slopes are at lower elevations. The previously glaciated basins deviate from the overall trend of the region, which is for slope to increase with increasing elevation. This is supported by Robl et al. (2015) who described fluvially shaped catchments (which they term "premature") as generally increasing in slope with increasing elevation, whereas in glacially carved landscapes, slope only increases with elevation up to the ELA, where slopes begin to decrease due to glacial cirque formation, before suddenly steeply rising at the highest elevations where isolated forms such as nunataks rise sharply above their surroundings (figure 2.2).

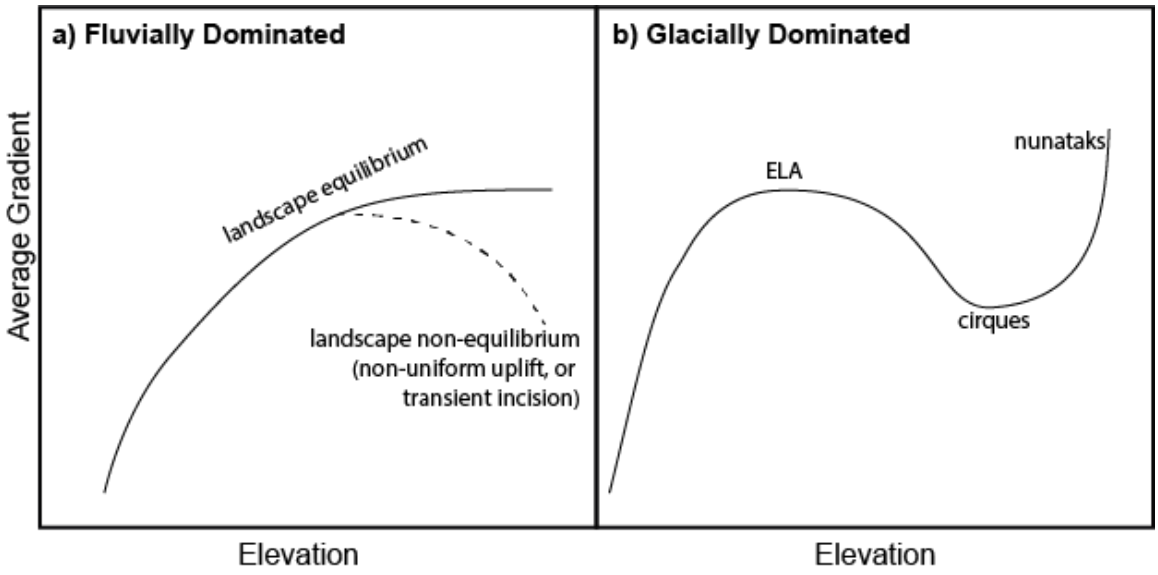

Figure A4. *Idealized slope-elevation distributions of a single profile from headwaters to trunk stream, characteristic of a) a landscape shaped by fluvial processes, and b) a landscape shaped by glacial processes. In landscape (a), the solid line represents a landscape in equilibrium, meaning it has adapted to its present boundary conditions and the entire landscape is responding to the same forcing. The dotted line represents a landscape that is not in equilibrium, which could be either because the landscape is experiencing non-uniform uplift, or because it is experiencing transient incision, meaning a change in base level has*

occurred within the landscape's response time and is still being communicated across the landscape. Glacial erosion erases local relief above the ELA and forms cirques (b), where slope gradient decreases, and can form nunataks, horns, and arêtes at the summit where rock is exposed above the glacial ice with extremely steep (near vertical) slopes. Figure adapted from Robl et al. (2015).

In addition to these direct links between glaciers and chemical weathering, the morphology left behind after glaciers recede may continue to influence chemical weathering for thousands of years. This is because soil chemical and physical weathering may depend on landscape characteristics; processes that move soil are slope-dependent, and glacial topography controls hydrologic flow that helps water flow along the surface or deep into the regolith, where it catalyzes chemical weathering reactions. Topography has been demonstrated to influence physical erosion rates (Roering et al., 2007), soil thickness and soil production rates (Dietrich et al. 1995; Heimsath, 1997) and chemical weathering rates (Riebe et al., 2004; West and Bickle, 2004; Ferrier and Kirchner, 2008; Yoo et al., 2009).

Glaciers as a Global Climate Regulator

Glaciers have been suggested to act as a global climate regulator due to their power to erode material and create fresh mineral surfaces, thus accelerating weathering and causing the sequestration of atmospheric CO_2 (Molnar and England, 1990; Raymo and Ruddiman, 1992; Hallet et al., 1996; Zhang et al., 2001); however, this argument is widely debated (Koppes and Montgomery, 2009; Portenga and Bierman, 2011; Sadler and Jerolmack, 2014; Willenbring and Jerolmack, 2016). Silicate weathering can influence the concentration of carbon dioxide in the atmosphere (Berner et al., 2003) and at least partly helps regulate climate (e.g. Walker et al., 1981), as silicate weathering reactions draw down carbon dioxide:

$$CO_2 + (Ca, Mg)SiO_3 \rightarrow (Ca, Mg)CO_3 + SiO_2 \cdot \qquad \text{(Equation 9)}$$

Rapid physical erosion, as occurs as a result of rapid rock uplift or during glaciation, may logically produce rapid chemical erosion, increasing CO_2 drawdown (Raymo et al., 1988). It is possible that tectonically driven uplift of the Himalayas and western North America may have caused such rapid erosion so as to induce global cooling in the late Cenozoic (Ruddiman and Kutzbach, 1989; Raymo and Ruddiman, 1992), or that global cooling formed glaciers that then did so much erosive work that they induced cooling and possibly even isostatic uplift of mountains (Molnar and England, 1990; Zhang et al., 2001; Molnar, 2004). However, this argument is based on a direct increase in chemical weathering with physical erosion rate, which is not always the case. Modeled chemical erosion rates my instead reach a maximum at an intermediate physical erosion rate and then decrease, approaching zero as physical erosion rates increase (e.g., Ferrier and

Kirchner, 2008). Chemical weathering in rapidly uplifting mountain belts may not contribute as significantly to global weathering as previously thought, primarily due to the low intensity of weathering in these systems and their small global area (Dixon and von Blanckenburg, 2012). The climate-driven erosion hypothesis also assumes that glaciers are a more efficient erosive agent than rivers (Hallet et al., 1996; Brozovich et al., 1997); however this point has been widely debated (Small and Anderson, 1998; Whipple et al., 1999; Koppes and Montgomery, 2009; Yanites and Ehlers, 2012). Furthermore, recent research casts doubt on whether denudation rates did increase in the late Cenozoic at all (Sadler and Jarolmack, 2014; Naylor et al, 2015; Willenbring and Jarolmack, 2016). Some of the methods used to demonstrate that denudation increased in the last 10 My, including ocean sediment accumulation (Hay et al., 1998; Métivier et al., 1999; Zhang et al., 2001; Molnar, 2004) and thermochronologic exhumation ages (Herman et al., 2013) may have a problem of scale, so that rates of accumulation or exhumation appear to decrease as the measurement interval is expanded (Sadler, 1981, 1994; Schumer and Jerolmack, 2009). While climate, tectonics, erosion, and weathering certainly interact in complex ways and feed back on each other, the ability of glaciers to instigate drastic global cooling or mountain uplift is far from certain (Willenbring and Jerolmack, 2016).

Local Geology and Setting of the Bitterroot Valley

The Bitterroot and Sapphire Mountains, which border the Bitterroot Valley in western Montana, provide an ideal natural laboratory for studying the effects of climate history on morphology and soil evolution. The Bitterroot Mountains occupy the eastern edge of the Idaho Batholith; bordering the Idaho Batholith to the east is the Bitterroot Valley, and across the valley the Sapphire Mountains. The Idaho Batholith is composed of quartz monzonite whose mineralogic composition varies but is mainly quartz, orthoclase, oligoclase, and biotite (Ross 1950). The texture is coarse-grained to porphyritic. Along the Bitterroot range front adjacent to the valley is a gneissic and schistose border zone that dips 18-26° east and which has a closely spaced joint pattern (Lindgren 1904, Ross 1950). This makes it highly susceptible to glacial erosion, so that glacial drift deposited outside the canyon mouths has a high percentage of this gneissic lithology. In this gneiss biotite grains form thin, discontinuous laminae, which are roughly parallel to the long axis of the quartz and feldspar grains (Ross 1950).

The Bitterroot Mountains are composed of a series of east-west-trending parallel catchments carved by valley glaciers during the Pleistocene. North-facing slopes are carved by cirque glaciers, while cirque glacier growth was inhibited on south-facing slopes by higher solar insolation (Beaty, 1961; Evans and Cox, 2005). Naylor and Gabet (2007) took advantage of this difference and the lithologic homogeneity across the Bitterroot Mountains to assess the relative erosional potential of glacial processes on north-facing slopes and nonglacial processes on south-facing slopes.

The Bitterroots' glacial history was first described by Lindgren (1904). Pardee (1910, 1942) examined the geomorphic evidence of the historical extent of Glacial Lake Missoula. Alden (1953) surveyed the physiography of Bitterroot glaciations including piedmont surfaces, stream terraces, and moraines. Alden (1953) found evidence for three major glaciations in the Bitterroot Mountains correlating to Early Pleistocene, Illinoian (or Early Wisconsin), and Wisconsin ages. This was based on glacial deposits at the mouths of several canyons, and on a Pleistocene chronology Alden had already developed from work in eastern Montana (Alden, 1932). Weber (1972) built on this work by mapping three drift sequences, which he refers to as the Judd Drift (pre-Wisconsin), Charlos Drift (early Wisconsin), and Lost Horse Drift (late Wisconsin). These approximate ages are based on granite-weathering ratios, topographic position, soil development, and correlations with Glacial Lake Missoula lake stands. Weber (1972) mapped six end moraines composed of Lost Horse Drift outside the mouth of Roaring Lion Canyon, suggesting there were at least six glacial advances. He also noted that evidence of glaciation increases to the south. Four canyons (Carlton, One Horse, Bass, and Kootenai Creeks) toward the north were found to lack the signature U-shape of glaciation and terminal moraine. The Judd glaciation seems to have been the most extensive, as Judd Drift is present beyond drift of other sequences, and because Judd Drift mapped between Lost Horse and Rock Creeks indicates that the glaciers from these two creeks merged beyond the canyon mouths.

Naylor and Gabet (2007) used field mapping and analysis of DEMs and aerial photography to compare north- and south-facing slopes in the Bitterroot Mountains in order to compare differing erosional regimes: due to unequal solar insolation, north-facing sides of the valleys were glaciated, while south-facing slopes were not, allowing the formation of larger cirque glaciers on north-facing slopes (Beaty, 1961; Evans and Cox, 2005). This is shown through the asymmetric ridges, as ridge-to-valley distances on north-facing slopes are ~1.5x that of south-facing slopes. Glaciated slopes are found to be less steep than non-glaciated slopes (portions of south-facing slopes that are judged to be glaciated are excluded from this analysis). This is despite equal precipitation rates and no significant redistribution of snow latitudinally, according to late Pleistocene weather reconstructions that show that anticyclonic easterlies were dominant in the northwest (Kutzbach and Ruddiman, 1993; Hostetler and Clark, 1997). The differences are also not due to lithology, as most of the range is underlain by a massive granite assemblage without discrete structural features (Lonn and Berg, 1996; Lewis, 1998). Using a spline surface fit across ridgelines to approximate the volume of material eroded (e.g. Brocklehurst and Whipple 2006), glaciers are found to have removed almost twice as much rock as nonglacial processes. Part of this is through vertical incision but the dominant impact of glaciers is lateral erosion by headwall retreat. Naylor and Gabet (2007) concluded that glacial processes operating on north-facing slopes are more efficient at headward erosion than the nonglacial processes operating on south-facing slopes, causing ridgelines to be pushed southward. This is in accordance with the findings

of Brocklehurst and Whipple (2002, 2006) that glacial erosion exceeds fluvial erosion, principally through horizontal headwall incision, based on analysis of fluvial and glacial longitudinal profiles.

Pederson and Egholm (2013) used the Bitterroot Range in their investigation into the effect of multiple glacial cycles. They compare Bear Creek to the unglaciated Aldeire catchment in the Spanish Sierra Nevada, which they refer to as a fluvial landscape with no hypsometric maximum, by simulating snowline lowering in each catchment. In the Sierra Nevada catchment, glaciers grow steadily when snowline is lowered. The simulation in Bear Creek, on the other hand, shows that glaciers are slow to grow at first but when the snowline gets lowered below the hypsometric maximum, glaciers grow quickly. The Sierra Nevada shows a linear relationship between snowline altitude and glacial area, and in the Bitterroots the relationship is nonlinear. In the second part of the experiment, a model landscape is subjected to a simulation of glacial erosion processes and isostatic flexure subjected to climatic changes similar to what Earth has experienced over the last 2 My: phase 1) symmetric, constant magnitude 40 ky climate cycles; 2) a transition period representing the mid-Pleistocene transition; and phase 3) asymmetric constant-magnitude 100-kyr climate cycles. During phase 1, the topography forms the typical glacial hypsometry and by the end of phase 1 glaciers become smaller as much of the topography above the snowline has been removed. During phase 2, there is an abundance of topography just below what was previously the snowline, so when the snowline advances even a small amount, ice volume increases greatly (ice volume doubles for only ~90m lowering of snowline). The snowline progressively lowers, and glacial extent increases quickly. The authors find that the degree of glacial modification already present at the onset of a climatic cooling influences the extent of subsequent glaciation and sensitivity of the landscape to climate change. In landscapes that were not glaciated before, glacial area increases linearly with cooling; in previously glaciated landscapes, however, glaciers are slow to grow at first because there is little topography above the snowline but expand rapidly once the snowline reaches the hypsometric maximum, even when the landscapes have extensive area at similar elevations. This shows that early Pleistocene glaciations (before a transition at approx. 950 kya) preconditioned the landscape for more extensive glaciations and valley deepening in the later Pleistocene. This agrees with existing exposure dating and low-temperature thermochronologic dating from the European Alps. This experiment shows that long-term history of a region influences the relation between climate and glacial extent through a constantly changing topographic control.

Input from dust has been shown to significantly impact soils in other regions of

the Idaho Batholith, west of the Bitterroots. This is important for using mass balance to infer rock-to-soil chemical weathering losses. Granitic soils at two transects at the South Fork Salmon River in Idaho showed enrichment of mafic elements (Ti, Fe, Mg), implying that a mafic-rich dust has been aerially deposited, possibly from glacial outburst flood

sediments in Eureka Flat, WA (Ferrier, 2009). In order to determine the deposition rate of dust to this site, Ferrier (2009) carried out a mass-balance analysis using two immobile elements instead of one and combined this with soil production rates determined from cosmogenic nuclides and concluded that dust deposition rate would be 3-13 t km^{-2} yr^{-1}.

The degree of chemical weathering at the same sites in the South Fork Salmon River mentioned above has been demonstrated to be strongly influenced by moisture availability and almost not at all by temperature. Ferrier (2009) used time series measurements from soil moisture and temperature probes and found that the degree of chemical weathering is strongly controlled by the annual duration of high soil moisture conditions, which is primarily dependent on the annual duration of snow cover in this setting. Additionally, soils at these sites become more chemically weathered with increasing soil residence time, which implies that weathering is kinetically limited.

References Cited

Ahnert, F. 1967. in *L'evolution des Versants* (ed. Macar, P.) 23–41 (Univ. Liege).

Ahnert, F., 1970. Functional relationships between denudation, relief, and uplift in large, mid-latitude drainage basins. *American Journal of Science*, *268*(3), pp.243-263.

Amundson, R, Heimsath, A., Owen, J., Yoo, K., and Dietrich, WE. 2015. Hillslope soils and vegetation: A review. *Geomorphology*, 234: 122-132.

Anderson, S.P., Dietrich, W.E. and Brimhall, G.H., 2002. Weathering profiles, mass-balance analysis, and rates of solute loss: Linkages between weathering and erosion in a small, steep catchment. *Geological Society of America Bulletin*, *114*(9), pp.1143-1158.

Anderson, R.S., Riihimaki, C.A., Safran, E.B. and MacGregor, K.R., 2006. Facing reality: Late Cenozoic evolution of smooth peaks, glacially ornamented valleys, and deep river gorges of Colorado's Front Range. *Geological Society of America Special Papers*, *398*, pp.397-418.

Berner, R.A. 2003. The long-term carbon cycle, fossil fuels and atmospheric composition. *Nature*, *426*(6964), pp.323-326.

Brantley, S. L., and M. Lebedeva. 2011. Learning to read the chemistry of regolith to understand the Critical Zone. *Annu. Rev. Earth Planet. Sci.*, 39, 387–416, doi:10.1146/annurev-earth-040809-152321.

Brardinoni, F. and Hassan, M.A., 2006. Glacial erosion, evolution of river long profiles, and the organization of process domains in mountain drainage basins of coastal British Columbia. *Journal of Geophysical Research: Earth Surface*, *111*(F1).

Brardinoni, F. and Hassan, M.A., 2007. Glacially induced organization of channel-reach morphology in mountain streams. *Journal of Geophysical Research: Earth Surface*, *112*(F3).

Brimhall, G.H., Alpers, C.N. and Cunningham, A.B., 1985. Analysis of supergene ore-forming processes and ground-water solute transport using mass balance principles. *Economic Geology*, *80*(5), pp.1227-1256.

Brimhall, G.H., Lewis, C.J., Ague, J.J., Dietrich, W.E. and Hampel, J., 1988. Chemically mature aeolian dust. *Nature*, *333*, p.30.

Brimhall, G.H., Ford, C., Bratt, J., Taylor, G. and Warin, O., 1991. Quantitative geochemical approach to pedogenesis: importance of parent material reduction, volumetric expansion, and eolian influx in lateritization. *Geoderma*, *51*(1), pp.51-91.

Brimhall, G., Chadwick, O., Lewis, C., Compston, W., Williams, I., Danti, K., Dietrich, W., Power, M., Hendricks, D. and Bratt, J., 1992. Deformational mass transport and invasive processes in soil evolution. *Science*, *255*(5045), pp.695-702.

Brimhall, G.H. and Dietrich, W.E., 1987. Constitutive mass balance relations between chemical composition, volume, density, porosity, and strain in metasomatic hydrochemical systems: results on weathering and pedogenesis. *Geochimica et Cosmochimica Acta*, *51*(3), pp.567-587.

Brocklehurst, S.H. and Whipple, K.X., 2002. Glacial erosion and relief production in the Eastern Sierra Nevada, California. *Geomorphology*, *42*(1), pp.1-24.

Brocklehurst, S.H. and Whipple, K.X., 2004. Hypsometry of glaciated landscapes. *Earth Surface Processes and Landforms*, *29*(7), pp.907-926.

Brocklehurst, S.H. and Whipple, K.X., 2006. Assessing the relative efficiency of fluvial and glacial erosion through simulation of fluvial landscapes. *Geomorphology*, *75*(3), pp.283-299.

Brozović, N., Burbank, D.W. and Meigs, A.J., 1997. Climatic limits on landscape development in the northwestern Himalaya. Science, 276, 571–574.

Burbank, D.W., Leland, J., Fielding, E., Anderson, R.S., Brozovic, N., Reid, M.R. and Duncan, C. 1996. Bedrock incision, rock uplift and threshold hillslopes in the northwestern Himalayas. *Nature*, *379*(6565), pp.505-510.

Carson, M.A. and Kirkby, M.J., 1972. Hillslope form and process.

Carson, M.A. and Petley, D.J. 1970. The Existence of Threshold Hillslopes in the Denudation of the Landscape. *Transactions of the Institute of British Geographers* 49(49):71.

Chadwick, O.A., Brimhall, G.H. and Hendricks, D.M., 1990. From a black to a gray box—a mass balance interpretation of pedogenesis. *Geomorphology*, *3*(3), pp.369-390.

Chadwick, O.A., Roering, J.J., Heimsath, A.M., Levick, S.R., Asner, G.P. and Khomo, L., 2013. Shaping post-orogenic landscapes by climate and chemical weathering. *Geology*, *41*(11), pp.1171-1174.

Colin, F., Alarcon, C. and Vieillard, P., 1993. Zircon: an immobile index in soils?. *Chemical Geology*, *107*(3-4), pp.273-276.

Collins, B.D. and Montgomery, D.R., 2011. The legacy of Pleistocene glaciation and the organization of lowland alluvial process domains in the Puget Sound region. *Geomorphology*, *126*(1), pp.174-185.

Cornu, S., Breeze, D., Saada, A. and Baranger, P., 2003. The influence of pH, electrolyte type, and surface coating on arsenic (V) adsorption onto kaolinites. *Soil Science Society of America Journal*, *67*(4), pp.1127-1132.

Culling, W.E.H., 1960. Analytical theory of erosion. *The Journal of Geology*, pp.336-344.

Culling, W.E.H., 1963. Soil creep and the development of hillside slopes. *The Journal of Geology*, pp.127-161.

DiBiase, R.A., Whipple, K.X., Heimsath, A.M. and Ouimet, W.B., 2010. Landscape form and millennial erosion rates in the San Gabriel Mountains, CA. *Earth and Planetary Science Letters*, *289*(1), pp.134-144.

DiBiase, R.A., Heimsath, A.M. and Whipple, K.X., 2012. Hillslope response to tectonic forcing in threshold landscapes. *Earth Surface Processes and Landforms*, *37*(8), pp.855-865.

Dietrich, W.E. and Montgomery, D.R., 1998. Hillslopes, channels, and landscape scale. *Scale dependence and scale invariance in hydrology*, pp.30-60.

Dietrich, W. E., Reiss, R., Hsu, M.-L. & Montgomery, D. R. 1995. A process-based model for colluvial soil depth and shallow landsliding using digital elevation data. *Hydrol. Proc.* **9,** 383–400.

Dietrich, W.E., Bellugi, D.G., Sklar, L.S., Stock, J.D., Heimsath, A.M. and Roering, J.J. 2003. Geomorphic transport laws for predicting landscape form and dynamics. *Prediction in geomorphology*, pp.103-132.

Dixon JL, Heimsath AM, Amundson RC. 2009. The critical role of climate and saprolite weathering in landscape evolution. *Earth Surface Processes and Landforms* **34** : 1507–1521.

Dixon, J.L., Hartshorn, A.S., Heimsath, A.M., DiBiase, R.A. and Whipple, K.X., 2012. Chemical weathering response to tectonic forcing: A soils perspective from the San Gabriel Mountains, California. *Earth and Planetary Science Letters*, *323*, pp.40-49.

Dixon, J.L. and von Blanckenburg, F. 2012. Soils as pacemakers and limiters of global silicate weathering. *Comptes Rendus Geoscience*, *344*(11), pp.597-609.

Dixon JL, Riebe CS. 2014. Tracing and pacing soil across slopes. *Elements* **10** : 363–368.

Dixon, JL., von Blanckenburg, F, Stuwe, K., and Christl, M. 2016. Glaciation's topographic control on Holocene erosion at the eastern edge of the Alps. *Earth Surf. Dynam. Discuss.*, doi:10.5194/esurf-2016-29, 2016

D'Odorico, P., Ridolfi, L., Porporato, A. and Rodriguez-Iturbe, I., 2000. Preferential states of seasonal soil moisture: The impact of climate fluctuations. *Water Resources Research*, *36*(8), pp.2209-2219.

Egholm, D.L., Nielsen, S.B., Pedersen, V.K. and Lesemann, J.E., 2009. Glacial effects limiting mountain height. *Nature*, *460*(7257), pp.884-887.

Fernandes, N.F. and Dietrich, W.E., 1997. Hillslope evolution by diffusive processes: The timescale for equilibrium adjustments. *Water Resources Research*, *33*(6), pp.1307-1318.

Ferrier, K., 2009. Effects of climate, physical erosion, parent mineralogy, and dust on chemical erosion rates in mountainous terrain.

Ferrier, K.L. and Kirchner, J.W., 2008. Effects of physical erosion on chemical denudation rates: a numerical modeling study of soil-mantled hillslopes. *Earth and Planetary Science Letters*, *272*(3), pp.591-599.

Ferrier, K.L., Kirchner, J.W., Riebe, C.S. and Finkel, R.C., 2010. Mineral-specific chemical weathering rates over millennial timescales: measurements at Rio Icacos, Puerto Rico. *Chemical Geology*, *277*(1), pp.101-114.

Ferrier, K.L., Kirchner, J.W. and Finkel, R.C., 2011. Estimating millennial-scale rates of dust incorporation into eroding hillslope regolith using cosmogenic nuclides and immobile weathering tracers. *Journal of Geophysical Research: Earth Surface*, *116*(F3).

Ferrier, K.L., Kirchner, J.W. and Finkel, R.C., 2012. Weak influences of climate and mineral supply rates on chemical erosion rates: Measurements along two

altitudinal transects in the Idaho Batholith. *Journal of Geophysical Research: Earth Surface*, *117*(F2).

Gilbert, GK. 1877. *Report on the Geology of the Henry Mountains*. Department of the Interior: Washington, DC.

Gilbert, G.K., 1904, Systematic asymmetry of crest lines in the high Sierra of California: *The Journal of Geology*, v. **12** pp. 579-588.

Gilbert GK. 1909. The convexity of hilltops. *Journal of Geology* **17** : 344–350.

Hack, J.T., 1960. *Interpretation of erosional topography in humid temperate regions*. Bobbs-Merrill.

Hallet, B., Hunter, L. and Bogen, J., 1996. Rates of erosion and sediment evacuation by glaciers: a review of field data and their implications. Global Planet. Change, 12(1), 213–235.

Hay, W.W., Sloan, J.L. and Wold, C.N., 1988. Mass Age Distribution and Composition of Sediments on the Ocean-Floor and the Global Rate of Sediment Subduction. J. Geophys. Res.-Solid Earth, 93(B12), 14933–14940.

Heimsath, A.M., Dietrich, W.E., Nishiizumi, K. and Finkel, R.C., 1997. The soil production function and landscape equilibrium. *Nature*, *388*(6640), pp.358-361.

Heimsath, A.M., Dietrich, W.E., Nishiizumi, K. and Finkel, R.C., 1999. Cosmogenic nuclides, topography, and the spatial variation of soil depth. *Geomorphology*, *27*(1), pp.151-172.

Heimsath, A.M., Chappell, J., Dietrich, W.E., Nishiizumi, K. and Finkel, R.C., 2000. Soil production on a retreating escarpment in southeastern Australia. *Geology*, *28*(9), pp.787-790.

Heimsath, A.M., Dietrich, W.E., Nishiizumi, K. and Finkel, R.C., 2001a. Stochastic processes of soil production and transport: Erosion rates, topographic variation and cosmogenic nuclides in the Oregon Coast Range. *Earth Surface Processes and Landforms*, *26*(5), pp.531-552.

Heimsath, A.M., Chappell, J., Dietrich, W.E., Nishiizumi, K. and Finkel, R.C., 2001b. Late Quaternary erosion in southeastern Australia: a field example using cosmogenic nuclides. *Quaternary International*, *83*, pp.169-185.

Heimsath AM, Furbish DJ, Dietrich WE. 2005. The illusion of diffusion: Field evidence for

depth-dependent sediment transport. *Geology* **33** : 949–952.

Heimsath, A.M., Chappell, J., Finkel, R.C., Fifield, K. and Alimanovic, A., 2006. Escarpment erosion and landscape evolution in southeastern Australia. *Geological Society of America Special Papers*, *398*, pp.173-190.

Heimsath, A.M., Fink, D. and Hancock, G.R., 2009. The 'humped'soil production function: eroding Arnhem Land, Australia. *Earth Surface Processes and Landforms*, *34*(12), pp.1674-1684.

Heimsath, A.M., DiBiase, R.A. and Whipple, K.X., 2012. Soil production limits and the transition to bedrock-dominated landscapes. *Nature Geoscience*, *5*(3), pp.210-214.

Herman, F., Seward, D., Valla, P.G., Carter, A, Kohn, B., Willett, S.D. and Ehlers, T.A., 2013. Worldwide acceleration of mountain erosion under a cooling climate. Nature, 504, 423–426.

Hicks, D.M., McSaveney, M.J., and Chinn, T.J.H., 1990, Sedimentation in proglacial Ivory Lake, Southern Alps, New Zealand: *Arctic and Alpine Research*, v. 22p. 26-42.

Hole, F.D., 1981. Effects of animals on soil. *Geoderma*, *25*(1), pp.75-112.

Hostetler, S.W., and Clark, P.U., 1997, Climatic controls of western U.S. glaciers at the Last Glacial Maximum: *Quaternary Science Reviews*, v. **16** pp. 505-511 doi: 10.1016/S0277-3791 (96)00116-3.

Howard, A.D., 1994. A detachment-limited model of drainage basin evolution. *Water resources research*, *30*(7), pp.2261-2285.

Howard AD. 1997. Badland morphology and evolution: interpretation using a simulation model. Earth Surface Processes and Landforms 22: 211–227.

Hurst, M.D., Mudd, S.M., Walcott, R., Attal, M. and Yoo, K., 2012. Using hilltop curvature to derive the spatial distribution of erosion rates. *Journal of Geophysical Research: Earth Surface*, *117*(F2).

Jerolmack, D. and Sadler, P., 2007. Transience and persistence in the depositional record of continental margins. J. Geophys. Res., 112, F03S13

Jin, L., R. Ravella, B. Ketchum, P. R. Bierman, P. Heaney, T. White, and S. L. Brantley. 2010. Mineral weathering and elemental transport during hillslope evolution at

the Susquehanna/Shale Hills Critical Zone Observatory. *Geochim. Cosmochim. Acta*, 74, 3669–3691

Kirchner, J.W., Finkel, R.C., Riebe, C.S., Granger, D.E., Clayton, J.L., King, J.G. and Megahan, W.F., 2001. Mountain erosion over 10 yr, 10 ky, and 10 my time scales. *Geology*, *29*(7), pp.591-594.

Kirkbride, M. and Matthews, D., 1997. The role of fluvial and glacial erosion in landscape evolution: the Ben Ohau Range, New Zealand. *Earth Surface Processes and Landforms*, *22*(3), pp.317-327.

Koppes, M.N. and Hallet, B., 2002. Influence of rapid glacial retreat on the rate of erosion by tidewater glaciers. *Geology*, *30*(1), pp.47-50.

Koppes, M.N. and Montgomery, D.R., 2009. The relative efficacy of fluvial and glacial erosion over modern to orogenic timescales. Nature Geosci., 2(9), 644– 647.

Kurtz, A.C., Derry, L.A., Chadwick, O.A. and Alfano, M.J., 2000. Refractory element mobility in volcanic soils. *Geology*, *28*(8), pp.683-686.

Kutzbach, J.E. and Ruddiman, W.F., 1993. Model description, external forcing, and surface boundary conditions. *Global climates since the last glacial maximum*, pp.12-23.

Lewis, R.S., 1998, Geologic map of the Montana part of the Missoula West 30′ × 60′ quadrangle: Montana Bureau of Mines Open-File Report 373, scale 1:100,000.

Lindgren, Waldemar, 1904, A geological recon- naissance across the Bitterroot Range and Clear- water Mountains in Montana and Idaho: U.S. Geol. Survey Prof. Paper 27, 222 p.

Lonn, J.D., and Berg, R.B., 1996, Preliminary geologic map of the Bitterroot Valley, Montana: Montana Bureau of Mines Open-File Report 340, scale 1:100,000.

Lutz, H.J., 1960. Movement of rocks by uprooting of forest trees. *American Journal of Science*, *258*(10), pp.752-756.

Lutz, H.J. and Griswold, F.S., 1939. The influence of tree roots on soil morphology. *American Journal of Science*, *237*(6), pp.389-400.

Matsuoka, N., 1990. Mechanisms of rock breakdown by frost action: an experimental approach. *Cold Regions Science and Technology*, *17*(3), pp.253-270.

Métivier, F., Gaudemer, Y., Tapponier, P. and Klein, M., 1999. Mass accumulation rates in Asia during the Cenozoic. Geophys. J. Int., 137, 280–318.

McKean, J.A., Dietrich, W.E., Finkel, R.C., Southon, J.R. and Caffee, M.W., 1993. Quantification of soil production and downslope creep rates from cosmogenic ^{10}Be accumulations on a hillslope profile. *Geology*, *21*(4), pp.343-346.

Merrill, G.P., 1897. *A treatise on rocks: Rock-weathering and soils*. Macmillan Company.

Mitchell, P.B., 1988. The influence of vegetation, animals and micro-organisms on soil processes.

Mitchell, S.G. and Montgomery, D.R., 2006. Influence of a glacial buzzsaw on the height and morphology of the Cascade Range in central Washington State, USA. *Quaternary Research*, *65*(1), pp.96-107.

Molnar, P., 2004, Late Cenozoic increase in accumulation rates of terrestrial sediment: How might climate change have affected erosion rates?: Annual Review of Earth and Planetary Sciences, v. 32, p. 67–89, doi: 10.1146/ annurev.earth.32.091003.143456.

Molnar, P. and England, P., 1990. Late Cenozoic uplift of mountain ranges and global climate change: chicken or egg?. *Nature*, *346*(6279), pp.29-34.

Montgomery, D.R. 2001. Slope distributions, threshold hillslopes, and steady-state topography. *American Journal of Science*, *301*(4-5), pp.432-454.

Montgomery, D.R. and Brandon, M.T. 2002. Topographic controls on erosion rates in tectonically active mountain ranges. *Earth and Planetary Science Letters*, *201*(3), pp.481-489.

Moon, S., Chamberlain, C.P., Blisniuk, K., Levine, N., Rood, D.H. and Hilley, G.E., 2011. Climatic control of denudation in the deglaciated landscape of the Washington Cascades. *Nature Geoscience*, *4*(7), pp.469-473.

Mudd, S.M. and Furbish, D.J., 2007. Responses of soil-mantled hillslopes to transient channel incision rates. *Journal of Geophysical Research: Earth Surface*, *112*(F3).

Naylor, M., Sinclair, H.D., Bernet, M., van der Beek, P., and Kirstein, L. 2015. Bias in detrital fission track grain-age populations: implications for reconstructing changing erosion rates. *Earth Planet. Sci. Lett.*, 422, 94-104.

Naylor, S. and Gabet, E.J., 2007. Valley asymmetry and glacial versus nonglacial erosion in the Bitterroot Range, Montana, USA. *Geology*, *35*(4), pp.375-378.

Norman, J.M., Kustas, W.P. and Humes, K.S., 1995. Source approach for estimating soil and vegetation energy fluxes in observations of directional radiometric surface temperature. *Agricultural and Forest Meteorology*, *77*(3), pp.263-293.

Norton, K.P., Molnar, P. and Schlunegger, F., 2014. The role of climate-driven chemical weathering on soil production. *Geomorphology*, *204*, pp.510-517.

Ouimet, W.B., Whipple, K.X. and Granger, D.E., 2009. Beyond threshold hillslopes: Channel adjustment to base-level fall in tectonically active mountain ranges. *Geology*, *37*(7), pp.579-582.

Paton, T.R., 1995. *Soils: a new global view*. CRC Press.

Pedersen, V.K., Egholm, D.L. and Nielsen, S.B., 2010. Alpine glacial topography and the rate of rock column uplift: a global perspective. *Geomorphology*, *122*(1), pp.129-139.

Pedersen, V.K. and Egholm, D.L., 2013. Glaciations in response to climate variations preconditioned by evolving topography. *Nature*, *493*(7431), pp.206-210.

Penck, A., 1905. Glacial features in the surface of the Alps. *The Journal of Geology*, *13*(1), pp.1-19.

Porder, S., Hilley, G.E. and Chadwick, O.A., 2007. Chemical weathering, mass loss, and dust inputs across a climate by time matrix in the Hawaiian Islands. *Earth and Planetary Science Letters*, *258*(3), pp.414-427.

Portenga, E.W. and Bierman, P.R., 2011. Understanding Earth's eroding surface with 10 Be. *GSA Today*, *21*(8), pp.4-10.

Porter, S.C., 1989. Late Holocene fluctuations of the fiord glacier system in Icy Bay, Alaska, USA. *Arctic and Alpine Research*, pp.364-379.

Rasmussen, C., Brantley, S., Blum, A., Dixon, J. and White, A.F., 2011. Strong climate and tectonic control on plagioclase weathering in granitic terrain. *Earth and Planetary Science Letters*, *301*(3), pp.521-530.

Raymo, M.E. and Ruddiman, W.F., 1992. Tectonic forcing of late Cenozoic climate. *Nature*, *359*(6391), pp.117-122.

Raymo, M.E., Ruddiman, W.F. and Froelich, P.N., 1988. Influence of late Cenozoic mountain building on ocean geochemical cycles. *Geology*, *16*(7), pp.649-653.

Riebe, C.S., Kirchner, J.W., Granger, D.E. and Finkel, R.C., 2001. Minimal climatic control on erosion rates in the Sierra Nevada, California. *Geology*, *29*(5), pp.447-450.

Riebe, C.S., Kirchner, J.W. and Finkel, R.C., 2004a. Erosional and climatic effects on long-term chemical weathering rates in granitic landscapes spanning diverse climate regimes. *Earth and Planetary Science Letters*, *224*(3), pp.547-562.

Riggins, S.G., Anderson, R.S., Anderson, S.P. and Tye, A.M., 2011. Solving a conundrum of a steady-state hilltop with variable soil depths and production rates, Bodmin Moor, UK. *Geomorphology*, *128*(1), pp.73-84.

Robl, J., Prasicek, G., Hergarten, S. and Stüwe, K., 2015. Alpine topography in the light of tectonic uplift and glaciation. *Global and Planetary Change*, *127*, pp.34-49.

Roering, J.J., Kirchner, J.W. and Dietrich, W.E., 1999. Evidence for nonlinear, diffusive sediment transport on hillslopes and implications for landscape morphology. *Water Resources Research*, *35*(3), pp.853-870.

Roering, J.J., Kirchner, J.W., Sklar, L.S. and Dietrich, W.E., 2001a. Hillslope evolution by nonlinear creep and landsliding: An experimental study. *Geology*, *29*(2), pp.143-146.

Roering, J.J., Kirchner, J.W. and Dietrich, W.E., 2001b. Hillslope evolution by nonlinear, slope-dependent transport: Steady state morphology and equilibrium adjustment timescales. *Journal of Geophysical Research: Solid Earth*, *106*(B8), pp.16499-16513.

Roering, J.J., Perron, J.T. and Kirchner, J.W., 2007. Functional relationships between denudation and hillslope form and relief. *Earth and Planetary Science Letters*, *264*(1), pp.245-258.

Ross, C. P., 1950, The eastern front of the Bitterroot Range, Montana: U.S. Geol. Survey Bull. 974-E, p. 135-174.

Ruddiman, W.F., 2010. A paleoclimatic enigma. Science, 328(5980), 838–839.

Ruddiman, W.F. and Kutzbach, J.E., 1989. Forcing of late Cenozoic northern hemisphere climate by plateau uplift in southern Asia and the American West. *Journal of Geophysical Research: Atmospheres*, *94*(D15), pp.18409-18427.

Sadler, P.M., 1981. Sediment accumulation rates and the completeness of stratigraphic sections. J. Geol., 89, 569–584.

Sadler, P.M., 1994. The expected duration of upward-shallowing carbonate cycles and their terminal hiatuses. Geol. Soc. Am. Bull., 106, 791–802.

Sadler, P. and Jerolmack, D.J., 2014. Scaling laws for aggradation, denudation and progradation rates: the case for time-scale invariance at sediment sources and sinks. Geol. Soc. London Spec. Publ., 404, SP404.

Salcher, B.C., Kober, F., Kissling, E. and Willett, S.D., 2014. Glacial impact on short-wavelength topography and long-lasting effects on the denudation of a deglaciated mountain range. *Global and Planetary Change, 115*, pp.59-70.

Schaetzl, R.J. and Follmer, L.R., 1990. Longevity of treethrow microtopography: implications for mass wasting. *Geomorphology*, *3*(2), pp.113-123.

Schlunegger, F. and Norton, K.P., 2013. Water versus ice: The competing roles of modern climate and Pleistocene glacial erosion in the Central Alps of Switzerland. *Tectonophysics, 602*, pp.370-381.

Schmidt, K.M. and Montgomery, D.R. 1995. Limits to relief. *Science, 270* (5236), p.617.

Schumer, R. and Jerolmack, D.J., 2009. Real and apparent changes in sediment deposition rates through time (2003–2012). J. Geophys. Res.-Earth Surface, 114, F3.

Small, E.E. and Anderson, R.S., 1998. Pleistocene relief production in Laramide mountain ranges, western United States. *Geology*, *26*(2), pp.123-126.

Small, Eric E., Robert S. Anderson, and Gregory S. Hancock. 1999. Estimates of the rate of regolith production using ^{10}Be and 26Al from an alpine hillslope. *Geomorphology* 27.1 : 131-150.

Strahler, A.N., 1950. Davis' concepts of slope development viewed in the light of recent quantitative investigations. *Annals of the Association of American Geographers*, *40*(3), pp.209-213.

Stallard, R.F. and Edmond, J.M., 1983. Geochemistry of the Amazon: 2. The influence of geology and weathering environment on the dissolved load. *Journal of Geophysical Research: Oceans*, *88*(C14), pp.9671-9688.

Sudom, M.D. and St. Arnaud, R.J., 1971. Use of quartz, zirconium and titanium as indices in pedological studies. *Canadian Journal of Soil Science*, *51*(3), pp.385-396.

Taboada, T., Cortizas, A.M., García, C. and García-Rodeja, E., 2006. Particle-size fractionation of titanium and zirconium during weathering and pedogenesis of granitic rocks in NW Spain. *Geoderma*, *131*(1), pp.218-236.

Tucker GE, Bras RL. 1998. Hillslope processes, drainage density, and landscape morphology. Water Resources Research 34: 2751–2764. DOI. 10.1029/98wr01474

Van Der Beek, P., Van Melle, J., Guillot, S., Pécher, A., Reiners, P.W., Nicolescu, S. and Latif, M., 2009. Eocene Tibetan plateau remnants preserved in the northwest Himalaya. Nat. Geosci., 2, 364–368.

Walker, J.C., Hays, P.B. and Kasting, J.F., 1981. A negative feedback mechanism for the long-term stabilization of Earth's surface temperature. *Journal of Geophysical Research: Oceans*, *86*(C10), pp.9776-9782.

Weber, W.M., 1972, Correlation of Pleistocene glaciation in the Bitterroot Range, Montana, with fluctuations of Glacial Lake Missoula, Montana: Bureau of Mines and Geology Memoir 42p. 44 p.

West, A.J., Galy, A. and Bickle, M., 2005. Tectonic and climatic controls on silicate weathering. *Earth and Planetary Science Letters*, *235*(1), pp.211-228.

Wilkinson MT, Chappell J, Humphreys GS, Fifield K, Smith B, Hesse PP. 2005. Soil production in heath and forest, Blue Mountains, Australia: influence of lithology and palaeoclimate. *Earth Surface Processes and Landforms* **30** : 923–934.

Willenbring, J.K. and Jerolmack, D.J., 2016. The null hypothesis: globally steady rates of erosion, weathering fluxes and shelf sediment accumulation during Late Cenozoic mountain uplift and glaciation. *Terra Nova*, *28*(1), pp.11-18.

Whipple, K., Kirby, E. and Brocklehurst, S., 1999. Geomorphic limits to climatically induced increases in topographic relief. *Nature*, 401, 39–43.

White, A.F., Blum, A.E., Schulz, M.S., Vivit, D.V., Stonestrom, D.A., Larsen, M., Murphy, S.F. and Eberl, D., 1998. Chemical weathering in a tropical watershed, Luquillo Mountains, Puerto Rico: I. Long-term versus short-term weathering fluxes. *Geochimica et Cosmochimica Acta*, *62*(2), pp.209-226.

White, A.F., Blum, A.E., Schulz, M.S., Huntington, T.G., Peters, N.E., and Stonestrom, D.A., 2002. Chemical weathering of the Panola granite: Solute and regolith elemental fluxes and the weathering rate of biotite, *in* Hellmann, R., and Wood,

S.A., eds., Water rock interaction, ore deposits, and environmental geochemistry, a tribute to David A. Crerar: *Geochemical Society Special Publication* 7,. 37-59.

Yanites, B.J. and Ehlers, T.A., 2012. Global climate and tectonic controls on the denudation of glaciated mountains. Earth Planet. Sci. Lett., 325–326, 63–75.

Yoo, K., Mudd, S.M., Sanderman, J., Amundson, R. and Blum, A., 2009. Spatial patterns and controls of soil chemical weathering rates along a transient hillslope. *Earth and Planetary Science Letters*, *288*(1), pp.184-193.

Zhang, P., Molnar, P. and Downs, W.R., 2001. Increased sedimentation rates and grain sizes 2–4 Myr ago due to the influence of climate change on erosion rates. Nature, 410, 891–897.

APPENDIX H

DETAILED SAMLPING METHODS

Surface samples consist of soil and rock pairs from each location. Surface sample locations were selected with the objective of representing various hillslope positions, slope gradients, and aspect angles. To take a sample, we first lay out the 3x3 m string grid at a sample location and estimate the percent soil cover in each of the 9 squares. We would auger to the depth of refusal at a point within 1 m of the grid.

Soil sample: We choose to sample the top 10 cm of the regolith in order to measure that material which will be delivered to the river channel. The top 10 cm of regolith was sampled in the center of each of the nine squares. If there is a clear layer of organic debris on the ground, for example a layer of pine needles, that organic material was brushed aside and discounted from the 10 cm (in later steps, ignition will be used to remove organic material within the sample, but where there is a thick layer of biomass on top of the ground we want to exclude it). The sample was stored in a labeled freezer-quality quart-size Ziploc bag. Once transported to the lab, sample bags were set out with the bag open for 2 days to dry. A subsample of selected samples was sent off for X-ray fluorescence by ALS Global in Reno, NV (see below). Material was shaken up and moved around within the Ziploc bag, and a scoop was used to collect 30-40 g of material from the full length of the bag.

Rock sample: In sampling surface rock, we aim to take a spatially integrated sample so that any anomalous rock present at the surface will not significantly throw off our measurements. We acknowledge that using surface rock to represent parent material is problematic; however, we take measures to minimize error that may come from heterogeneities in bedrock. To take a rock sample, we break off fragments of ~5 large rocks present within the sample grid using a rock hammer. Where little or no rocks are present within the sample grid, we sample rocks within 10 m of the sample grid (this was rarely the case). We target large rocks, mostly big boulders ~1m on a side, rather than 10 cm rock fragments that might by lying on the ground and are more likely to be transported a great distance. However, most of the rocks sampled are boulders that might have been transported from upslope, not outcrops that are rooted in bedrock. By sampling approximately five rocks at each sample site, we minimize the effects of heterogeneities such as veins in bedrock. We further minimize the effect of “nuggets” of anomalous composition when we subsample for XRF analysis: after the bags are set out to dry, the samples that were selected for XRF analysis were crushed by covering the whole sample with a cloth and smashing with a sledgehammer to ~1 cm fragments. Then a mixture of these crushed fragments was sent to ALS Global where it was powdered for XRF analysis (see below).

X-ray Fluorescence: 118 samples were sent for XRF at ALS Global in Reno, NV to be crushed (ALS code and description: PUL-31, “pulverize split to 85% < 75 μm”), incorporated into XRF pellets and fused beads. They were measured for major elements (ME-XRF06 “whole rock package”) and trace-level XRF analysis (ME-XRF-05 “trace level XRF analysis”).

Samples were processed by:

ALS Global
4977 Energy Way, Reno, NV 89502. (775) 356-5395

APPENDIX I

DISTRIBUTION OF LAND COVER TYPE WITH SLOPE GRADIENT

While field measurements of soil thickness and weathering extent show no correlation with topographic metrics, land cover type as defined by the National Land Cover Database does correlate with slope gradient in both Lost Horse Creek and Rye Creek. We compare NLCD classifications by slope gradient, binning by 5° slope increments (figure A3). The results reveal that forest abundance starts high at low elevations, decreases with increasing slope gradient until approximately 35° slope, and then rises again; meanwhile, nonforest categories ("perennial ice/snow", "barren land (rock/sand/clay)", "shrub/scrub", and "grassland/herbaceous") are almost nonexistent at low slopes and increases in abundance until the forest and non-forest are almost equal at ~35° slope, and then nonforest decreases again. Our analysis of NLCD data also suggests that a slope threshold for soil cover exists in both catchments and that this threshold is slightly higher in Lost Horse (~25°) than Rye Creek (~20°), based on analysis of what portion of forest or non-forest occurs at each 5° slope bin. Forest occupies more than its share of low elevations while nonforest occupies more of its share at higher elevations. This difference is more pronounced in Lost Horse. This is important because it suggests that morphology, including the topographic legacy left by glaciation, can influence the distribution of ecological communities.

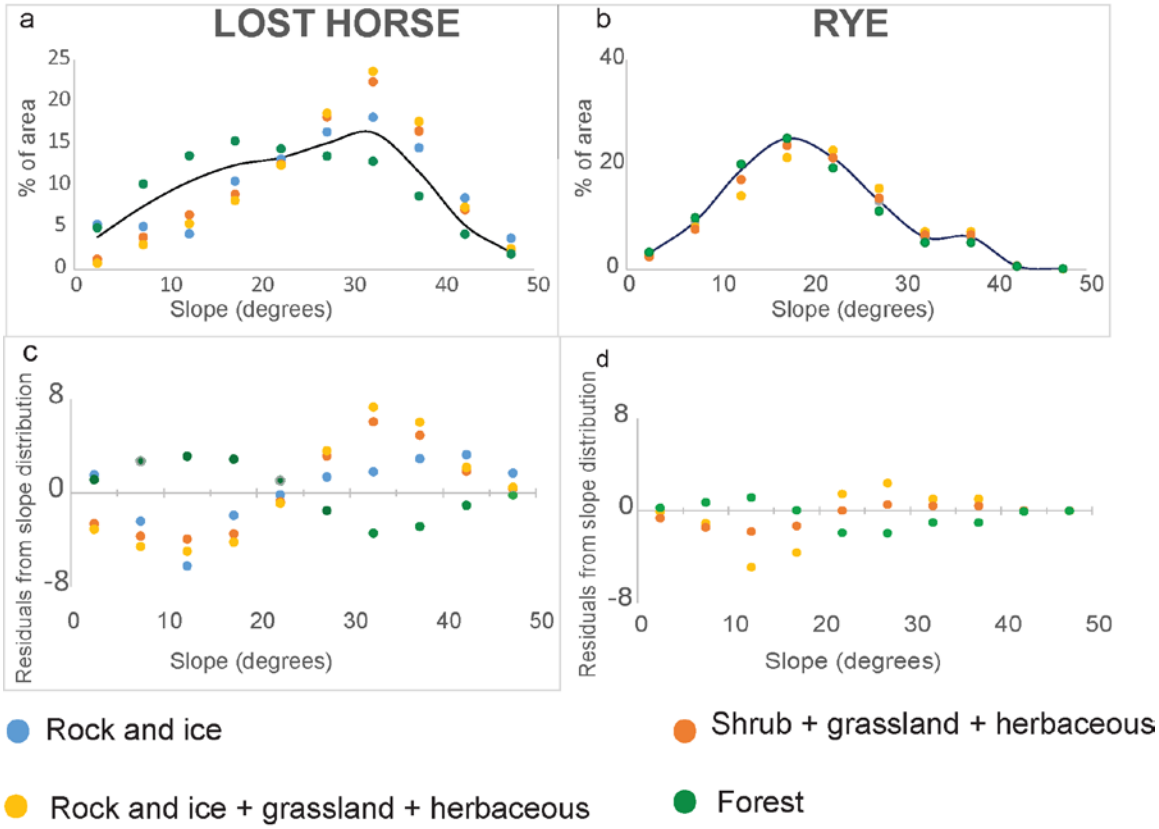

***A.3.**. Land cover type distribution across Lost Horse and Rye Creeks. A and b show the amount of each land cover type (ex. forest) present at a given slope range (for example, between 10-15°), while the black line reflects the overall frequency distribution of slope values within each catchment. Notice that a large portion of Lost Horse Creek has a slope gradient of ~30°, and a large portion of Rye Creek has a slope of ~15°. The bottom two panels, c and d, represent the amount of a land cover type present, normalized with respect to slope. The purpose of this analysis is to show how abundance of different land cover classes may change with respect to local slope gradient. This shows the dominance of a land cover type compared to the others at any given slope interval. In Lost Horse Creek, forest is a greater portion of the land area at low elevations than at high elevations, where rock and ice become more dominant. Shrubs also become more ubiquitous at higher elevations. There appears to be a threshold where forest becomes less dominant and the other categories become more dominant around 25° slope. In Rye Creek, we find a more subtle decrease in forest cover at slopes near 20°.*